Young massive star clusters

Simon F. Portegies Zwart
Leiden Observatory, Leiden University,
P.O. Box 9513, NL-2300 RA Leiden, The Netherlands
email: spz@strw.leidenuniv.nl

Stephen L.W. McMillan
Department of Physics, Drexel University, Philadelphia, PA 19104, USA
email: steve@physics.drexel.edu

Mark Gieles
European Southern Observatory, Casilla 19001, Santiago 19, Chile
email: mgieles@eso.org

February 10, 2010

Abstract

Young massive clusters are dense aggregates of young stars that form the fundamental building blocks of galaxies. Several examples exist in the Milky Way Galaxy and the Local Group, but they are particularly abundant in starburst and interacting galaxies. The few young massive clusters that are close enough to resolve are of prime interest for studying the stellar mass function and the ecological interplay between stellar evolution and stellar dynamics. The distant unresolved clusters may be effectively used to study the star-cluster mass function, and they provide excellent constraints on the formation mechanisms of young cluster populations. Young massive clusters are expected to be the nurseries for many unusual objects, including a wide range of exotic stars and binaries. So far only a few such objects have been found in young massive clusters, although their older cousins, the globular clusters, are unusually rich in stellar exotica.

In this review we focus on star clusters younger than $\sim 100\,\mathrm{Myr}$, more than a few current crossing times old, and more massive than $\sim 10^4\,\mathrm{M}_\odot$, irrespective of cluster size or environment. We describe the global properties of the currently known young massive star clusters in the Local Group and beyond, and discuss the state of the art in observations and dynamical modeling of these systems. In order to make this review readable by observers, theorists, and computational astrophysicists, we also review the cross-disciplinary terminology.

1 Introduction

Stars form in clustered environments (Lada & Lada 2003). In the Milky Way Galaxy, evidence for this statement comes from the global clustering of spectral O-type stars (Parker & Goodwin 2007), of which $\sim 70\%$ reside in young clusters or associations (Gies 1987), and $\sim 50\%$ of the remaining field population are directly identified as runaways (de Wit et al. 2005). de Wit et al. (2005) found that only $\sim 4\%$ of O-type stars can be considered as having formed outside a clustered environment; further analysis has shown that a few of even those 4% may actually be runaway stars (Gvaramadze & Bomans 2008, Schilbach & Röser 2008), further strengthening the case for clustered formation. Additional evidence that clusters are the primary mode of star formation comes from the observed formation rate of stars in embedded clusters ($\sim 3 \times 10^3\,\mathrm{M_\odot\,Myr^{-1}\,kpc^{-2}}$; Lada & Lada 2003) which is comparable to the formation rate of field stars (~ 3–$7 \times 10^3\,\mathrm{M_\odot\,Myr^{-1}\,kpc^{-2}}$; Miller & Scalo 1979). Finally, some 96% of the stars in the nearby Orion B star-forming region are clustered (Clarke, Bonnell & Hillenbrand 2000).

In nearby young starburst galaxies at least 20%, and possibly all, of the ultraviolet light appears to come from young star clusters (Meurer et al. 1995); this also seems to be the case for the observed $H\alpha$ and B-band luminosities in interacting galaxies, such as the Antennae (Fall, Chandar & Whitmore 2005) and NGC 3256 (Zepf et al. 1999). The fossil record of an early episode of star formation is evidenced by the present-day population of old globular clusters, although the first (population III) stars seem not to have formed in clusters (Abel, Bryan & Norman 2002).

1.1 Scope of this review

In this review we focus on the *young massive clusters* (hereafter YMCs) found in an increasing number of galaxies. We adopt a deliberately broad definition of this term, concentrating on observations of star clusters younger than about 100 Myr and more massive than $10^4\,\mathrm{M_\odot}$. In addition, implicit throughout most of our discussion is the assumption that the clusters under study are actually *bound*. This may seem obvious but, as we will discuss in §2, some very young objects satisfying our age and mass criteria may well be unbound, expanding freely into space following the loss of the intracluster gas out of which they formed. We find that imposing a third requirement, that the age of the cluster exceed its current dynamical time (the orbit time of a typical star—see §1.3.3) by a factor of a few, effectively distinguishes between bound clusters and unbound associations.

Our adopted age limit is somewhat arbitrary, but represents roughly the epoch at which a cluster can be said to have survived its birth (phase 1, see §3) and the subsequent early phase of vigorous stellar evolution (phase 2, see §4), and to be entering the long-term evolutionary phase during which its lifetime is determined principally by stellar dynamical processes and external influences (phase 3, see §3). This latter, "stellar dynamical" phase generally starts after about 100 Myr and is not the principal focus of this review.

The mass limit is such that lower-mass clusters are unlikely to survive for more than 1 Gyr. Based on the lifetimes presented in §4 (in particular see Eq. 19), we estimate that a cluster with an initial number of stars $N \simeq 10^5$ will survive for ~ 10 Gyr. Since young clusters more massive than $10^5\,\mathrm{M_\odot}$ are relatively rare, we relax our criterion to include star clusters with masses as low as $10^4\,\mathrm{M_\odot}$. We place no limits on cluster size, metallicity, or

galactic location, for the practical reason that this would further reduce our already small sample of YMCs, even though it seems likely that clusters such as the Arches and Quintuplet systems near the Galactic center (see Tab. 2) are likely to dissolve within a gigayear.

Thus, any young cluster massive enough to survive for a significant fraction of a Hubble time—regardless of its current location—meets our criteria for inclusion in this review. Within the current context we cannot make a strong connection between cluster properties and environment, but from the discussion around Fig. 10 below it is evident that environment has at least some influence on global cluster characteristics (see §2.4.2).

The masses and projected lifetimes of YMCs coincide with those of the old globular clusters (hereafter GCs) that populate the bulges and halos of many galaxies, including our own. Indeed, YMCs are sometimes referred to in the literature as "young globular clusters." This possible connection between YMCs and GCs offers the exciting prospect of studying in the local universe physical processes that may have occurred during the otherwise practically unobservable formative stages of the GC population.[a] However, although the characterization is highly suggestive, the extent to which today's YMCs will someday come to resemble GCs remains unclear.

As we will see, the size distribution of YMCs does appear to be consistent with them evolving into GCs (Maíz-Apellániz 2002), and we can reasonably expect that after (say) 10 Gyr they will be roughly spherical in shape and will have surface brightness distributions similar in character to those of the GCs, but other properties are not so easy to assess. Except for a few nearby cases, such as Westerlund 1 and the Arches cluster (see Tab. 2 in §2), observations of YMCs are limited to stellar masses $\gtrsim 1\,M_\odot$, whereas the most massive stars observed in GCs are less than $1\,M_\odot$. Thus there is no guarantee that the stellar mass function in YMCs below $\sim 1M_\odot$ resembles the initial mass functions of known GCs, although we note that the stellar mass functions in nearby open clusters are consistent with the distribution of low-mass stars in GCs (Chabrier 2003; Bastian, Covey & Meyer 2010). Similar uncertainties apply to cluster binary populations. The initial binary fractions inferred for GCs are generally small, whereas YMCs appear to be binary-rich (see §5.1). But the known binaries in massive clusters tend to be found among massive stars, while the binary properties of low-mass stars in YMCs are unknown. Again, any comparison is complicated by the absence of any significant overlap in the observed stellar mass spectra.

Our objective in this review is to summarize the current state of knowledge of YMCs, to describe the key physical processes governing their evolution and survival, and to assess the extent to which we expect them to evolve into systems comparable to the old GCs observed today.

In this review we will use the terms *young*, *dense*, and *massive* in relation to star clusters. Although not precise, these descriptions do have specific connotations. As already indicated, "young" means star clusters that are still in the early, violent mass-loss phase during the first 100 Myr (see §4). "Dense" indicates that in some clusters the stars are packed together so closely that stellar collisions start to play an important role (see §3.4.2). In terms of the Safronov number,[b] young dense clusters have $\Theta \lesssim 10^2$. As a practical matter, we consider a cluster to be dense if its half-mass relaxation time (Eq. 16) is less than $\sim 10^8$ years

[a] "Real" young globular clusters at $z \sim 5$ are expected to be ∼2 magnitudes brighter than the detection limit of the James Webb Space Telescope.

[b] The Safronov (1969) number Θ is defined as the square of the ratio of the escape velocity from the stellar

(Portegies Zwart, McMillan & Makino 2007). "Massive" indicates that we expect the cluster to survive for ~ 10 Gyr, into the "old globular cluster" regime. Tab. 1 summarizes the main parameters of the three different populations of star clusters.

cluster	age [Gyr]	$m_{\rm to}$ [$M_\odot$]	M [$M_\odot$]	$r_{\rm vir}$ [pc]	ρ_c [$M_\odot/pc^3$]	Z [$Z_\odot$]	location	$t_{\rm dyn}$ [Myr]	$t_{\rm rh}$ [Myr]
OC	$\lesssim$ 0.3	$\lesssim 4$	$\lesssim 10^3$	1	$\lesssim 10^3$	~ 1	disk	~ 1	$\lesssim 100$
GC	$\gtrsim 10$	~ 0.8	$\gtrsim 10^5$	10	$\gtrsim 10^3$	< 1	halo	$\gtrsim 1$	$\gtrsim 1000$
YMC	$\lesssim$ 0.1	$\gtrsim 5$	$\gtrsim 10^4$	1	$\gtrsim 10^3$	$\gtrsim 1$	galaxy	$\lesssim 1$	$\lesssim 100$

Table 1: Comparison of fundamental parameters for star cluster families relevant to this review: open cluster (OC), globular cluster (GC), and young massive cluster (YMC). The numbers in the columns are intended to be indicative of the population and are rounded-off, and should be used with care, but they provide some flavor of the various cluster types. The second column gives cluster age, followed by the turn-off mass (in $M_\odot$), the total cluster mass (in $M_\odot$), the virial radius $r_{\rm vir}$ (see §1.3.2), the core density, and the metallicity. The last three columns give the location in the Galaxy where these clusters are found, and the dynamical and relaxation time scales, defined in §1.3.3.

Figs. 1 and 2 compare the distributions of massive open star clusters, YMCs, and GCs in the Milky Way Galaxy. The spatial distribution of the YMCs (Fig. 1) clearly identify them as a disk population comparable to the open clusters, but in the mass-radius diagram (Fig. 2), YMCs seem more closely related to GCs.

1.2 Properties of Cluster Systems

The Milky Way Galaxy contains some 150 GCs, with mass estimates ranging from $\sim 10^3\,M_\odot$ (for AM4, a member of the Sgr dwarf spheroidal galaxy) to $2.2 \times 10^6\,M_\odot$ (for NGC 5139, Omega Centauri)[c]. If we assume constant $M/L = 2$, the current total mass in GCs in the Harris (1996) catalog is $\sim 3.5 \times 10^7\,M_\odot$, or $\sim 0.07\%$ of the baryonic mass of the Galaxy and 0.005% of the total mass (including dark matter). The luminosity function of GCs in the Galaxy peaks at $M_V \approx -7.4$ mag, corresponding to a typical mass of $\sim 2 \times 10^5\,M_\odot$, and has a (Gaussian) width of $\simeq 1.2$ mag (Harris 2001). The total initial mass for GCs is estimated to be $\sim 4 - 8 \times 10^8\,M_\odot$ (Fall & Zhang 2001). Apparently, more than 90% of all globular star clusters have been disrupted during the last ~ 12 Gyr (Chernoff & Weinberg 1990); the inferred total mass in disrupted clusters is comparable to the total mass of the Galactic

surface to the rms ($\langle v^2 \rangle^{1/2}$) velocity in the cluster:

$$\Theta = \frac{1}{2} \left(\frac{v_{\star,\rm esc}}{\langle v^2 \rangle^{1/2}} \right)^2 . \quad (1)$$

[c]These estimates are made assuming a constant mass-to-light ratio $M/L = 2$, with data from the (Harris 1996) catalog of Milky Way GCs `http://www.physics.mcmaster.ca/Globular.html`. Another useful catalog for Milky Way globular cluster data is available online `http://www.astro.caltech.edu/~george/glob/data.html` (Djorgovski & Meylan 1993).

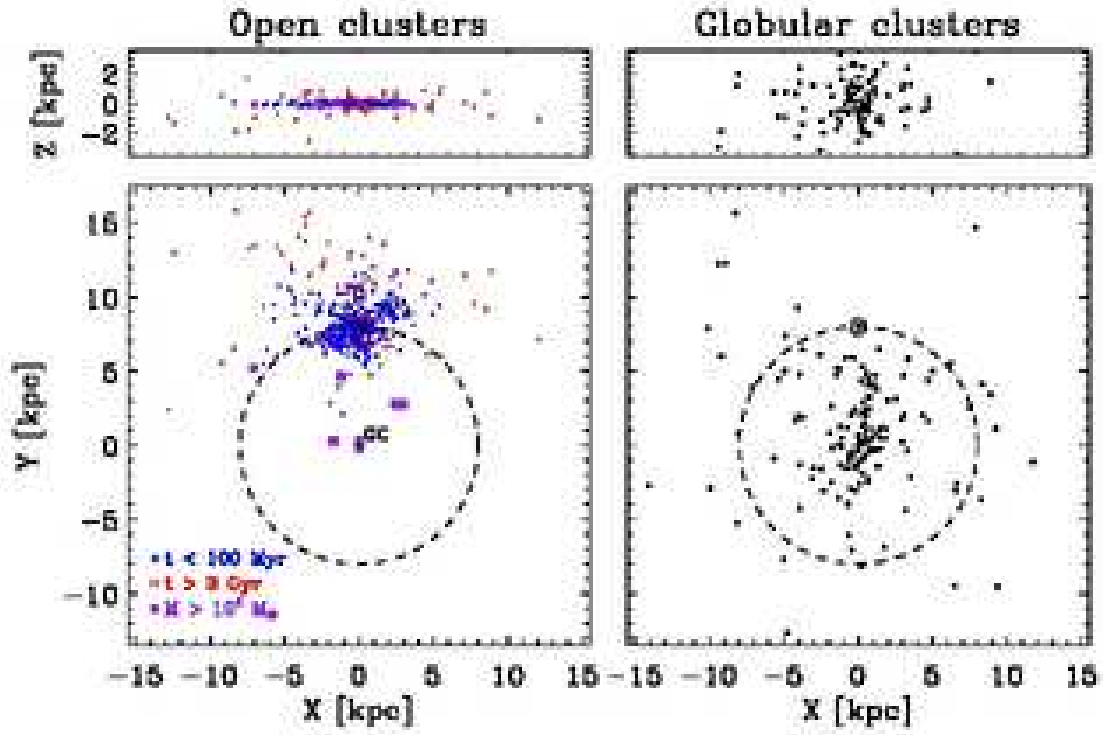

Figure 1: Left: Distribution of young (< 100 Myr, bullets) and old (> 3 Gyr, circles) open clusters in the Galactic plane, based on the catalog of Dias et al. (2002). The old open clusters are found preferentially towards the Galactic anti-center and above the plane. The young massive clusters (squares) seem to be concentrated in the same quadrant as the Sun, which is an observational selection effect. Right: Distribution of old globular clusters, data from the Harris (1996) catalog.

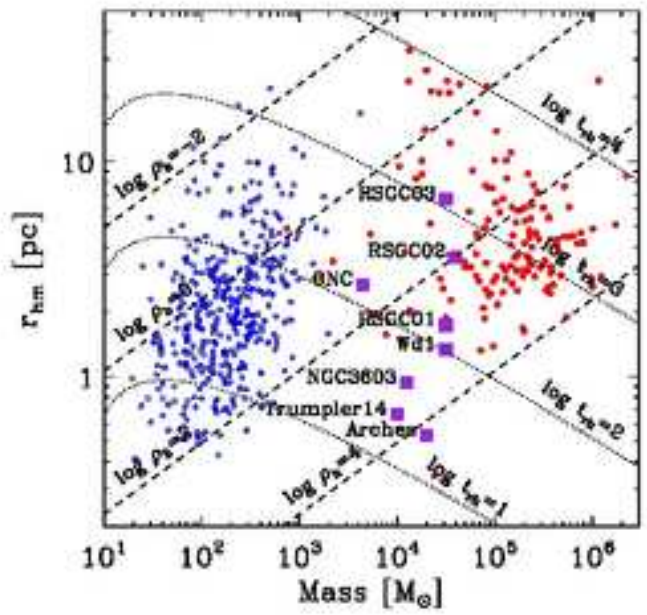

Figure 2: Radius–mass diagram of Milky Way open clusters, young massive clusters and old globular clusters. Open cluster half-mass radii $r_{\rm hm}$ (see §1.3.2) and masses are taken from Dias et al. (2002) and Lamers et al. (2005, private communication), respectively. Data for the YMCs are discussed in more detail in §2. Globular cluster data are taken from the Harris catalog. Dashed and dotted lines represent constant half-mass density $\rho_{\rm h} = 3M/8\pi {r_{\rm hm}}^3$ and half-mass relaxation time $t_{\rm rh}$ (Eq. 17), respectively.

stellar halo (Hut & Djorgovski 1992, Bell et al. 2008, see also §4), although we note that the spatial distributions of halo stars and GCs differ (Forte, Vega & Faifer 2009).

The open cluster databases of Kharchenko et al. (2005) and Piskunov et al. (2008), with 81 clusters, are probably complete to a distance of $\sim 600\,$pc and have a mean cluster mass of $\sim 500\,{\rm M}_\odot$. With an open cluster birth rate of 0.2–0.5 $\rm Myr^{-1}\,kpc^{-2}$ (Battinelli & Capuzzo-Dolcetta 1991, Piskunov et al. 2006), the implied total star formation rate in open clusters is $\sim 2\times10^2\,{\rm M}_\odot\,{\rm Myr}^{-1}\,{\rm kpc}^{-2}$. For an average cluster age of $\sim 250\,$Myr these estimates imply a total of about 23,000–37,000 open star clusters currently in the Galaxy. However, the formation rate of embedded clusters (still partly or completely enshrouded in the molecular cloud from which they formed) is considerably higher—$2-4\,{\rm Myr}^{-1}\,{\rm kpc}^{-2}$ (Lada & Lada 2003)—and with a similar cluster mean mass the total star formation rate in embedded clusters is $\sim 3\times10^3\,{\rm M}_\odot\,{\rm Myr}^{-1}\,{\rm kpc}^{-2}$, comparable to the formation rate of field stars in the disk ($3-7\times10^3\,{\rm M}_\odot\,{\rm Myr}^{-1}\,{\rm kpc}^{-2}$; Miller & Scalo 1979). Although the uncertainties are large, this suggests that the majority of stars form in embedded clusters, but only a relatively small fraction ($\sim 10\%$) of clusters survive the embedded phase.

These estimates are sensitive to the underlying assumptions made about the star-formation history of the Galaxy and the duration of the embedded phase, as well as to observational selection effects. For example, the open cluster sample used by Battinelli & Capuzzo-Dolcetta (1991) is based on a luminosity limited sample of 100 clusters from the Lynga (1982) catalog, which

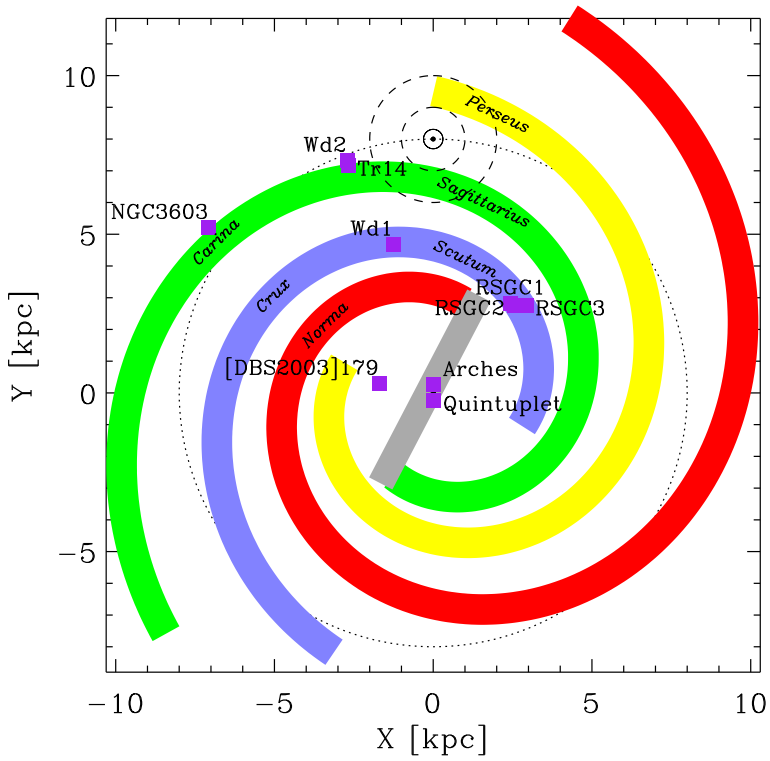

Figure 3: Top view of the Milky Way Galaxy, with the known spiral pattern (Vallée 2008) and young star clusters more massive than $\gtrsim 10^4\,M_\odot$ identified. Basic cluster parameters are listed in Tab. 2. The location of the Sun is indicated by $\odot$, and its orbit by the dotted circle. Dashed lines indicate circles of 1 kpc and 2 kpc around the sun.

claims to be complete to a distance of 2 kpc, but the mass of open clusters in this catalog between 600 pc and 2 kpc averages several thousand solar masses. The much higher mean mass of open clusters at large distance indicates that care has to be taken in using these catalogs, as there appear to be selection effects with respect to distance. Another problem arises from confining the analysis to a distance of 600 pc around the Sun, since the cluster sample does not include any nearby spiral arms, where many young clusters form; Lada & Lada (2003) considered a sample of clusters within 2 kpc of the sun, which therefore includes many objects in the Perseus and Sagittarius arms (Fig. 3). These differences complicate direct comparison of cluster samples.

1.3 Terminology

The study of star clusters has suffered from conflicting terminology used by theorists and observers. In this section we attempt to clarify some terms, with the goal of making this review more readable by all.

1.3.1 Cluster center

Determining the center of a star cluster sounds like a trivial exercise, but in practice it is not easy. The cluster center is not well defined observationally, although theorists have reached some consensus about its definition.

von Hoerner (1963) defined the center of a simulated (N-body) cluster as a density-weighted average of stellar positions:

$$\bar{x}_{d,j} = \frac{\sum_i x_i \rho_i^{(j)}}{\sum_i \rho_i^{(j)}}, \tag{2}$$

where $\rho_i^{(j)}$ is the density estimator of order j around star i, and x_i is the (3-dimensional) position vector of star i.

In direct N-body simulations (see §A.3), alternatives to Eq. 2 are preferred due to the computational expense of determining the local density $\rho_i^{(j)}$. The center of mass, often used in simple estimates, is generally *not* a good measure of the cluster center, as distant stars tend to dominate. This has led to approximate, but more efficient, estimators, such as the "modified" density center (Portegies Zwart et al. 2001), which iteratively determines the weighted mean of the positions of a specified Lagrangian fraction (typically $\sim 90\%$) of stars, relative to the modified density center (Heggie, Inagaki & McMillan 1994). In general, it agrees well with the density center defined above.

Observationally, the cluster center is considerably harder to define, both because of the lack of full 3-dimensional stellar positions, and also because of observational selection effects, including the influence of low-luminosity stars and remnants, crowding, and the broad range in luminosities of individual stars. Both number-averaged and luminosity-averaged estimators are found in the literature. In principle, the 2-dimensional equivalent of Eq. 2 could be used, but observers often prefer the point of maximal symmetry of the observed projected stellar distribution. An example is the technique adopted by McLaughlin et al. (2006) to determine the center of GC 47 Tuc.

1.3.2 Size scales

Massive star clusters tend to be approximately spherically symmetric in space, or at least circular on the sky, so the radius of a cluster is a meaningful measure of its size. Theorists often talk in terms of Lagrangian radii—distances from the center containing specific fractions of the total cluster mass. For observers, a similar definition can be formulated in terms of isophotes containing given fractions of the total luminosity. The *half-mass radius* ($r_{\rm hm}$; the 50% Lagrangian radius) is the distance from the cluster center containing half of the total mass. Observationally, the projected half-light radius—the effective radius $r_{\rm eff}$—is often used, although the total cluster light, which is obviously required to define the Lagrangian radii, can be hard to determine and is not the same as $r_{\rm hm}$ in projection when the mass-to-light ratio varies with the distance to the cluster centre.

Arguably more useful cluster scales are the virial radius $r_{\rm vir}$, the core radius $r_{\rm c}$ (see Eq. 6), and the tidal radius $r_{\rm t}$. We now define them in turn.

The *virial radius* is defined as

$$r_{\rm vir} \equiv \frac{GM^2}{2|U|}. \tag{3}$$

Here M is the total cluster mass, U is the total potential energy and G is the gravitational constant. This is clearly a theoretical definition, as neither the total mass nor the potential energy are actually observed. The potential energy may be obtained directly from the stellar masses and positions in an N-body simulation (see §4.1), or from a potential–density pair by $U = 2\pi \int \rho(r)\phi(r)\, r^2\, dr$.

From an observational point of view, the parameter $\eta \equiv 6r_{\rm vir}/r_{\rm eff}$ is generally introduced to determine the dynamical mass of star clusters. In virial equilibrium ($U = -2T$, where T is the total kinetic energy of the cluster stars), $T/M = \frac{1}{2}\langle v^2\rangle = \frac{3}{2}{\sigma_{\rm 1D}}^2$ for an isotropic system. The line-of-sight velocity dispersion $\sigma_{\rm 1D}$ can be directly measured, yielding the cluster mass

$$M_{\rm vir} = \eta \left(\frac{{\sigma_{\rm 1D}}^2 r_{\rm eff}}{G}\right). \tag{4}$$

In Fig. 4 we present the dependence of η on the parameters of some typical density profiles: the concentration parameter $c \equiv \log(r_{\rm t}/r_{\rm c})$ of a King (1966) model or the parameter γ in an Elson, Fall & Freeman (1987, hereafter EFF87) surface brightness profile,

$$\Sigma(r) = \Sigma_0 \left(1 + \frac{r^2}{a^2}\right)^{-\gamma/2}, \tag{5}$$

where a is a scale parameter, the 3-dimensional density profile has a logarithmic slope of $-\gamma_{\rm 3D} = -(\gamma + 1)$ for $r \gg a$, and $r_{\rm c}$ and $r_{\rm t}$ are, respectively, the core radius and tidal radius of the cluster (to be defined below).

A Plummer (1911) density profile has $\gamma = 4$, $r_{\rm vir}/r_{\rm eff} = 16/3\pi$, and therefore $\eta \simeq 10$. The value $\eta = 9.75$, corresponding to $r_{\rm vir} = 1.625 r_{\rm eff}$, is a reasonable and widely used choice for clusters with relatively shallow density profiles—$\gamma \gtrsim 4$ or $c \lesssim 1.8$. For $\gamma \leq 2$ the EFF87 profile has infinite mass, and the ratio $r_{\rm vir}/r_{\rm eff}$ drops sharply for $\gamma \lesssim 2.5$. The choice for $\eta = 9.75$ should be made cautiously, since many young clusters tend to have relatively shallow density profiles with $2 \lesssim \gamma \lesssim 3$, for which $\eta \lesssim 9$ (see Fig. 4 and also §2). In addition, mass segregation can have a severe effect on η, resulting in a variation of more than a factor of $\sim$3 (Fleck et al. 2005).

Observers generally define the cluster *core radius*, $r_{\rm c}$, as the distance from the cluster center at which the surface brightness drops by a factor of two from the central value. Unfortunately, theorists use at least two distinct definitions of $r_{\rm c}$, depending on context. When the central density ρ_0 and velocity dispersion $\langle v^2\rangle_0$ are easily and stably defined, as is often the case for analytic, Fokker–Planck, and Monte Carlo models (see §4.1 and the Appendix A for more details), the definition

$$r_{\rm c} = \sqrt{\frac{3\langle v^2\rangle_0}{4\pi G \rho_0}} \tag{6}$$

(King 1966) is often adopted. For typical cluster models this corresponds roughly to the radius at which the three-dimensional stellar density drops by a factor of 3, and the surface density by ~ 2.

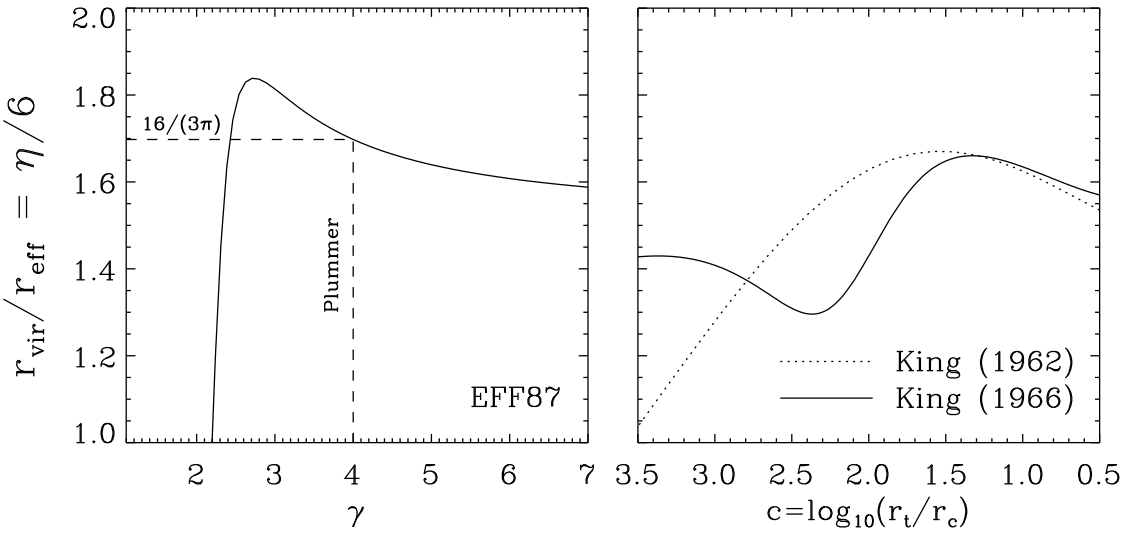

Figure 4: The ratio $r_{\rm vir}/r_{\rm eff}$ and the parameter η used to convert an observed 1-D velocity dispersion and half-light radius into a dynamical mass (Eq. 4) for Eq. 5 (left) and King (1962) and King (1966) models (right). The dashed line in the left panel indicates the analytical result for a Plummer (1911) model ($\gamma = 4$ in Eq. 5).

In N-body simulations, however, both ρ_0 and $\langle v^2 \rangle_0$ are difficult to determine, as they are subject to substantial stochastic fluctuations. As a result, a density-weighted core radius is used instead. Specifically, for each star a local density ρ_i is defined using the star's k nearest neighbors (Casertano & Hut 1985), where $k = 12$ is a common choice. A density center is then determined, either simply the location of the star having the greatest neighbor density, or as a mean stellar position, as in Eq. 2, except that the density estimator is ρ_i^2. [The square is used rather than the first power, as originally suggested by Casertano & Hut (1985), to stabilize the algorithm and make it less sensitive to outliers.] The core radius then is the ρ_i^2-weighted rms stellar distance from the density center:

$$r_{\rm c} = \sqrt{\frac{\sum_i \rho_i^2 r_i^2}{\sum_i \rho_i^2}}. \tag{7}$$

Despite their rather different definitions, in practice the two "theoretical" core radii (Eqs. 6 and 7) behave quite comparably in simulations.

For simple models, the values of $r_{\rm c}$ and $r_{\rm vir}$ determine the density profile, which is generally assumed to be spherically symmetric. This is the case for the empirical King (1962) profiles and dynamical King (1966) models, both of which fit the observed surface brightness distribution of many Milky Way GCs. The dynamical King models are often parameterized by a quantity W_0 representing the dimensionless depth of the cluster potential well. Centrally concentrated clusters have $W_0 \gtrsim 8$ ($c \gtrsim 1.8$), whereas shallow models have $W_0 \lesssim 4$ ($c \lesssim 0.8$). The empirical and dynamical King profiles are in good agreement for $W_0 \lesssim 7$ ($c \lesssim 1.5$).

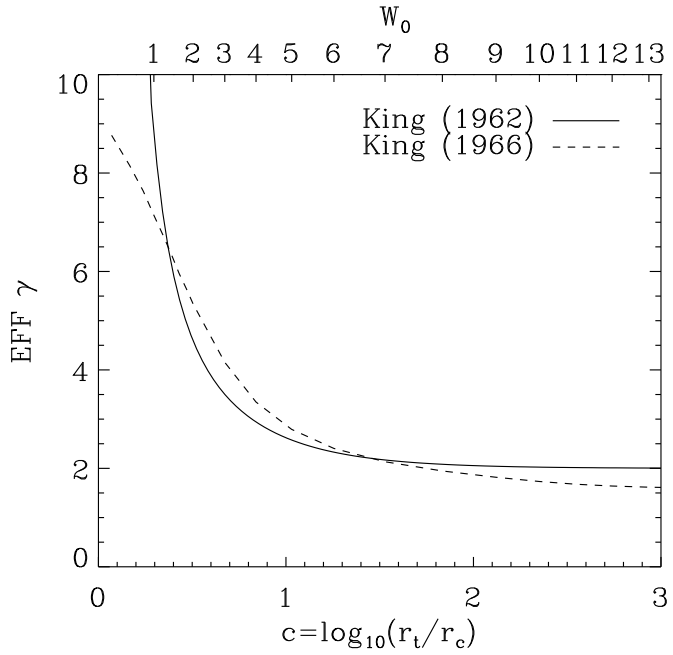

Figure 5: EFF87 model fits (with power-law index γ) to King surface brightness profiles (characterized by King concentration parameter $c = \log_{10} r_t/r_c$). The fits of Eq. 5 to the King profiles/models are done within half the cluster tidal radius.

Galactic GCs are well fit by King models, but the observed surface brightness profiles of young clusters in, for example, the LMC are not (see e.g. Mackey & Gilmore 2003). They are much better represented by EFF87 profiles (Eq. 5), which have cores (different from the King-model cores) and power-law halos. For a King model with concentration $c \gtrsim 1$ ($W_0 \gtrsim 5$), the surface brightness drops to approximately half of its central value at $r = r_c$, as defined by Eq. 6, so the observed core radius is a good measure of the core radius of the underlying three-dimensional stellar density distribution. The "King" core radius of the EFF87 surface brightness profile often adopted by observers is

$$r_c = a \left(2^{2/\gamma} - 1\right)^{1/2} . \tag{8}$$

Here a is the scale parameter in the EFF87 profile. Thus, when an EFF87 surface brightness profile is fit to an observed cluster, Eq. 8 can be used to determine with good confidence the 3-dimensional core radius r_c of Eq. 6.

In Fig. 5 we compare the EFF87 profiles with the empirical King profiles and (projected) King models, by fitting Eq. 5 to each within the inner half-mass radius. For $c \to \infty$ the King (1962) surface brightness profile tends to a power-law with index -2, which has (logarithmically) infinite mass. The King (1966) model in that case becomes an isothermal sphere ($\rho \propto r^{-2}$), also with (linearly) infinite mass, corresponding to $\gamma = 1$ in Eq. 5.

The *tidal radius*, r_t, is the distance from the center of a star cluster where the gravitational acceleration due to the cluster equals the tidal aceleration of the parent Galaxy (von Hoerner 1957). In Fig. 6 we show the equipotential curves of a cluster in the tidal potential of its parent galaxy (the galactic center is to the left in the figure). The equipotential

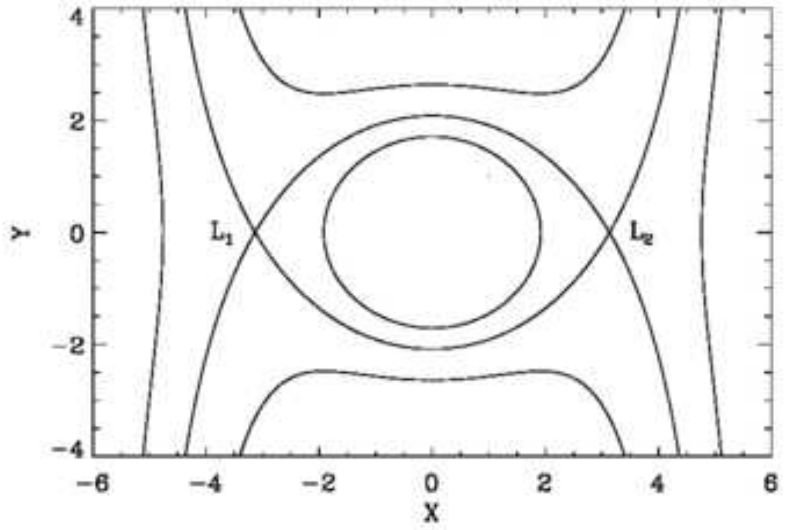

Figure 6: Equipotential surfaces for a $W_0 = 3$ star cluster in an external point-mass tidal field. The galactic center is to the left. The Jacobi surface is delineated by the two crossing equipotentials, passing through the L_1 Lagrangian point to the left and the L_2 point to the right. (Data from Fig. 2 of Fukushige & Heggie 2000).

surface through the two Lagrangian points (L_1 and L_2 at $x \approx \pm 3.1$ in the figure) is the *Jacobi surface*, defining the effective extent of the cluster in the external field. Stars within this surface may be regarded as cluster members (Read et al. 2006). Stars do not escape from the cluster in random directions, but instead do so through the L_1 and L_2 points (Heggie 2001). As a practical matter, the *Jacobi radius* $r_{\rm J}$, the distance from the center to the L_1 point, is a commonly used measure of the cluster's "size." For clusters on circular orbits $r_{\rm J}$ is defined by the cluster mass, M, the orbital angular frequency in the galaxy, ω, and the galactic potential, ϕ, by (King 1962)

$$r_{\rm J} = \left(\frac{GM}{2\omega^2}\right)^{1/3} . \tag{9}$$

Here, $\omega \equiv V_G/R_G$, where R_G is galactocentric distance and V_G is the circular orbital speed around the galaxy center, and we have assumed a flat rotation curve: $\phi(R_G) = V_G^2 \ln(R_G)$. Note that a factor 2/3 is sometimes included to correct for the elongation in the direction along the line connecting L_1 and L_2 (Innanen, Harris & Webbink 1983).

For "Roche lobe filling" clusters that exactly fill their Jacobi surfaces, the Jacobi radius is often identified with the truncation radius of a King (1966) model. However, we emphasize that there is no compelling reason why a star cluster should exactly fill its Jacobi surface, nor is there necessarily any connection in general between the King truncation radius and the properties (or even the existence) of an external tidal field. Observationally, the truncation radius is not measured directly, but instead is inferred from King model fits.

1.3.3 Time scales

The two fundamental time scales of a self-gravitating system are the dynamical time scale $t_{\rm dyn}$, and the relaxation time scale $t_{\rm rl}$.

The dynamical time scale is the time required for a typical star to cross the system; it is also the time scale on which the system (re)establishes dynamical equilibrium. A convenient formal definition in terms of conserved quantities is

$$t_{\rm dyn} = \frac{GM^{5/2}}{(-4E)^{3/2}}, \tag{10}$$

where $E \equiv T + U$ is the total energy of the cluster. In virial equilibrium, $2T + U = 0$ and this expression assumes the more familiar form (Spitzer 1987)

$$t_{\rm dyn} = \left(\frac{GM}{r_{\rm vir}^3}\right)^{-1/2} \tag{11}$$

$$\sim 2 \times 10^4 \,{\rm yr} \left(\frac{M}{10^6 \,{\rm M}_\odot}\right)^{-1/2} \left(\frac{r_{\rm vir}}{1 \,{\rm pc}}\right)^{3/2}, \tag{12}$$

The relaxation time, $t_{\rm rl}$, is typically much longer than $t_{\rm dyn}$. It the time scale on which two-body encounters transfer energy between individual stars and cause the system to establish thermal equilibrium. The local relaxation time is (Spitzer 1987)

$$t_{\rm rl} = \frac{\langle v^2 \rangle^{3/2}}{15.4 G^2 m \rho \ln \Lambda}, \tag{13}$$

where m is the local mean stellar mass and ρ is the local density. The value of the parameter Λ is $0.4N$ for the theoretical case where all stars have the same mass and are distributed homogeneously with an isotropic velocity distribution (Spitzer 1987). Giersz & Heggie (1994) find empirically $\Lambda \sim 0.11N$ for systems where all stars have the same mass. For systems with a significant range of stellar masses, the effective value of Λ may be considerably smaller than this value.

For a cluster in virial equilibrium we can replace all quantities by their cluster-wide averages, writing $\langle v^2 \rangle = GM/2r_{\rm vir}$ and $\bar{\rho} \approx 3M/8\pi r_{\rm vir}^3$, where we ignore the distinction between virial and half-mass quantities, so $r_{\rm hm} \approx r_{\rm vir}$. We thus obtain the "half-mass" two-body relaxation time (Spitzer 1987)

$$t_{\rm rh} \simeq \frac{0.065 \langle v^2 \rangle^{3/2}}{G^2 \langle m \rangle \bar{\rho} \ln \Lambda} \tag{14}$$

$$= 0.14 \frac{N^{1/2} {r_{\rm vir}}^{3/2}}{G^{1/2} \langle m \rangle^{1/2} \ln \Lambda} \tag{15}$$

$$\approx \frac{N}{7 \ln \Lambda} \, t_{\rm dyn} \,, \tag{16}$$

where $\langle m \rangle \equiv N/M$ is the global mean stellar mass and N is the total number of stars in the cluster. If, for simplicity, we adopt $\ln \Lambda = 10$ as appropriate for the range in cluster masses

of interest in this review, Eq. 14 becomes

$$t_{\rm rh} \sim 2 \times 10^8 \,{\rm yr} \, \left(\frac{M}{10^6 {\rm M}_\odot} \right)^{1/2} \left(\frac{r_{\rm vir}}{1{\rm pc}} \right)^{3/2} \left(\frac{\langle m \rangle}{{\rm M}_\odot} \right)^{-1} . \quad (17)$$

Finally, we note that in real stellar systems the one-parameter simplicity of Eq. 16 is broken by the introduction of a third time scale independent of the dynamical properties of the cluster—the stellar evolution time scale $t_S \sim 10$ Myr for YMCs, but a complication here is that t_S depends on time. This simple fact underlies almost all of the material presented in this review.

2 Properties of young massive star clusters

2.1 General characteristics

Traditionally, astronomers have drawn a clear distinction between the relatively young and low mass Milky Way open clusters associated with the Galactic disk and the old and massive globular clusters that reside mostly in the bulge and halo (see Fig. 1 and Tab. 1). According to our definition in §1, the Milky Way hosts several clusters that fill the gap between these populations, in terms of both mass and density (Fig. 2), indicating that the formation of clusters with masses comparable to old GCs is not restricted to the early universe. This becomes even more evident when we look at the Magellanic clouds, which host massive clusters spanning a broad range of ages (Hunter et al. 2003, de Grijs & Anders 2006), as well as many YMCs that have received considerable attention since the 1960s (Hodge 1961).

The ages of the YMCs in the Magellanic Clouds are comparable to those of many Milky Way open clusters (up to a few hundred megayears), but the masses and core densities of these clusters exceed those of open clusters in the Milky Way, in some cases by several orders of magnitude (e.g. Elson & Fall 1985b, see Table 1). A prominent example is R 136, whose core was once believed to be a single stellar object at least 2000 times more massive and about 10^8 times brighter than the Sun. Weigelt & Baier (1985) unambiguously resolved it into a group of stars, and now we know it is a cluster of $\sim 10^5$ young stars, rather than a single extraordinary object (Massey & Hunter 1998, Andersen et al. 2009, Campbell et al. 2010, and left panel of Fig. 7). YMCs such as R 136 are responsible for the giant HII regions found in other galaxies (Kennicutt & Chu 1988, and right panel in Fig. 7) and appear to be much more common phenomena than was previously thought.

YMCs more massive than R 136 were already known several decades ago. Ground-based observations revealed numerous "bluish knots" and "super-star clusters" in the starburst galaxies M82 and NGC 1569 (van den Bergh 1971, Arp & Sandage 1985), and in the relatively local ongoing galaxy mergers NGC 7252 and NGC 3597 (Schweizer 1982, Lutz 1991). HST has since confirmed many extragalactic YMCs, starting with those in the interacting galaxy NGC 1275 (Holtzman et al. 1992). These and later well studied examples have been cited as promising candidates for the latest generation of "young globular clusters" (Whitmore 2003, Larsen 2006).

We review here the basic characteristics of known YMCs and attempt to assess the similarities and differences between the young and old populations (see also §5.4 for a number

Figure 7: Left: A region of $50 \times 50\,\mathrm{pc}^2$ around the $\sim 10^5\,\mathrm{M}_\odot$ cluster R 136 in the 30 Doradus region of the LMC, at a distance of $\sim 50\,\mathrm{kpc}$. Right: Many young star clusters forming in M83 at a distance of 3.6 Mpc. Credit: NASA, ESA, the Wide Field Camera 3 Science Oversight Committee, and the Hubble Heritage Team (STScI/AURA) and F. Paresce R. O'Connell (R136) and R. O'Connell (M83).

of well studied cases). In the limited space available in this section we highlight only the most relevant observed properties. For more in-depth reviews of YMC populations we refer to Whitmore (2003) and Larsen (2006, 2009b). Some interesting individual cases are discussed in depth in de Grijs & Parmentier (2007).

We have collected data on clusters for which estimates of the age, (photometric) mass and half-light (or effective) radius exist in the literature. If more information on structural parameters is available, we determine $r_{\rm vir}$ using the relation presented in Fig. 4. If only an estimate of $r_{\rm eff}$ is available, we determine $r_{\rm vir}$ using the Plummer value of $r_{\rm vir}/r_{\rm eff} = 16/(3\pi) \approx 1.6$. We then calculate $t_{\rm dyn}$ from $r_{\rm vir}$ and the mass using Eq. 12. We assume here that the observed clusters are in virial equilibrium, which results in an overestimate for $t_{\rm dyn}$ for unbound (expanding) clusters. The data are presented in Tables 2, 3 and 4.

As illustrated in Figure 2 of Pfalzner (2009), young star clusters appear to show two evolutionary sequences: (1) a compact configuration starting at a radius of ~ 0.5 pc, which we refer to as (dense) *clusters*, and (2) a sequence with radii ~ 5 pc, which we call *associations*. (These two groups are referred to as "starburst" and "leaky" clusters by Pfalzner 2009.) A more quantitative distinction may be found in the ratio age/$t_{\rm dyn}$, since for bound objects this ratio should be large and for unbound objects it is expected to remain small. We note that the two groups identified by Pfalzner (2009) can be divided in this way, with a boundary at age/$t_{\rm dyn} \approx 3$. This division is indicated in the tables. More physical interpretations of these sequences are presented in §4.

2.2 Mass segregation

Nearby clusters that can be resolved into individual stars are excellent laboratories for studies of stellar populations, and their derived properties can be used as input parameters to models of cluster evolution. Two well known examples of resolved YMCs are the Arches and Quintuplet clusters near the Galactic center (Figer et al. 2002, Figer, McLean & Morris 1999). The Arches has an age of just 1–2 Myr and a central density of $\sim 10^5\,{\rm M}_\odot\,{\rm pc}^{-3}$; its stellar initial mass function (IMF) has been the topic of much debate (Stolte et al. 2002, 2005, Kim et al. 2006). (See also Harfst, Portegies Zwart & Stolte 2009, who reconstruct the cluster's initial conditions by iterated N-body simulations.) We will refrain from commenting in detail on this debate, and instead refer to the recent review by Bastian, Covey & Meyer (2010) for an in-depth discussion of this topic. The current consensus seems to be that "evidence for IMF variations is absent, although this is not evidence for their absence." A Salpeter (1955)[d] distribution cannot be ruled out for the stellar IMF of the Arches cluster (Kim et al. 2006).

Stolte et al. (2002) find evidence for mass segregation within the Arches cluster based on a steepening of the stellar mass function (MF) with increasing distance from the cluster center. However, Espinoza, Selman & Melnick (2009) suggest that the apparent mass segregation could simply be an observational bias, and that a Salpeter MF in the core is still consistent with their observations. The differential extinction across the cluster and the total visual extinction of $A_V \approx 30$ magnitudes make this a challenging cluster to study. See also

[d]Here we use the term "Salpeter" as a possibly universal power-law mass function (with exponent -2.35) for stars more massive than $\sim 1\,{\rm M}_\odot$. At present, given the range of detectable masses, it is not possible to distinguish more finely between the various mass functions commonly adopted by theorists.

(1) Name	(2) Ref	(3) Age [Myr]	(4) $\log M_{\rm phot}$	(5) $\log M_{\rm dyn}$	(6) $r_{\rm c}$ [pc]	(7) $r_{\rm eff}$ [pc]	(8) γ	(9) $\sigma_{\rm 1D}$ [km s^{-1}]	(10) $r_{\rm vir}$ [pc]	(11) $t_{\rm dyn}$ [Myr]	(12) Age/$t_{\rm dyn}$
Arches	1	2.00	4.30	–	0.20	0.40	–	–	0.68	0.06	33.86
DSB2003	4	3.50	3.80	–	–	1.20	–	–	2.04	0.55	6.41
NGC 3603	5	2.00	4.10	–	0.15	0.70	2.00	–	1.19	0.17	11.62
Quintuplet	6	4.00	4.00	–	1.00	2.00	–	–	3.40	0.93	4.29
RSGC 01	6	12.00	4.50	4.70	–	1.50	–	3.70	2.55	0.34	35.22
RSGC 02	8	17.00	4.60	4.80	–	2.70	–	3.40	4.58	0.73	23.18
RSGC 03	9	18.00	4.50	–	–	5.00	–	–	8.49	2.07	8.68
Trumpler 14	10	2.00	4.00	–	0.14	0.50	2.00	–	0.85	0.12	17.15
Wd 1	11	3.50	4.50	4.80	0.40	1.00	4.00	5.80	1.74	0.19	18.27
Wd 2	4	2.00	4.00	–	–	0.80	–	–	1.36	0.24	8.48
hPer	4	12.80	4.20	–	–	2.10	–	–	3.57	0.80	16.06
χPer	4	12.80	4.10	–	–	2.50	–	–	4.24	1.16	11.02
CYgOB	4	2.50	4.40	–	–	5.20	–	–	8.83	2.47	1.01
IC 1805	4	2.00	4.20	–	–	12.50	–	–	21.22	11.58	0.17
I Lac 1	4	14.00	3.40	–	–	20.70	–	–	35.14	61.97	0.23
Lower Cen-Crux	4	11.50	3.30	–	–	15.00	–	–	25.46	42.89	0.27
NGC 2244	4	2.00	3.90	–	–	5.60	–	–	9.51	4.90	0.41
NGC 6611	4	3.00	4.40	–	–	5.90	–	–	10.02	2.98	1.01
NGC 7380	4	2.00	3.80	–	–	6.50	–	–	11.03	6.88	0.29
ONC	13	1.00	3.65	–	0.20	2.00	2.00	–	3.40	1.40	0.72
Ori Ia	4	11.40	3.70	–	–	16.60	–	–	28.18	31.50	0.36
Ori Ib	4	1.70	3.60	–	–	6.30	–	–	10.70	8.26	0.21
Ori Ic	4	4.60	3.80	–	–	12.50	–	–	21.22	18.35	0.25
Upper Cen-Crux	4	14.50	3.60	–	–	22.10	–	–	37.52	54.30	0.27
U Sco	4	5.50	3.50	–	–	14.20	–	–	24.11	31.38	0.18

Table 2: Properties of YMCs (top) and associations (bottom) in the Milky Way, with the distinction based on age/$t_{\rm dyn}$. 1: Figer, McLean & Morris (1999); 2: Figer et al. (2002); 3: Stolte et al. (2002); 4: Pfalzner (2009); 5: Harayama, Eisenhauer & Martins (2008); 6: Figer et al. (2006); 7: Davies et al. (2008); 8: Davies et al. (2007); 9: Clark et al. (2009); 10: Ascenso et al. (2007); 11: Mengel & Tacconi-Garman (2007); 12: Brandner et al. (2008); 13: Hillenbrand & Hartmann (1998).

(1) Gal	(2) Name	(3) Ref	(4) Age [Myr]	(5) M_V [mag]	(6) $\log M_{\rm phot}$	(7) $\log M_{\rm dyn}$	(8) $r_{\rm c}$ [pc]	(9) $r_{\rm eff}$ [pc]	(10) γ	(11) $\sigma_{\rm 1D}$ [km s^{-1}]	(12) $r_{\rm vir}$ [pc]	(13) $t_{\rm dyn}$ [Myr]	(14) Age/$t_{\rm dyn}$
LMC	R136	1,2,3,4	3.0	−11.74	4.78	–	0.10	1.70	1.50	–	2.89	0.30	10.14
LMC	NGC 1818	2,3	25.1	−9.62	4.42	–	2.07	5.39	3.30	–	9.76	2.80	8.96
LMC	NGC 1847	2,3	26.3	−9.67	4.44	–	1.73	32.58	2.05	–	10.33	2.98	8.82
LMC	NGC 1850	2,3	31.6	−10.52	4.86	5.22	2.69	11.25	2.05	3.00	3.56	0.37	84.83
LMC	NGC 2004	2,3	20.0	−9.60	4.36	–	1.41	5.27	2.90	–	9.81	3.03	6.59
LMC	NGC 2100	2,3	15.8	−9.77	4.36	–	0.99	4.41	2.30	–	6.32	1.57	10.12
LMC	NGC 2136	2,3	100.0	−8.60	4.30	–	1.59	3.42	3.50	–	6.10	1.59	62.85
LMC	NGC 2157	2,3	39.8	−9.10	4.31	4.90	1.99	5.39	3.05	2.80	9.95	3.27	12.16
LMC	NGC 2164	2,3	50.1	−8.65	4.18	5.15	1.48	4.76	2.95	4.30	8.84	3.19	15.72
LMC	NGC 2214	2,3	39.8	−8.40	4.03	5.28	1.83	8.13	2.45	3.90	14.24	7.74	5.14
LMC	NGC 1711	2,3	50.1	−8.82	4.24	–	1.91	5.19	2.70	–	9.70	3.42	14.66
M31	KW246	5	75.9	−7.80	4.19	–	–	3.20	–	–	5.43	1.52	50.01
M31	B257D	6	79.4	−8.84	4.45	–	3.16	15.14	–	–	25.70	11.57	6.86
M31	B318	6	70.8	−8.76	4.38	–	0.19	6.61	–	–	11.22	3.62	19.57
M31	B327	6	50.1	−8.95	4.38	–	0.20	4.47	–	–	7.59	2.01	24.91
M31	B448	6	79.4	−9.20	4.58	–	0.20	16.22	–	–	27.54	11.05	7.19
M31	Vdb0	7	25.1	−10.00	4.85	–	1.40	7.40	–	–	12.56	2.49	10.07
M31	KW044/B325	5	58.9	−9.20	4.59	–	–	10.00	–	–	16.98	5.29	11.14
M31	KW120	5	87.1	−8.80	4.57	–	–	2.60	–	–	4.41	0.72	121.43
M31	KW208	5	56.2	−7.70	4.01	–	–	2.90	–	–	4.92	1.61	34.93
M31	KW272	5	53.7	−9.00	4.50	–	–	9.00	–	–	15.28	5.01	10.73
M31	B015D	6	70.8	−9.71	4.76	–	0.24	16.60	–	–	28.18	9.30	7.61
M31	B040	6	79.4	−9.00	4.50	–	0.55	12.88	–	–	21.87	8.57	9.27
M31	B043	6	79.4	−8.81	4.43	–	0.72	3.98	–	–	6.76	1.60	49.77
M31	B066	6	70.8	−8.43	4.25	–	0.38	6.76	–	–	11.48	4.35	16.29
NGC 6822	Hubble IV	8,9	25.1	−8.00	4.00	–	0.40	2.00	–	–	3.40	0.93	26.93
SMC	NGC 330	2,3	25.1	−9.94	4.56	5.64	2.34	6.11	2.55	6.00	11.17	2.92	8.60
M31	KW249	5	5.0	−10.50	4.30	–	–	13.50	–	–	22.92	11.58	0.43
M31	KW258	5	5.0	−9.90	4.05	–	–	3.40	–	–	5.77	1.95	2.57
M33	NGC 595	10	4.0	−11.40	4.50	–	–	26.90	–	–	45.67	25.87	0.15
M33	NGC 604	10	3.5	−12.60	5.00	–	–	28.40	–	–	48.21	15.78	0.22
SMC	NGC 346	11	3.0	-	5.60	–	–	9.00	–	–	15.28	1.41	2.13

Table 3: Same as Table 2, but now for the Local Group. 1: Hunter et al. (1995); 2: Mackey & Gilmore (2003); 3: McLaughlin & van der Marel (2005); 4: Andersen et al. (2009); 5: Vansevičius et al. (2009); 6: Barmby et al. (2009); 7: Perina et al. (2009); 8: Wyder, Hodge & Zucker (2000); 9: Chandar, Bianchi & Ford (2000); 10: Maíz-Apellániz (2001); 11: Sabbi et al. (2008).

(1) Gal	(2) Name	(3) Ref	(4) Age [Myr]	(5) M_V [mag]	(6) $\log M_{\rm phot}$	(7) $\log M_{\rm dyn}$	(8) $r_{\rm c}$ [pc]	(9) $r_{\rm eff}$ [pc]	(10) γ	(11) $\sigma_{\rm 1D}$ [km s^{-1}]	(12) $r_{\rm vir}$ [pc]	(13) $t_{\rm dyn}$ [Myr]	(14) Age/$t_{\rm dyn}$
ESO338-IG	23	1	7.08	−15.50	6.70	7.10	–	5.20	–	32.50	4.26	0.15	39.22
M51	3cl-a	2	15.85	−11.10	5.04	–	1.60	5.20	2.00	–	7.13	0.52	6.10
M51	3cl-b	2	5.01	−12.25	5.91	–	0.86	2.30	2.60	–	8.83	1.18	46.07
M51	a1	2	5.01	−12.15	5.47	–	0.65	4.20	1.90	–	5.55	0.24	12.82
M82	MGG 9	3,4,5	9.55	−13.42	5.92	6.36	–	2.60	–	15.90	4.41	0.15	46.04
M82	A1	6,5	6.31	−14.85	5.82	5.93	1.30	3.00	3.00	13.40	5.77	0.31	28.36
M82	F	7	60.26	−14.50	6.70	6.08	–	2.80	3.00	13.40	3.90	0.09	99.10
NGC 1140	1	8	5.01	−14.80	6.04	7.00	–	8.00	–	24.00	5.86	0.32	9.40
NGC 1487	2	9	8.51	–	5.20	5.30	0.71	1.20	–	11.10	5.19	0.40	63.64
NGC 1487	1	9	8.32	–	5.18	6.08	0.97	2.30	–	13.70	2.72	0.07	23.40
NGC 1487	3	9	8.51	–	4.88	5.78	0.71	2.10	–	14.30	5.18	0.08	19.02
NGC 1569	A	10,11,12	12.02	−14.10	6.20	5.52	–	2.30	–	15.70	3.78	0.15	77.49
NGC 1569	C	13	3.02	–	5.16	–	–	2.90	–	–	4.50	0.24	15.13
NGC 1569	B	14	19.95	−12.85	5.74	5.64	0.70	2.10	2.50	9.60	8.83	0.17	49.47
NGC 1569	30	11,12	91.20	−11.15	5.55	–	0.75	2.50	2.50	–	13.58	0.71	33.37
NGC 1705	1	7	15.85	−13.80	5.90	5.68	–	1.60	–	11.40	6.11	0.26	96.15
NGC 4038	S2_1	9	8.91	–	5.47	5.95	0.60	3.70	–	11.50	10.19	0.90	16.09
NGC 4038	W99-1	15	8.13	−14.00	5.86	5.81	–	3.60	–	9.10	13.58	0.46	26.11
NGC 4038	W99-16	15	10.00	−12.70	5.46	6.51	–	6.00	–	15.80	2.38	0.08	7.76
NGC 4038	W99-2	9	6.61	–	6.42	6.48	1.30	8.00	–	14.10	6.11	0.27	14.82
NGC 4038	W99-15	9	8.71	–	5.70	6.00	–	1.40	–	20.20	6.11	0.32	89.94
NGC 4038	S1_1	9	7.94	–	5.85	6.00	0.58	3.60	–	12.50	1.53	0.05	25.77
NGC 4038	S1_2	9	8.32	–	5.70	5.90	0.72	3.60	–	11.50	6.11	0.17	21.75
NGC 4038	S1_5	9	8.51	–	5.48	5.60	1.35	0.90	–	12.00	6.28	0.43	135.26
NGC 4038	2000_1	9	8.51	–	6.23	6.38	0.42	3.60	–	20.00	4.24	0.21	40.09
NGC 4038	S2_2	9	8.91	–	5.60	5.60	0.40	2.50	–	9.50	5.09	0.35	33.64
NGC 4038	S2_3	9	8.91	–	5.38	5.40	0.60	3.00	–	7.00	3.90	0.30	19.86
NGC 4449	N-1	13	10.96	–	6.57	–	–	16.90	–	–	2.04	0.11	5.92
NGC 4449	N-2	13	3.02	–	5.00	–	–	5.80	–	–	3.57	0.36	4.45
NGC 5236	805	16	12.59	−12.17	5.29	5.62	0.70	2.80	2.60	8.10	4.92	0.43	17.80
NGC 5236	502	16	100.00	−11.57	5.65	5.71	0.70	7.60	2.14	–	34.97	9.10	25.27
NGC 5253	I	13	11.48	–	5.38	–	–	4.00	–	–	44.65	17.30	13.11
NGC 5253	VI	13	10.96	–	4.93	–	–	3.10	–	–	33.27	17.64	11.41
NGC 6946	1447	16	11.22	−13.19	5.64	6.25	1.15	10.00	2.10	8.80	20.03	2.83	22.57
NGC 2403	I-B	13	6.03	–	4.82	–	–	26.30	–	–	50.93	15.81	0.39
NGC 2403	I-C	13	6.03	–	4.42	–	–	19.60	–	–	28.01	4.21	0.38
NGC 2403	I-A	13	6.03	–	5.06	–	–	20.60	–	–	56.02	12.47	0.75
NGC 2403	II	13	4.47	–	5.35	–	–	11.80	–	–	25.97	4.42	2.35
NGC 2403	IV	13	4.47	–	5.07	–	–	30.00	–	–	36.84	12.39	0.42
NGC 4214	VI	13	10.96	–	4.93	–	–	35.90	–	–	142.43	34.58	0.29
NGC 4214	V	13	10.96	–	5.73	–	–	83.90	–	–	60.95	24.31	0.20
NGC 4214	VII	13	10.96	–	5.33	–	–	40.40	–	–	68.59	18.31	0.38
NGC 4214	I-A	13	3.47	–	5.44	–	–	16.50	–	–	28.69	1.19	1.55
NGC 4214	I-B	13	3.47	–	5.40	–	–	33.00	–	–	9.85	1.46	0.52
NGC 4214	I-D	13	8.91	–	5.30	–	–	15.30	–	–	6.79	0.54	1.57
NGC 4214	II-C	13	2.00	–	4.86	–	–	21.70	–	–	23.43	7.38	0.51
NGC 5253	IV	13	3.47	–	4.72	–	–	13.80	–	–	5.26	0.62	0.89

Table 4: Same as Table 2, but now for objects outside the Local Group. 1: Östlin, Cumming & Bergvall (2007); 2: Bastian et al. (2008); 3: McCrady, Gilbert & Graham (2003); 4: Bastian et al. (2006); 5: McCrady & Graham (2007); 6: Smith et al. (2006); 7: Smith & Gallagher (2001); 8: Moll et al. (2007); 9: Mengel et al. (2008); 10: Ho & Filippenko (1996); 11: Hunter et al. (2000); 12: Anders et al. (2004); 13: Maíz-Apellániz (2001); 14: Larsen et al. (2008); 15: Mengel et al. (2002); 16: Larsen & Richtler (2004).

Ascenso, Alves & Lago (2009) for a general discussion on observational challenges in studies on mass segregation in the dense central regions of clusters.

Currently the most massive young cluster known in our Galaxy is Westerlund 1 (Clark et al. 2005). Due to its relative proximity ($\sim$4 kpc), its lower extinction (although still a considerable $A_V \approx 10$ magnitudes), and slightly lower intrinsic stellar density, it represents a somewhat easier target than the Arches and Quintuplet for studies of its stellar content. The MF and structural parameters of Westerlund 1 and the somewhat less massive NGC 3603 have been investigated by several space-based instruments and from the ground using adaptive optics. Evidence for an overabundance of massive stars within the half-mass radius has been found in both these clusters (Harayama, Eisenhauer & Martins 2008; Brandner et al. 2008). Probably the best known example of a mass segregated cluster is the (much closer) Orion Nebula Cluster (ONC) (Hillenbrand & Hartmann 1998, Huff & Stahler 2006). Radial variations of the stellar MF have also been found for slightly older ($\sim 10 - 25$ Myr) star clusters in the LMC (de Grijs et al. 2002a, Gouliermis et al. 2004).

Clusters at much larger distances have also been used for studies of mass segregation. McCrady, Graham & Vacca (2005) show that cluster F in the starburst galaxy M82 appears to be smaller at red wavelengths than at blue wavelengths, which they attribute to mass segregation. The reasoning is that the most massive stars are red (super)giants and if these are more centrally concentrated the cluster would appear smaller in the red. A note of caution is added by Bastian et al. (2007), however, who point out that M82-F is a complicated case because of differential extinction across the cluster. A negative correlation between radius and wavelength was also found for NGC 1569-B (Larsen et al. 2008). Gaburov & Gieles (2008) modeled mass segregated clusters and projected them in different filters, and showed that mass segregation can only explain differences in measured $r_{\rm c}$ in different filters at the 5% level. This because the massive stars are much more luminous than the average cluster member and dominate the light profile at all wavelengths, so if a cluster is mass segregated it should appear smaller at all wavelengths. It is thus not clear why NGC 1569-B and M82-F should appear smaller at redder wavelengths.

If stars with masses greater than some mass m are found to be more centrally concentrated than the average stellar mass $\langle m \rangle$, and if the cluster is much younger than the dynamical friction time scale for stars of mass m ($\sim \langle m \rangle t_{\rm rh}/m$; see Eq. 20 in §3), then an obvious conclusion is that the observed mass segregation is primordial—that is, the cluster formed with stars more massive than M preferentially closer to the center. This is generally consistent with simulations of cluster formation (Klessen 2001, Bonnell & Bate 2006). However, the time scale argument only holds for a spherically symmetric stellar system in virial equilibrium. If clusters form through mergers of smaller sub-clumps, the degree of mass segregation of the merger product is higher than would be expected from these simple dynamical arguments (McMillan, Vesperini & Portegies Zwart 2007; Allison et al. 2009; Moeckel & Bonnell 2009). From studies of star clusters that are still embedded in their natal molecular clouds, it is evident that stars form in a clumpy hierarchical fashion (Lada & Lada 2003, Gutermuth et al. 2005), and that some merging has to occur during the early (embedded) evolution. A YMC with a clear lack of mass segregation would therefore be an very interesting object to study.

The degree of mass segregation at a young age has important consequences for the further evolution of a cluster, as we discuss in more detail in §3 and §4.

2.3 Structural Parameters

Studies of the structural parameters of YMCs often involve the rich cluster population of the LMC. Due to their vicinity, these clusters can be spatially resolved and studied from the ground. As mentioned in §1.3.2, unlike the old GCs, whose surface brightness profiles are best described by (tidally truncated) King profiles, the surface brightness profiles of YMCs are best described by power-law profiles with a core (Eq. 5; EFF87). A typical range for the power-law index is $2.2 \lesssim \gamma \lesssim 3.2$ (EFF87; Mackey & Gilmore 2003). Similar slopes are found for extragalactic clusters, with tentative evidence for an increase of γ with age (Larsen 2004).

Several studies have reported a striking increase of $r_{\rm c}$ with age for LMC clusters (Elson, Freeman & Laue de Grijs et al. 2002b; Mackey & Gilmore 2003). Bastian et al. (2008) finds a similar increase for $r_{\rm c}$ of massive clusters in M51 and in a compilation of literature data. Brandner et al. (2008) have shown that $r_{\rm eff}$ of YMCs in the Milky Way increases with age. Fig. 8 shows the increase of $r_{\rm c}$ and $r_{\rm eff}$ with age for all the clusters in Tables 2–4. There may be a rather strong selection bias toward dense objects in the studies that consider $r_{\rm c}$, i.e., there may be young clusters with large $r_{\rm c}$ which simply have not been classified as star clusters or do not have a $r_{\rm c}$ measurement available. This becomes clear immediately when we look at $r_{\rm eff}$, where we have many more values available for the associations (open symbols). The values of $r_{\rm c}$ are not determined for these objects, resulting in a depletion of points at the top left of Fig. 8.

At an age of 100 Myr there is a large spread in $r_{\rm c}$. Elson, Freeman & Lauer (1989) show that mass loss due to stellar evolution from stellar populations with different IMF slopes gives rise to different expansion rates. Mackey et al. (2008) invoke different degrees of (primordial) mass segregation and retention fractions of black holes to explain a range of growth rates for $r_{\rm c}$ (see §3.4.3 for further discussion). From the lower envelope of points in the right panel of Fig. 8 it seems that $r_{\rm eff}$ rises monotonically with age, with no obvious increase in the spread with age.

An increase of a factor of 5–10 in radius has dramatic implications for the evolution of these clusters, since it implies that in a very short time the densities drop by two or three orders of magnitudes. However, if very young clusters are mass segregated (§2.2), the observed $r_{\rm c}$ and $r_{\rm eff}$ (measured from the projected luminosity profile, see §1.3.2) could be considerably smaller than the true values (Fleck et al. 2006, Gaburov & Gieles 2008). We will return to this topic, and the various physical mechanisms that drive cluster expansion at these ages, in more detail in §3 and §4.

Several studies have discussed the lack of any clear correlation between the size of a cluster and its mass or luminosity (Zepf et al. 1999, Larsen 2004, Scheepmaker et al. 2007). If this is how clusters form, it places important constraints on models of cluster formation, since molecular clouds and dense cores do follow a (virial) scaling relation between mass and radius (Larson 1981). A variable star formation efficiency that is higher for massive clumps could weaken or erase the molecular cloud mass-radius relation (Ashman & Zepf 2001).

Fig. 9 shows the masses and radii of all clusters and associations listed in Tables 2–4. The sample is divided into two age bins: less than 10 Myr (left panel) and $10 - 100$ Myr (right panel). We tentatively overplot lines of constant density, which might indicate a trend with $\rho_{\rm hm} \approx 10^{3\pm1}\,{\rm M}_\odot$ for the younger cluster sample. This mass-radius correlation seems to contradict earlier findings, but it is important to bear in mind that we have limited ourselves

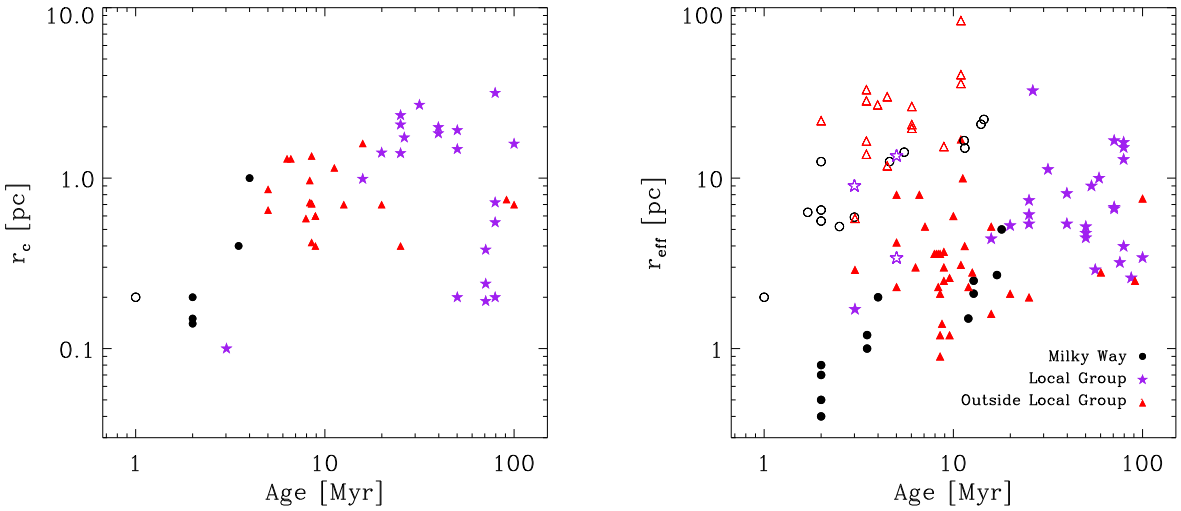

Figure 8: Core radius (r_c, left) and effective radius ($r_{\rm eff}$, right) as functions of age for the clusters in Tables 2, 3 & 4. The filled symbols are clusters and the open symbols are associations.

to a narrow range of (young) ages, and show the data for the clusters (age$> 3\,t_{\rm dyn}$) with different (and more distinct) symbols, whereas most literature studies do not separate the data in this way. The distinction between clusters and assocations is of course a density cut (Eq. 12), corresponding to $\rho_{\rm hm} \approx 10\,M_\odot\,{\rm pc}^{-3}$ at an age of 10 Myr, causing the upper envelope of cluster points (filled) to line up with the constant density lines. However, the lower envelope of points in the left panel seems more consistent with constant density than with constant radius. For the older clusters (right panel) the lower envelope seems quite consistent with constant radius. A correlation between mass and radius, or indeed the lack of one, would have important implications for the cluster's long-term survival, as we discuss in more detail in §4.

2.4 Global properties

The YMCs in the Magellanic Clouds and other nearby galaxies, such as M31 (Narbutis et al. 2008, Barmby et al. 2009, Ma et al. 2009, Vansevičius et al. 2009, Hodge et al. 2009, Caldwell et al. 2009, Peacock et al. 2010) and M33 (e.g. Chandar et al. 1999; Park, Park & Lee 2009; Sarajedini & Mancone 20(San Roman et al. 2009) provide opportunities for population studies. Observational studies of these systems suffer less from the problematic distance and extinction effects that challenge studies of Milky Way star clusters. They provide a more global view of cluster populations, and are better targets for studies of cluster age distributions (Elson & Fall 1985b, Hodge 1987, Girardi et al. 1995, de Grijs & Anders 2006, Parmentier & de Grijs 2008) and luminosity functions (Elson & Fall 1985a).

A comparison between Table 2 and Table 3 reveals the striking absence of Milky Way YMCs with ages between 10 and 100 Myr, whereas in the SMC and LMC, all YMCs except R 136 have ages spanning this range. This may well be an observational effect: Due

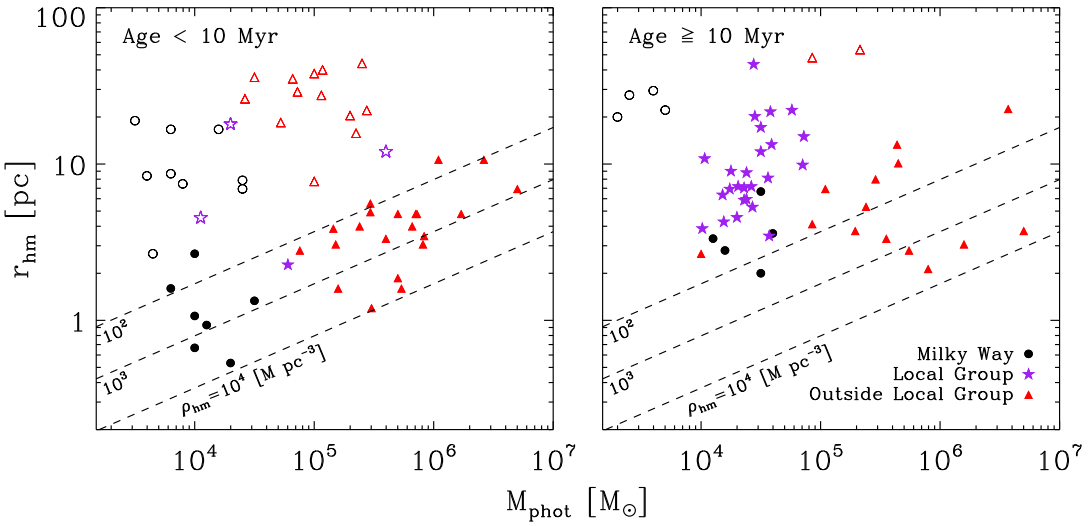

Figure 9: Mass-radius relation for all clusters (filled symbols) and associations (open symbols) from Tables 2, 3 & 4, using $r_{\rm hm} = (4/3)r_{\rm eff}$. Lines of constant half-mass density, $\rho_{\rm hm} \equiv 3M/(8\pi {r_{\rm hm}}^3)$, are overplotted. The values of the densities shown correspond to $0.07{\rm Myr} \lesssim t_{\rm dyn} \lesssim 0.7{\rm Myr}$ (Eq. 10). The clusters are subdivided into two groups: younger than 10 Myr (left) and older than 10 Myr (right).

to extinction and foreground and background stars in the Milky Way, it is hard to discover clusters without nebular emission and the luminous evolved stars found in very young systems. There might be a population of slightly older (10–100 Myr) YMCs in the Milky Way still awaiting discovery.

2.4.1 The cluster luminosity function

YMCs have been observed and identified well beyond the Local Group, providing exciting new opportunities for studies of star formation and population synthesis. They are found in abundance in galaxies with high star formation rates, such as merging and interacting galaxies (e.g. Holtzman et al. 1992, Miller et al. 1997, Whitmore et al. 1999). However, they are also found in quiescent spirals (e.g. Larsen & Richtler 2000; Larsen 2004; Cantiello, Brocato & Blakeslee 2009), and there are many similarities between the young cluster populations in these different environments. For example, the luminosity function (LF), defined as the number of clusters per unit luminosity ($\mathrm{d}N/\mathrm{d}L$) is well described by a power-law $\mathrm{d}N/\mathrm{d}L \sim L^{-\alpha}$ with ($\alpha \approx 2$) (e.g. Whitmore & Schweizer 1995, Miller et al. 1997, Larsen 2002, de Grijs et al. 2003), and tends to be slightly steeper at the bright end (Whitmore et al. 1999, Larsen 2002, Gieles et al. 2006a).

An appealing property of an $\alpha = 2$ power-law is the fact that the luminosity of the most luminous object, $L_{\rm max}$, increases linearly with the total number of clusters, $N_{\rm cl}$. Whitmore (2003) showed that the value of $L_{\rm max}$ for clusters in different galaxies scales as $L_{\rm max} \propto {N_{\rm cl}}^{\eta}$, with

$\eta \approx 0.75$ (see also Larsen 2002). The index η is a proxy for the shape of the bright end of the LF, since for a pure power-law $\eta = 1/(\alpha - 1)$ (Hunter et al. 2003). A value of $\eta = 0.75$ corresponds to $\alpha = 2.4$, supporting the finding that the bright end of the LF is steeper than L^{-2}, since the $L_{\rm max}$ method traces the brightest clusters.

If a universal correlation between $L_{\rm max}$ and $N_{\rm cl}$ exists, it means that $L_{\rm max}$ is the result of the size of the sample. It is therefore determined by statistics, and no special physical conditions are needed to form brighter clusters. A similar scaling between $L_{\rm max}$ and the star formation rate (SFR) was found by Weidner, Kroupa & Larsen (2004) and Bastian (2008). This has been interpreted in various ways. Bastian (2008) uses the similarity between the $L_{\rm max} - N_{\rm cl}$ and $L_{\rm max} -$ SFR relations to conclude that the cluster formation efficiency is roughly constant ($\sim 10\%$) over a large range of SFR. Weidner, Kroupa & Larsen (2004) interpret it as an increase of the most massive cluster mass, $M_{\rm max}$, with SFR and they conclude that $M_{\rm max}$ is set by the SFR of the host galaxy, much like the Weidner & Kroupa (2006) relation between the most massive star and the mass of the parent cluster. Larsen (2009a) showed that the $L_{\rm max}$ clusters have a large range of ages, with the brightest ones on average being younger than the fainter ones. This implies a dependence of M/L on $L_{\rm max}$, such that the mass of the most *massive* cluster ($M_{\rm max}$) increases more slowly with $N_{\rm cl}$ (and the SFR) than $L_{\rm max}$, and hence that $M_{\rm max}$ does not follow the size of sample prediction of the pure power-law LF.

2.4.2 The cluster initial mass function

It is tempting to interpret the LF as the underlying cluster mass function. As discussed above, it is not trivial to gain information about the mass function from the LF, since the LF consists of clusters with different ages, and clusters fade rapidly during their first ~ 1 Gyr due to stellar evolution. Determinations of cluster initial mass functions (CIMFs) are rare, since it is hard to acquire the cluster ages needed to select the youngest and to convert luminosity into mass. Several CIMF determinations have also found power-law functions with indices close to -2 (Zhang & Fall 1999, McCrady & Graham 2007, Bik et al. 2003), and other studies have found evidence for a truncation of this power-law at the high-mass end (Gieles et al. 2006b, Bastian 2008, Larsen 2009a, Vansevičius et al. 2009). The functional form of the initial mass function for young star clusters is well represented by a Schechter (1976) distribution

$$\phi(M) \equiv \frac{dN}{dM} = A\, M^{-\beta}\, \exp(-M/M_*). \tag{18}$$

Here $\beta \simeq 2$ and the Schechter mass M_* is equivalent to the more familiar L_* for the galaxy luminosity function. For Milky-Way type spiral galaxies $M_* \approx 2 \times 10^5\, {\rm M}_\odot$ (Gieles et al. 2006b, Larsen 2009a). For interacting galaxies and luminous infrared galaxies, Bastian (2008) obtains $M_* \gtrsim 10^6\, {\rm M}_\odot$.

The upper panel of Fig. 10 compares cluster mass functions for several galaxies with the Schechter function, Eq. 18. The lower panel compares the corresponding logarithmic slopes of the data with that of the Schechter function. Clearly the mass function of the Antennae clusters extends to higher masses, and this is not only due to the larger number of clusters, since the slope is also flatter at large masses. Thus the value of M_* seems to depend on the local galactic environment—it is possible to form more massive clusters in the Antennae galaxies than in more quiescent environments.

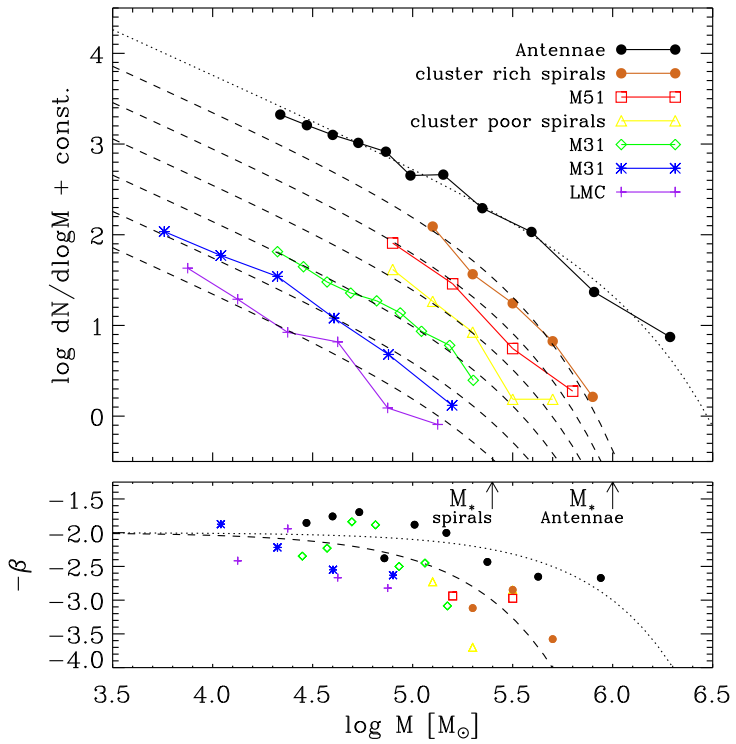

Figure 10: Top: Comparison of mass functions of clusters younger than $\sim 1\,\mathrm{Gyr}$ in different galaxies. The results are taken from Larsen (2009a) (LMC, cluster rich spirals and cluster poor spirals); Gieles (2009) (M51); Zhang & Fall (1999) (the Antennae galaxies) and Vansevičius et al. (2009) (two versions of the M31 cluster mass function). The cluster mass functions in spirals are compared to a Schechter function (Eq. 18) with $M_* = 2.5 \times 10^5\,\mathrm{M}_\odot$ (dashed curves); for the Antennae, $M_* = 10^6\,\mathrm{M}_\odot$ (dotted curve) is used. Bottom: the corresponding logarithmic slopes of the mass functions. The dotted and dashed curves are the logarithmic slopes of the functions shown in the top panel.

Indirect indications for a truncation of the cluster mass function also come from statistical arguments. If we temporarily ignore the (exponential) truncation, i.e. we adopt a power law with $\beta = 2$ without the exponential factor in Eq. 18, we can relate the cluster formation rate to the masses of the most massive clusters observed. For an overall star formation rate of $5000\,\mathrm{M_\odot\,Myr^{-1}\,kpc^{-2}}$ in the solar neighborhood (Miller & Scalo 1979), comparable to the average values found in external Milky-Way-type spirals (Kennicutt 1998), and assuming that $\sim 10\%$ of this mass ends up in bound star clusters, we find that the total mass formed in 10 Myr in clusters within 4 kpc of the Sun is $\sim 2 \times 10^5\,\mathrm{M_\odot}$. For our assumed power-law mass function, the most massive cluster contains $\sim 10\%$ of the total mass, so the mass of the most massive cluster is a few $\times 10^4\,\mathrm{M_\odot}$. Within a 4 kpc circle we find Westerlund 1, with a mass of $\sim 6 \times 10^4\,\mathrm{M_\odot}$ (see Tab. 2), in reasonable agreement with expectations.

Assuming the same star formation rate out to a distance of ~ 8 kpc from the sun, which is a conservative assumption since the star formation rate toward the Galactic center is probably higher than in the solar neighborhood, the expected most massive cluster becomes a factor of $8^2/4^2$ higher, or about $10^5\,\mathrm{M_\odot}$. Over a time span of 1 Gyr, clusters with masses of $\sim 10^7\,\mathrm{M_\odot}$ should have formed within that same distance, but if such a cluster existed it would most likely already have been discovered, unless it has been disrupted, which seems unlikely. This implies that for a quiescent environment like the Milky Way Galaxy, the truncation of the cluster mass function must occur at considerably lower mass than in a starburst environment. Similar arguments hold for external galaxies, where the entire disk can be seen, and it is found that the high-mass end of the cluster mass function falls off more steeply than a power-law with exponent -2 (see Fig. 10).

2.4.3 Cluster formation efficiency

The number of globular clusters in a galaxy is often expressed in terms of the specific frequency, the number of GCs per unit luminosity of the host. For young clusters, this is probably not a very meaningful quantity, since these clusters form with a power-law mass function (or Schechter function, as in Eq. 18), and the luminosity of the host galaxy depends strongly on the age of the field star population. For this reason, Larsen & Richtler (2000) introduce the *specific luminosity*, $T_L = 100\,L_{\mathrm{clusters}}/L_{\mathrm{galaxy}}$ for samples of cluster populations in different galaxies. They show that, in the U-band, T_L increases strongly with the star formation rate per unit area (Σ_{SFR}, see Fig. 11). This suggests that in galaxies with a higher Σ_{SFR} a larger fraction of the newly formed stars end up in star clusters. The light in this blue filter is dominated by (short-lived) hot stars, making T_L a tracer of current star and star cluster formation. A compelling aspect of Fig. 11 is that both axes are independent of distance. More recently, Bastian (2008) has used the L_{max}–SFR relation to derive a cluster formation efficiency of $\sim 8\%$. Both these estimates suffer from (unknown) extinction effects, and the best way to derive the cluster formation efficiency would be to compare the fraction of the mass that forms in clusters to Σ_{SFR} for a sample of galaxies.

The cluster formation efficiency is important for understanding the extent to which YMCs can be used as tracers of star formation. An interesting example is the lack of clusters with ages between 4 Gyr and 12 Gyr in the LMC (e.g. van den Bergh 1991). This "age gap" could be the result of cluster disruption processes, or due to a global pause in the SFR of the whole LMC. From comparison of the SFR history and the age–metallicity relation of LMC field

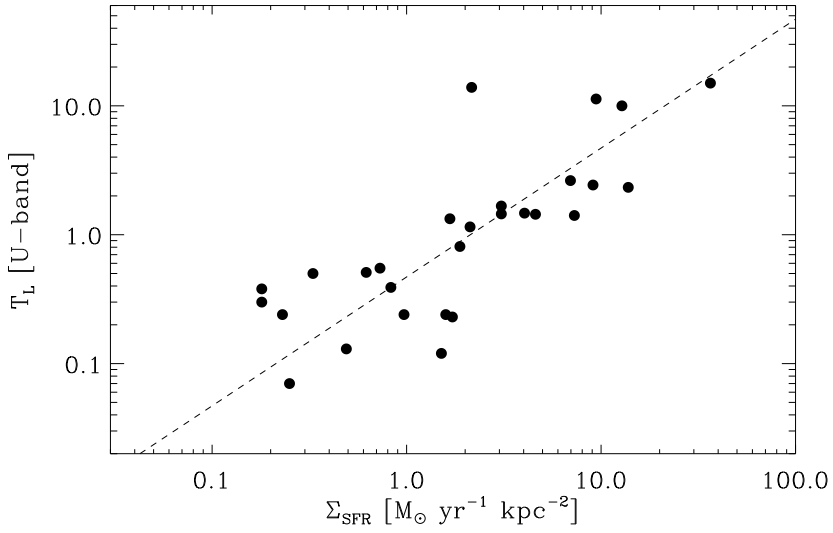

Figure 11: Specific U-band luminosity (T_L) for various cluster populations, as a function of $\Sigma_{\rm SFR}$ of the parent galaxy. The dashed line shows a linear relation ($T_L \propto \Sigma_{\rm SFR}$). Data from Larsen & Richtler (2000).

stars, the latter scenario seems preferred, i.e. the LMC had a low SFR between 4 and 12 Gyr ago, and this is reflected in both the field stars and the star clusters (Harris & Zaritsky 2009). This suggests that YMCs and their age distributions can be powerful tools in determining star formation histories in more distant galaxies where individual stars cannot be resolved. We return to the interpretation of the age distribution and its consequences for cluster lifetimes in §4.

3 Dynamical processes in star clusters

Studies of the evolution of a young star cluster split naturally into three phases: (1) the first few megayears, during which stars are still forming and the cluster contains significant amounts of ambient gas, (2) a subsequent period when the cluster is largely gas-free, but stellar mass loss plays an important role in the overall dynamics, and (3) a late stage, during which purely stellar dynamical processes dominate the long-term evolution of the cluster. An upper limit on the dividing line between phase 1 and phase 2 is the time of the first supernovae in the cluster, some 3 Myr after formation (Eggleton 2006), since these expel any remaining gas not already ejected by winds and radiation from OB stars. The dividing line between phase 2 and phase 3 may be anywhere between 100 Myr and 1 Gyr, depending on the initial mass, radius, and density profile of the cluster and the stellar mass function.

The evolution of the cluster during the first phase is a complex mix of gas dynamics, stellar dynamics, stellar evolution, and radiative transfer, and is currently incompletely understood (see Elmegreen 2007, Price & Bate 2009). Unfortunately this leaves uncertain many basic (and critical) cluster properties, such as the duration and efficiency of the star-formation process, and hence the cluster survival probability and the stellar mass function at the

beginning of phase 2 (see §4).

Together, phases 2 aqnd 3 span the "N-body simulation" stage familiar to many theorists. Phase 3 is the domain of traditional dynamical simulations; phase 2 is the "kitchen sink" phase, during which stellar interactions, stellar evolution, and large-scale stellar dynamics all contribute (see §4.1 and Appendix A). As discussed in more detail below, the processes driving the dynamical evolution during these phases are mostly well known and readily modeled, allowing significant inroads to be made into the task of interpreting cluster observations. However, since the outcome of phase 1 provides the initial conditions for phase 2, the proper starting configuration for these simulations remains largely a matter of conjecture. Theoretical studies generally consist of throughput experiments, mapping a set of assumed initial conditions into the subsequent observable state of the cluster at a later age.

Setting aside the many uncertainties surrounding the early (phase 1) evolution of the cluster, in this section we mainly describe the assumed state of the cluster at the start of phase 2 and the physical processes driving its subsequent evolution. For better or worse, N-body simulations generally assume quite idealized initial conditions (summarized in Tab. 5), with a spherically symmetric, gas-free cluster in virial equilibrium, with all stars already on the zero-age main-sequence.

3.1 Initial conditions

In the absence of a self-consistent understanding of cluster evolution during phase 1, assumptions must be made about the following key cluster properties before a phase 2 calculation can begin (Kroupa 2008). It must be noted that, in almost all cases, the choices are poorly constrained by observations.

Table 5: Commonly adopted initial conditions for particle-based simulations of YMCs.

cluster property	parameter	min	max
number of stars	N	10^3	10^6
mass function	single power law: $\phi(m) \propto m^{-2.35}$	$0.1\mathrm{M}_\odot$	$100\mathrm{M}_\odot$
equilibrium	$Q = -T/U$	0.5	
density distribution	Plummer, King		
tidal field	$r_\mathrm{t}/r_\mathrm{J}$	0.25	1
concentration	W_0	1	16
binary fraction	f_b	0	1
mass ratio	$\psi(q) = 1$	0	1
eccentricity	$\Xi(e) = 2e$	0	1
orbital period	$\Gamma(P) \propto 1/P$	RLOF	hard

- The *stellar mass function* $\phi(m) = dN/dm$ is typically taken to be a "standard" distribution derived from studies of the solar neighborhood (e.g. Salpeter 1955, Miller & Scalo 1979,

Kroupa 2001) although it has been suggested that the mass functions of some YMCs may be deficient in low-mass stars and/or "top-heavy" (Smith & Gallagher 2001), in the sense that the slope $d\log N/d\log m$ of the mass function at the high-mass end is shallower (i.e. less negative) than the standard Salpeter value of -2.35.

In addition to the mass function, in many cases minimum and maximum stellar masses are imposed. This is necessary for a pure power law, since the total mass would in general otherwise diverge, and is often desirable for other distributions, for which convergence is not an issue. Often the minimum mass $m_{\rm min}$ is chosen to be a relatively high, $m_{\rm min} \gtrsim 1{\rm M}_\odot$, to emulate a more massive cluster simply by ignoring the low-mass stars. This may suffice if one is interested in clusters younger than 100 Myr (phase 2), but for older clusters the lower-mass stellar population is important, e.g. to reproduce the proper relaxation time. The maximum mass $m_{\rm max}$ rarely poses a practical problem, although there may be some interesting correlations between the total cluster mass and the mass of the most massive star (Weidner & Kroupa 2004)

- *Mass Segregation.* Traditionally, dynamical simulations have begun without initial mass segregation—that is, the local stellar mass distribution is assumed not to vary systematically with location in the cluster. There is no good reason for this, other than simplicity. Evidence for initial mass segregation can be found in some young clusters (e.g. Hillenbrand & Hartmann 1998, Sabbi et al. 2008), simulations of star formation (e.g. Klessen 2001, Bonnell & Bate 2006), and dynamical evolution during phase 1 (McMillan, Vesperini & Portegies Zwart 2007; Allison et al. 2009). Several prescriptions have been used recently for initial mass segregation (Šubr, Kroupa & Baumgardt 2008; Baumgardt, De Marchi & Kroupa 2008; Vesperini, McMillan & Portegies Zwart 2009). They differ in detail, but lead to similar conclusions, namely that initial mass segregation may be critical to cluster survival (Vesperini, McMillan & Portegies Zwart 2009), since mass loss from centrally concentrated massive stars can be much more destructive than the same mass loss distributed throughout the body of the cluster (see §4).

- *Virial Ratio.* Simulations generally begin with a cluster in virial (dynamical) equilibrium, with virial ratio $Q \equiv -T/U = 1/2$. As with most of the other simplifying assumptions described here, the principal reason for this choice is reduction of the dimensionality of the initial parameter space, but there is no compelling physical reason for it. The gas expulsion that marks the end of phase 1 is expected to leave the cluster significantly out of equilibrium, and quite possibly unbound (e.g. Hills 1980). The time scale for a cluster to return to virial equilibrium may be comparable to the time scale on which mass loss due to stellar evolution subsequently modifies the cluster structure (see §4.2).

- *Spatial Density and Velocity Distributions.* The initial density profiles of young star clusters are poorly constrained. Several standard models are used to model the stellar distribution: Plummer (1911) and truncated Maxwellian (King 1966) models are the most common. Other distributions, such as isothermal and homogeneous spheres, are also used (e.g. Scally, Clarke & McCaughrean 2005). King models provide good fits to many observed GCs, although their relation to YMCs is unclear (see §2). In the absence

of strong observational constraints, the stellar velocity distribution is normally taken to be non-rotating and isotropic, with (for a Plummer model) the dispersion following the local potential with the assumed virial ratio (see §1.3.2).

- *Tidal Field.* Clusters do not exist in isolation, but rather are influenced by the local tidal field of their parent galaxy. In many cases (see §1.3.2), the field is modeled explicitly as an external potential or its quadrupole moment relative to the cluster center; however simple "stripping radius" prescriptions are also widely used. In practice, incorporating a simple stripping radius instead of a self-consistent tidal field reduces the cluster lifetime by about a factor of two if the stripping radius is taken as $r_{\rm J}$. This effect can be mitigated by adopting a larger cut-off radius (for example $2r_{\rm J}$). With few exceptions (e.g. Baumgardt & Makino 2003, Wilkinson et al. 2003) the parameters of the tidal field are held fixed in time, corresponding (for spherical or axisymmetric potentials) to an orbit at fixed galactocentric radius. For a given orbit and cluster mass, the initial ratio of the cluster limiting radius (e.g. the truncation radius of a King 1966, model, see §1.3.2) to the Jacobi radius of the cluster in the local tidal field is a free parameter, often taken to be of order unity. For a Plummer sphere, which extends to infinity, the tidal radius is often implemented as a simple cutoff at some relatively large distance.

- *Binary Fraction.* Binary stars are critical to cluster evolution during phase 2 and especially phase 3 (e.g. Hurley, Aarseth & Shara 2007; Portegies Zwart, McMillan & Makino 2007). It is not so clear how important they are during phase 1, when major structural changes are induced by mass loss and mass segregation (Clarke, Bonnell & Hillenbrand 2000; Bate, Bonnell & Bromm 2003). There are few, if any, observational constraints on the overall binary fraction in YMCs. Open clusters in the field typically have high binary fractions, approaching 100% in some cases (e.g. Sana et al. 2008; Mason et al. 2009; Bosch, Terlevich & Terlevich 2009). On the other hand, most recent studies of binaries in globular clusters suggest binary fractions of between $\sim$ 6% and $\sim$ 15% (Bellazzini et al. 2002, Sollima et al. 2007, Milone et al. 2008, Sommariva et al. 2009).

- *Binary Secondary Masses.* The mass of the secondary star in a binary is typically selected uniformly between some minimum mass and the mass of the primary (Duquennoy & Mayor 199 With this choice, a binary tends to be more massive than the average cluster star, resulting in additional mass segregation of the binary population. This effect can be removed if desired by randomly selecting primary stars and splitting them into primary and secondary components, in which case adding binaries does not affect the mass function of cluster members (single stars and binaries), but it does introduce a deviation from the initial stellar mass function among binary components (Kroupa 1995).

- *Orbital Elements of the Binaries.* In general, the choices made for binary orbital elements tend to be defensive, given the lack of observational guidance. Apart from the introduction of a whole new set of initial parameters, the presence of primordial binaries also introduces new mass, length, and time scales to the problem, greatly complicating direct comparison between runs having different initial conditions.

The initial distribution of binary periods is unknown, but is often assumed to follow the observed distribution in the solar neighborhood (Duquennoy & Mayor 1991), which is approximately a Gaussian in $\log P$ with mean $\log P = 4.8$ and dispersion $\sigma_{\log P} = 2.3$, with P in days. However, distributions flat in $\log P$ (Abt 1983) and $\log a$ (McMillan, Hut & Makino 1990) have also been adopted. Observations of YMCs are of little help, as there are at most a handful of binaries with measured orbital parameters in YMCs, and those have very short orbital periods and high-mass components. The eccentricity distribution is usually taken to be thermal (Duquennoy & Mayor 1991). Binary orbital orientation and initial phase are chosen randomly.

- *Higher order multiples.* Primordial multiple stars are rarely included in phase-2/3 dynamical simulations. There are a few examples of calculations with primordial triples (van den Berk, Portegies Zwart & McMillan 2007) or hierarchical planetary systems (Spurzem et al. 2009). The complications of adding primordial multiples greatly increase the already significant challenges of including binary dynamics and evolution.

3.2 Multiple stellar populations

The discovery of multiple populations of main-sequence stars and giants in an increasing number of globular clusters (Piotto et al. 2005, Piotto 2008) has led to the realization that star clusters are not idealized entities with single well defined stellar populations. In some clusters, the observed stellar populations appear to be separated by less than $\sim 10^8$ years, well within our age range for young clusters. The existence of multiple populations indicates that a second epoch of star formation must have taken place early in the cluster's lifetime (see §5.1.1). The differences in light-element abundances suggest that the second-generation (SG) stars formed out of gas containing matter processed through high-temperature CNO cycle reactions in first-generation (FG) stars.

The two main candidates currently suggested as possible sources of enriched gas for SG formation are rapidly rotating massive stars (Prantzos & Charbonnel 2006, Decressin et al. 2007) and massive (4–9 $M_\odot$) Asymptotic Giant Branch (AGB) stars (Ventura et al. 2001, Karakas & Lattanzio 20 In order to form the large fraction of SG stars suggested by observations (50% or more of the current mass of multiple-population clusters, Carretta et al. 2008), both scenarios require that either the IMF of the FG stars was highly anomalous, with an unusually large fraction of massive stars, or the FG population had a normal IMF but was initially at least ten times more massive than is now observed. Baumgardt & Kroupa (2007) have studied the subsequent evolution and mixing of the two-component cluster in the first scenario. D'Ercole et al. (2008) have presented simulations of the second, in which the SG stars form deep in the potential well of a FG cluster destabilized by early mass loss. Most of the FG cluster dissolves, leaving a mixed FG/SG system after a few gigayears.

If similar processes are operating today, multiple populations should be expected in at least some young star clusters, but it is currently not known whether, or to what extent, this phenomenon occurs in observed YMCs. For the unresolved extragalactic clusters, multiple populations will be hard to confirm, but for clusters in the local group this should be possible. At present, however, only one known cluster, Sandage 96, exhibits a young (10–16 Myr) population together with a relatively old (32–100 Myr) population (Vinkó et al. 2009) (see

also §5.3.1). Spreads in the main-sequence turn-off have been reported found for intermediate age clusters in the LMC, which has been interpreted as an age spread of $\sim 300\,\mathrm{Myr}$ (Mackey & Broby Nielsen 2007, Milone et al. 2009). If true, this has exciting implications for theories of the formation of star clusters and the general assumption that clusters are simple stellar populations. However, Bastian & de Mink (2009) find that the observed main sequence turn-off spread could be explained by stellar evolutionary effects induced by rotation. Obviously if multiple populations are common in YMCs, they significantly impact the assumptions made for simulations of phase 2 and the long-term cluster evolution during phase 3. Except where noted, we will not explicitly address the possibility of delayed SG star formation in this review.

3.3 Overview of cluster dynamical evolution

Most numerical studies start with initial conditions as described in §3.1. To the extent that stellar mass loss can be neglected, we can understand the dynamical evolution of a star cluster from the fundamental physics of self-gravitating systems, driven by relaxation.

3.3.1 Evaporation

The relaxation time (Eq. 16) is the time scale on which stars tend to establish a Maxwellian velocity distribution. A fraction ξ_e of the stars in the tail of that distribution have velocities larger than v_esc and consequently escape. Assuming that this high-velocity tail is refilled every t_rh, the dissolution time scale is $t_\mathrm{dis} = t_\mathrm{rh}/\xi_\mathrm{e}$. For isolated clusters, $v_\mathrm{esc} = 2\,\langle v^2\rangle^{1/2}$. For a Maxwellian velocity distribution, a fraction $\xi_\mathrm{e} = 0.0074$ has $v > 2\,\langle v^2\rangle^{1/2}$, and hence $t_\mathrm{dis} = 137\,t_\mathrm{rh}$. For tidally limited cluster ξ_e is higher since v_esc is lower. For a typical cluster density profile $\xi_\mathrm{e} \approx 0.033$, implying $t_\mathrm{dis} \approx 30\,t_\mathrm{rh}$ (Spitzer 1987).

The escape fraction ξ_e is often taken to be constant (e.g. Gnedin & Ostriker 1997), althouh it depends on r_hm (through $\langle v^2\rangle^{1/2}$) and also on the strength of the tidal field, or r_J (through v_esc). Effectively, ξ_e depends on the ratio $r_\mathrm{hm}/r_\mathrm{J}$ (e.g. Spitzer & Chevalier 1973, Wielen 1988). Gieles & Baumgardt (2008) show that $\xi_\mathrm{e} \propto (r_\mathrm{hm}/r_\mathrm{J})^{3/2}$ for $r_\mathrm{hm}/r_\mathrm{J} \gtrsim 0.05$ (the so-called *tidal regime*). From Eq. 16 we then find, for clusters on circular orbits in the tidal regime, that $t_\mathrm{dis} \propto N/\omega$ (neglecting the slowly varying Coulomb logarithm). For a flat rotation curve, $t_\mathrm{dis} \propto R_G$ for a cluster of given mass (e.g. Chernoff & Weinberg 1990, Vesperini & Heggie 1997). This linear dependence of t_dis on R_G makes it difficult to explain the universality of the globular cluster mass function via dynamical evolution of a power-law initial cluster mass function (Vesperini et al. 2003), but this will not be discussed further here.

Baumgardt (2001) showed that t_dyn also enters into the escape rate and found, for equal-mass stars, $t_\mathrm{dis} \propto {t_\mathrm{rh}}^{3/4} {t_\mathrm{dyn}}^{1/4}$. The non-linear scaling of the dissolution time with the relaxation time results from the fact that a star with sufficient energy to escape may orbit the system many times before "finding" one of the Lagrangian points, through which escape actually occurs (Fukushige & Heggie 2000). Baumgardt & Makino (2003) found that this scaling also holds for models of clusters with a stellar mass spectrum, stellar evolution, and for different types of orbits in a logarithmic potential. Their result for t_dis can be summarized

as

$$t_{\rm dis} \approx 2\,{\rm Myr} \left(\frac{N}{\ln\Lambda}\right)^{3/4} \left(\frac{R_G}{\rm kpc}\right) \left(\frac{V_G}{220\,{\rm km\ s^{-1}}}\right)^{-1} (1-\varepsilon), \tag{19}$$

where ε is the eccentricity of the orbit. For an eccentric orbit, $\varepsilon > 0$ the distance to the galactic enter R_G is taken as the apogalcticon, whereas V_G is circular velocity, which is constant in a logarithmic potential. If the Coulomb logarithm is taken into account, the scaling is approximately $t_{\rm dis} \propto N^{0.65}$ in the range of about 10^3 to $10^6\,{\rm M}_\odot$ (Lamers, Gieles & Portegies Zwart 2005).

3.3.2 Core collapse

Self-gravitating systems are inherently unstable, and no final equilibrium state exists for a star cluster. The evaporation of high-velocity stars and the internal effects of two-body relaxation, which transfers energy from the inner to the outer regions of the cluster, result in core collapse (Antonov 1962, Lynden-Bell & Wood 1968, Cohn 1980, Lynden-Bell & Eggleton 1980, Makino 1996). During this phase, the central portions of the cluster accelerate toward infinite density while the outer regions expand. The process is readily understood by recognizing that, according to the virial theorem, a self-gravitating system has negative specific heat—reducing its energy causes it to heat up. Hence, as relaxation transports energy from the (dynamically) warmer central core to the cooler outer regions, the core contracts and heats up as it loses energy. The time scale for the process to go to completion (i.e. a core of zero size and formally infinite density) is $t_{\rm cc} \sim 15 t_{\rm rh}$ for an initial Plummer sphere of identical masses. Starting with a more concentrated King (1966) distribution shortens the time of core collapse considerably (Quinlan 1996), as does a broad spectrum of masses (Inagaki & Saslaw 1985).

In systems with a mass spectrum, two-body interactions accelerate the dynamical evolution by driving the system toward energy equipartition, in which the velocity dispersions of stars of different masses would have $\langle mv^2\rangle \sim$ constant. The result is mass segregation, where more massive stars slow down and sink toward the center of the cluster on a time scale (Spitzer 1969)

$$t_{\rm s} \sim \frac{\langle m\rangle}{m}\, t_{\rm rl}\,. \tag{20}$$

Portegies Zwart & McMillan (2002) and Gürkan, Freitag & Rasio (2004) find that, for a typical Kroupa (2001) mass function, the time scale for the most massive stars to reach the center and form a well defined high-density core is $\sim 0.2 t_{\rm rl}$, where $t_{\rm rl}$ is the relaxation time (see Eq. 13) of the region of interest containing a significant number of massive stars—the core of a massive cluster, or the half-mass radius of a smaller one (in which case $t_{\rm rl} = t_{\rm rh}$, see Eq. 16). For dense clusters, $t_{\rm s}$ may be shorter than the time scale for stellar evolution, or for the first supernovae to occur (Portegies Zwart et al. 1999).

Thus, a collisional stellar system inevitably evolves toward a state in which the most massive objects become concentrated in the high-density central core (see §3.4.2). Dynamical evolution provides a natural and effective mechanism for concentrating astrophysically interesting objects in regions of high stellar density.

3.4 Internal Heating

On longer time scales, the evolution of clusters that survive the early phases of mass loss is driven by the competition between relaxation and a variety of internal heating mechanisms. High central densities lead to interactions among stars and binaries. Many of these interactions can act as energy sources to the cluster on larger scales, satisfying the relaxation-driven demands of the halo and temporarily stabilizing the core against collapse (Goodman & Hut 1989; Gao et al. 1991; McMillan, Hut & Makino 1990, 1991; Heggie & Aarseth 1992; Fregeau et al. 2003). On long time scales, these processes lead to a slow (relaxation time) overall expansion of the cluster, with $r_{\rm vir} \propto t^{2/3}$, a result that follows from simple considerations of the energy flux through the half-mass radius (Hénon 1965).

While these processes are important to the long-term dynamical evolution (phase 3), their relevance is somewhat different during the first 100 Myr (Portegies Zwart, McMillan & Makino 2007), which is largely dominated by stellar mass loss (phase 2) and the segregation of the most massive stars. Often, their major effect is to enhance the rate of collisions and the formation of stellar exotica. We now consider in turn the following processes: binary heating (§3.4.1), stellar collisions (§3.4.2), and black-hole heating (§3.4.3).

3.4.1 Binary Interactions

Irrespective of the way they form, binaries are often described by dynamicists as either "hard" or "soft." A hard binary has binding energy greater than the mean stellar kinetic energy in the cluster (Heggie 1975): $|E_b| > \frac{1}{2}\langle mv^2\rangle \approx \frac{1}{2}\langle m\rangle\langle v^2\rangle$, where $\langle m\rangle$ and $\langle v^2\rangle^{1/2}$ are the local mean stellar mass and velocity dispersion. A binary with mass $m_b = m_1 + m_2$ and semi-major axis a_b has energy $E_b = -Gm_1m_2/2a_b$, so hard binaries have $a_b < a_{\rm hard}$, where

$$a_{\rm hard} \;=\; \frac{Gm_b^2}{4\langle m\rangle\langle v^2\rangle} \;\approx\; 9.5\times10^4\,{\rm R}_\odot \left(\frac{m_b}{{\rm M}_\odot}\right)^2 \left(\frac{\langle v^2\rangle^{1/2}}{\rm km\ s^{-1}}\right)^{-2}. \qquad (21)$$

Here we implicitely assumed that $m_1 = m_2 = \langle m\rangle$ to derive the right-hand expression. The hard–soft distinction is helpful when discussing dynamical interactions between binaries and other cluster members. However, we note the definition of hardness depends on local cluster properties, so the nomenclature changes with environment, and even within the same cluster a binary that is hard in the halo could be soft in the core.

The dynamical significance of "hard" binaries (see Eq. 21) has been understood since the 1970s (Heggie 1975, Hills 1975, Hut & Bahcall 1983) When a hard binary interacts with another cluster star, the resultant binary (which may or may not have the same components as the original binary) tends, on average, to be harder than the original binary, making binary interactions a net heat source to the cluster. Soft binaries tend to be destroyed by encounters. For equal-mass systems, the mean energy liberated in a hard-binary encounter is proportional to E_b: $\langle\Delta E_b\rangle = \gamma E_b$, where $\gamma = 0.4$ for "resonant" interactions (Heggie 1975), and $\gamma \sim 0.2$ when wider "flybys" are taken into account (Spitzer 1987).

The liberated energy goes into the recoil of the binary and single star after the interaction. Adopting terminology commonly used in this field, we write the binary energy as $E_b = -hkT$, where $\frac{3}{2}kT = \langle\frac{1}{2}mv^2\rangle$ and $h \gg 1$, so the total recoil energy, in the center of mass frame of the interaction, is γhkT. In the center of mass frame, a fraction $\frac{m_b}{m_b+m}$ of this energy goes to

the single star (of mass m) and $\frac{m}{m_b+m}$ to the binary. For equal-mass stars, these reduce to $\frac{2}{3}$ for the single star and $\frac{1}{3}$ for the binary. Neglecting the thermal motion of the center of mass frame, we identify three regimes:

1. If $\frac{2}{3}\gamma hkT < \frac{1}{2}m{v_{\rm esc}}^2 = 2m\langle v^2\rangle = 6kT$, i.e. $h < 45$, neither the binary nor the single star acquires enough energy to escape the cluster. Binaries in this stage are kicked out of the core, then sink back by dynamical friction, in a process that we call "binary convection."

2. If $\frac{2}{3}\gamma hkT > 6kT$ but $\frac{1}{3}\gamma hkT < 4m\langle v^2\rangle = 12kT$, i.e. $45 < h < 180$, the single star escapes, but the binary is retained. We refer to such a binary as a "bully."

3. If $h > 36/\gamma = 180$, both the binary and the single star are ejected. Such a binary is a "self-ejecter."

These numbers are only illustrative. For a binary with components more massive than average, as is often the case, the threshold for bullying behavior drops, while that for self-ejection increases.

Tab. 6 places these considerations in a more physical context. Note that, since the closest approach between particles in a resonant interaction may be as little as a few percent of the binary semi-major axis (Hut & Inagaki 1985), the hardest binaries may well experience physical stellar collisions rather than hardening to the point of ejection; and a collision tends to soften the surviving binary. Alternatively, before their next interaction, they may enter the regime in which internal processes, such as tidal circularization and/or Roche-lobe overflow, become important. The future of such a binary may be determined by the internal evolution of its component stars, rather than by further encounters.

Table 6: Terminology (first column) and characterization (second and third columns) for the various stages of a binary (see text). The subsequent columns give the orbital separation a of a binary (in units of AU) with a total mass $m_1 + m_2 \equiv m_b = 10\langle m\rangle$ or $m_b = 100\langle m\rangle$, in a cluster with a mass of $M = 10^5\,{\rm M}_\odot$ and virial radius $r_{\rm vir} = 1\,{\rm pc}$ and $r_{\rm vir} = 10\,{\rm pc}$.

Binary	relation	E_b	$M = 10^5\,{\rm M}_\odot$				Unit
		[kT]	$r_{\rm vir} = 1$pc		$r_{\rm vir} = 10$pc		
			$m_b = 10$	$m_b = 100$	$m_b = 10$	$m_b = 100$	$\langle m\rangle$
hard	$E_{\rm b} > \frac{3}{2}kT$	1	7.2×10^4	7.2×10^6	7.2×10^5	7.2×10^7	AU
bully	$v_{\rm rec} > v_{\rm esc}m/m_b$	10	1.7×10^3	1.7×10^6	1.7×10^4	1.7×10^7	AU
tenured	$t_{\rm enc} > t_{\rm rh}$	100	52	58	53	5.8	AU
self-eject	$v_{\rm rec} > v_{\rm esc}m_b/m$	100	0.016	1.6	33	3.3×10^3	AU

The binary encounter time scale is $t_{\rm enc} = (n\sigma\langle v^2\rangle^{1/2})^{-1}$, where n is the local stellar density and σ is the encounter cross section (see Eq. 24). If we arbitrarily compute the binary interaction cross section as that for a flyby within 3 binary semi-major axes, consistent with the encounters contributing to the Spitzer (1987) value $\gamma = 0.2$, and again assume equal masses ($m_b = 2m$), we find

$$t_{\rm enc} \sim 8ht_{\rm rl}, \tag{22}$$

where we have used Eq. 13 and taken $\ln \Lambda = 10$. Thus the net local heating rate per binary during the 100% efficient phase (#1 above), when the recoil energy remains in the cluster due to "binary convection" is

$$\mathcal{E}_{bin} = \gamma h k T \, {t_{\rm enc}}^{-1} \sim 0.1 kT/t_{\rm rl}, \tag{23}$$

that is, *on average*, each binary heats the cluster at a roughly constant rate. During the "bully" phase, the heating rate drops to just over one-third of this value. The limiting value of one-third is not reached since the ejected single stars still heat the cluster indirectly by reducing its binding energy by a few kT. For "self-ejecting" binaries, the heating rate drops almost to zero, with only indirect heating contributing.

Binary–binary interactions also heat the cluster, although the extra degrees of freedom complicate somewhat the above discussion. If the binaries differ widely in semi-major axes, the interaction can be handled in the three-body approximation, with the harder binary considered a point mass. If the semi-major axes are more comparable, as a rule of thumb the harder binary tends to disrupt the wider one (Bacon, Sigurdsson & Davies 1996).

Numerical experiments over the past three decades have unambiguously shown how initial binaries segregate to the cluster core, interact, and support the core against further collapse (McMillan, Hut & Makino 1990; Heggie & Aarseth 1992). The respite is only temporary, however. Sufficiently hard binaries are ejected from the cluster by the recoil from their last interaction (self-ejection, see Tab. 6), and binaries may be destroyed, either by interactions with harder binaries, or when two or more stars collide during the interaction. For large initial binary fractions, this binary-supported phase may exceed the age of the universe or the lifetime of the cluster against tidal dissolution. However, for low initial binary fractions, as appears to have been the case for the GCs observed today (Milone et al. 2008), the binaries can be depleted before the cluster dissolves, and core collapse resumes (Fregeau et al. 2003).

Thus binary dynamics drives the evolution of the cluster while, simultaneously, the combination of cluster dynamics and internal stellar processes determine the internal evolution of each binary. This interplay between stellar evolution and stellar dynamics is sometimes referred to as *star-cluster ecology* (Heggie 1992) or the *binary zoo* (Davies et al. 2006) or *stellar promiscuouity* (Hurley & Shara 2002).

3.4.2 Stellar Collisions

In systems without significant binary fractions—either initially or following the depletion of core binaries—core collapse may continue to densities at which actual stellar collisions occur. In young clusters, the density increase may be enhanced by rapid segregation of the most massive stars in the system to the cluster core. Since the escape velocity from the stellar surface greatly exceeds the rms speed of cluster stars ($\theta < 100$ in Eq. 1), collisions lead to mergers of the stars involved, with only small fractional mass loss (Benz & Hills 1987, Freitag & Benz 2001). If the merger products did not evolve, the effect of collisions would be to dissipate kinetic energy, and hence cool the system, accelerating core collapse (Portegies Zwart et al. 199 However, when accelerated stellar evolution is taken into account, the (time averaged) enhanced mass loss can result in a net heating effect (Chatterjee, Fregeau & Rasio 2008).

The cross section for an encounter between two objects of masses m_1 and m_2 and radii

r_1 and r_2, respectively, is

$$\sigma = \pi r^2 \left[1 + \frac{2G(m_1 + m_2)}{rv^2}\right] \tag{24}$$

(Hills & Day 1976), where v is the relative velocity at infinity and $r = r_1 + r_2$. For $r \ll G(m_1 + m_2)/v^2$, as is usually the case for the systems discussed in this review, the encounter is dominated by the second term (gravitational focusing), and Eq. 24 reduces to

$$\sigma \approx 2\pi r \frac{Gm}{v^2}, \tag{25}$$

which is nearly independent of the properties of the other stars.

Collisions between single stars are unlikely unless one (or both) of the stars is very large and/or very massive, or the local density is very high. Consider a large, massive star of mass m and radius r moving through a field of smaller stars, so the collision cross section is dominated by the properties of the massive star. The rate of increase of the star's mass due to collisions is

$$\begin{aligned} \frac{dM}{dt} &\approx \rho_c \sigma v \approx 2\pi G m r \rho_c / v \\ &= 0.6 \left(\frac{m}{100 \mathrm{M}_\odot}\right) \left(\frac{r}{100 \mathrm{R}_\odot}\right) \left(\frac{\rho_c}{10^6 \mathrm{M}_\odot/\mathrm{pc}^3}\right) \left(\frac{10 \mathrm{km\ s}^{-1}}{v}\right) \quad M_\odot/\mathrm{Myr}\,. \end{aligned} \tag{26}$$

Thus a massive star ($m/\mathrm{M}_\odot \sim r/\mathrm{R}_\odot \sim 1$) in a dense stellar core ($\rho_c \sim 10^6\,\mathrm{M}_\odot/\mathrm{pc}^3$) will experience numerous collisions during its $\sim 3 - 5$ Myr lifetime.

The presence of primoridal binaries can significantly increase the chance of a traffic accident. Hard binaries (see §3.4.1) are in the gravitational focusing regime, so the binary interaction cross section may be obtained by setting $r = a$ in Eq. 25. Such an encounter will likely lead to the hardening of the binary and possibly the ejection of the single star and also the binary, as just discussed. However, it may also lead to a hydrodynamical encounter, i.e. a physical collision between two of the stars. It is quite likely that the third star will also be engulfed in the collision product (Fregeau et al. 2004). Since binaries generally have semi-major axes much greater than the radii of the component stars, such *binary-mediated collisions* play important roles in determining the stellar collision rate in YMCs (Portegies Zwart & McMillan 2002), leading to significant numbers of mergers in lower-density, binary rich environments. Massive binaries in young dense clusters tend to be collision targets rather than heat sources (Gürkan, Freitag & Rasio 2004).

In a sufficiently dense system, repeated stellar collisions can lead to a so-called "collision runaway" (Portegies Zwart et al. 1999), in which a massive star or collision product suffers repeated mergers and grows enormously in mass before exploding as a supernova (Portegies Zwart & McMillan 2002; Portegies Zwart et al. 2004; Gürkan, Freitag & Rasio 2004). This has frequently been cited as a possible mechanism for producing intermediate-mass black holes (IMBHs) in star clusters. However, while the dynamics is simple, numerous uncertainties in the stellar evolution and mass loss of the resultant merger product have been pointed out in the recent literature, suggesting that the net growth rate, and hence the final mass of the resulting IMBH, may be much lower than suggested by purely dynamical simulations—perhaps as little as a few hundred solar masses (Yungelson et al. 2008,

Glebbeek et al. 2009, Vanbeveren et al. 2009). Alternative formation mechanisms for more massive IMBHs involve gas accretion onto a seed $\sim 100\,\mathrm{M}_\odot$ black hole during a second round of star formation early in the cluster's lifetime (Vesperini et al. 2009), or repeated collisions between stellar-mass black holes during the phase-3 evolution of the cluster (Miller & Hamilton 2002).

3.4.3 Black Hole Heating

An IMBH in a star cluster can be an efficient source of energy to the stellar system. Stars diffuse by two-body relaxation deeper and deeper into the IMBH's potential well, and eventually are tidally disrupted and consumed (Bahcall & Wolf 1976). The energy lost during the process heats the system. The heating rate for an IMBH of mass M_{BH} in a cluster core of density ρ_c and velocity dispersion v_c is

$$\mathcal{E}_{bh} \sim \frac{G^5\langle m\rangle\rho_c^2 M_{BH}^3 \ln\Lambda}{v_c^7}. \tag{27}$$

Although cores are promising environments for the formation of IMBHs, they may not be the best place to look for evidence of massive black holes today. Dynamical heating by even a modest IMBH is likely to lead to a cluster containing a fairly extended core (Baumgardt, Makino & Hut 2005). Comparing the outward energy flux from stars relaxing inward in the (Bahcall–Wolf) cusp surrounding the IMBH to the outward flux implied by two-body relaxation at the cluster half-mass radius, Heggie et al. (2007) estimate the equilibrium ratio of the half-mass ($r_{\rm hm}$) to the core ($r_{\rm c}$) radius in a cluster of mass M. Calibrating to simulations, they conclude that for systems with equal mass, except of course the black holes

$$\frac{r_{\rm hm}}{r_{\rm c}} \;\sim\; 0.23\left(\frac{M}{M_{BH}}\right)^{3/4}. \tag{28}$$

Trenti et al. (2007) has suggested that the imprint of this process can be seen in his "isolated and relaxed" sample of simulated open clusters having relaxation times less than 1 Gyr, a half-mass to tidal radius ratio $r_{\rm hm}/r_{\rm t} < 0.1$, and an orbital ellipticity of less than 0.1. Roughly half of the clusters in this sample have core radii substantially larger than would be expected on the basis of simple stellar dynamics and binary heating. However, Hurley (2007) has argued that such anomalously large core to half-mass ratios may also be explained by the presence of a stellar-mass BH binaries heating the cores of these clusters (see also Merritt et al. 2004, Mackey et al. 2007, 2008). Many of the results discussed above and much of our physical understanding of the dynamical evolution of star clusters have been developed and calibrated by means of simulations.

4 The survival of star clusters

The realization that the majority of star formation occurs in embedded clusters, whereas only a small fraction of stars in the Galactic disk currently reside in clusters (see §1), indicates that most clusters and associations are relatively short lived; they dissolve on time scales comparable to the median age of open clusters in the solar neighborhood (Kharchenko et al. 2005), which is about 250 Myr (see §1.2).

Historically, studies of the lifetimes of star clusters have focused on open clusters in the Milky Way. The scarcity of open clusters with ages $\gtrsim 1$ Gyr was reported independently in several studies (von Hoerner 1958; van den Bergh 1957; Oort, Kerr & Westerhout 1958), and has been attributed to their short median lifetimes (about 250 Myr; Wielen 1971), rather than, say, a variation in the formation history or a detection bias toward young objects. These short cluster lifetimes have been explained as due to the destructive effects of encounters with giant molecular clouds (GMCs) (Spitzer 1958). A typical Galactic cluster with a density of $\sim 1\,M_\odot\,\mathrm{pc}^{-3}$ can survive the heating due to passing GMCs for about 250 Myr. The remarkable agreement between the inferred mean lifetime and the expected survival time in the Galactic disk implicated GMCs as responsible for the destruction of open clusters (see §4.4). The argument is further supported by the radial offset of the old (few Gyrs) open clusters toward the anticenter of the Galactic disk and away from the plane of the disk, where the density of GMCs is low (van den Bergh & McClure 1980), as is illustrated in Fig. 1. The galactic bulge and spiral structure also contribute, though in lesser extend, to the destruction of open clusters (Weinberg 1994, Gieles, Athanassoula & Portegies Zwart 2007).

By comparing the age distributions of clusters in the Magellanic clouds with those in the Milky Way Galaxy, the former population is found to be on average older and also more massive than the local population (Elson & Fall 1985b, Hodge 1987). The higher average cluster mass in the sample of Magellanic cloud clusters is a consequence of the difficulty in detecting low mass clusters. The apparent longer lifetimes of the Magellanic clusters could imply that more massive clusters tend to live longer, although the longer lifetimes could also be explained by the lower density of GMCs, the absence of bulges and spiral structures and the overall weaker tidal fields in the Magellanic clouds. However, in §4.4.2 we argue that GMCs are unlikely to play an important role in the early evolution of a YMC, due to their high initial density. The mechanism leading to the destruction of star clusters is therefore of major importance for understanding the evolution of star clusters from youth to old age.

4.1 Simulating star clusters

The formation, evolution and death of star clusters is a complex problem combining stellar dynamics, gas dynamics, stellar evolution and the evolution of the potential of the parent galaxy, all of which contribute to the cluster's appearance over the entire lifetime of the cluster (see also §3). Over the past decade, significant progress has been made in modeling many of these processes simultaneously in numerical simulations of clusters during phase 2 and phase 3. A striking omission is the self-consistent treatment of the interaction between stars and gas during phase 1. We focus here on simulations of phase-2 and phase-3 clusters, first describing treatments of stellar dynamics (see below), then turning to the inclusion of other physical processes into the mix.

A broad spectrum of numerical methodologies is available for simulating the dynamical evolution of young star clusters. In approximate order of increasing algorithmic and physical complexity, but not necessarily in increasing numerical complexity, the various methods may be summarized as follows.

- *Static Models* are self-consistent potential–density pairs for specific choices of phase-space distribution functions (Plummer 1911, King 1966, Binney & Tremaine 2008).

They have been instrumental in furthering our understanding of cluster structure, and provide a framework for semi-analytical treatments of cluster dynamics. However, they do not lend themselves to detailed study of star cluster evolution, and we will not discuss them further here, instead referring the reader to the discussion in §1.3.2, or to (Spitzer 1987).

- *"Continuum" Models* treat the cluster as a quasi-static continuous fluid whose phase-space distribution function evolves under the influence of two-body relaxation and other energy sources (such as binary heating) that operate on relaxation time scales (see Eq. 14).
- *Monte Carlo Models* treat some or all components of the cluster as pseudo-particles whose statistical properties represent the continuum properties of the system, and whose randomly chosen interactions model relaxation and other processes driving the long-term evolution.
- *Direct N-body Models* follow the individual orbits of all stars in the system, automatically including dynamical and relaxation processes, and modeling other physical processes on a star-by-star basis.

Much of our current understanding of the evolution of star clusters comes from detailed numerical simulations, and the above techniques are used for the vast majority if simulations. In order to appreciate some of the details presented in §4.2 to §4.4.2 it may be important to have some rudimentary understanding of this range of techniques. However, since this is a rather technical discussion, we present it in an appendix (§A).

4.2 Early violent gas expulsion

Possibly the greatest discrepancy between star cluster simulations and observations lies in the first few million years of the evolution (phase 1 in §3). Real star clusters are formed in a complicated interaction between gas and gravity, which is imperfectly understood. Once a primordial gas cloud starts to condense into stars dynamical evolution also begins (Bate, Bonnell & Bromm 2003). At the end of the star formation process, probably brought about by the developing winds of the most massive stars or the first supernovae, the residual gas is ejected from the protostellar cluster. The gas expulsion phase is expected to be short—on the order of several dynamical times (Eq. 12)—and places the remaining stellar population in a super-virial state, making the young cluster vulnerable to dissolution. The sharp decrease in the number of young and embedded star clusters at an age of a few megayears is thought to be a consequence of this early process, and is often referred to as "infant mortality" (Lada & Lada 2003).

4.2.1 Theoretical considerations

The total mass $M = M_{\rm g} + M_*$ of the primordial cluster contains contributions from stars M_* and gas $M_{\rm g}$. In virial equilibrium, the rms velocity of the cluster is

$$\langle v^2 \rangle = \frac{GM}{2r_{\rm vir}}. \tag{29}$$

which in observable quantities becomes

$$\sigma_{\rm 1D}{}^2 = \frac{GM}{\eta r_{\rm eff}}, \tag{30}$$

with $\eta \approx 10$ (see §1.3.2).

The response of the cluster to the loss of the residual gas depends on the gas expulsion time scale $t_{\rm exp}$ relative to the dynamical time scale $t_{\rm dyn}$ of the cluster (see Eq. 10). For many young clusters $t_{\rm exp} \ll t_{\rm dyn}$, in which case removing the gas shocks the cluster. In the extreme case, the positions and velocities of the stars remains fixed during the gas expulsion phase, and the response of the cluster to losing a fraction of gas, $f_e \equiv M_*/M$, can be calculated under the assumption that the mass loss is instantaneous. The rms velocity of the stars immediately before and after gas loss is then given by Eq. 29; the stellar positions are also unchanged. As a consequence, the cluster expands and re-establishes equilibrium at a new virial radius given by (Hills 1980)

$$\frac{r_{\rm vir}}{r_{\rm vir}(t=0)} = \frac{f_e}{2f_e - 1}. \tag{31}$$

For high star formation efficiency ($f_e \gtrsim 0.5$) the arguments leading to Eq. 31 may be reasonable, as in this case a relatively small fraction of the stars is lost after the gas is expelled. However, the energy argument is too simple to determine the survival probability if $f_e \lesssim 0.5$. Losing more than half of the total mass ($f_e \leq 0.5$) by explosive gas expulsion is devastating for the cluster, leading to its complete dissolution in a few dynamical time scales. A low star formation efficiency may explain the majority of disrupted young and embedded clusters, but even for $f_e \lesssim 0.5$ some small portion of the cluster can in practice remain bound. There are several independent arguments for the survival of embedded clusters even for a star formation efficiency as low as $f_e \lesssim 0.1$.

The most important argument against the above simple analysis (Eq. 31) is the fact that the time scale for gas expulsion, $t_{\rm exp}$, in practice is short but not instantaneous. This time scale should not be compared to the (global) half-mass crossing time, but rather to the local dynamical time, which depends strongly on the distance to the cluster center. For example, the dynamical time scale in the cluster core has $t_{\rm core}/t_{\rm dyn} = (\rho_{\rm hm}/\rho_{\rm c})^{1/2}$ and this fraction ranges from $\lesssim 0.01$ for a concentrated cluster ($W_0 \gtrsim 12$, or $c > 2.7$) to ~ 0.2 for a shallow potential ($c < 1$ or $W_0 \lesssim 5$). For concentrated clusters ($c \gtrsim 2$), the gas expulsion occurs more or less instantaneously for stars in the outskirts, but stars in the core respond adiabatically to the loss of gas. If $t_{\rm exp} > t_{\rm dyn}$, the cluster is likely to survive; in particular, the core may respond with just a slight expansion (of at most a factor of 2), even in extreme cases, $f_e \lesssim 0.1$ (Geyer & Burkert 2001).

Further complications arise from the clumping of the gas and stellar distributions in the embedded cluster (Fellhauer, Wilkinson & Kroupa 2009). It is likely that the radial dependence of the star formation process causes the central part of the cluster to be depleted in gas, whereas the outskirts are relatively gas rich (Bonnell, Bate & Vine 2003). This radial variation of the star formation efficiency, combined with the process of competitive star formation (Bonnell, Bate & Vine 2003), may actually render the cluster subvirial after the gas is ejected, for example if stars formed in the collapsing cloud are dy-

namically cold (Lada, Margulis & Dearborn 1984), as suggested by the outcome of turbulent self-gravitating simulations of cluster formation (Offner, Hansen & Krumholz 2009). In that case, Eq. 31 depends on the fractional deviation from virial equilibrium $q_{\rm vir}$, to become $r_{\rm vir}/r_{\rm vir}(t=0) = f_e/(2f_e - q_{\rm vir}^2)$, i.e. the condition for complete disruption becomes $f_e = q_{\rm vir}^2/2$ (Proszkow et al. 2009, Goodwin 2009). The cluster survival probability then depends on the entire star formation process, not just on its overall efficiency (Goodwin & Bastian 2006). A further deviation from the simple formulation comes from the effect of high-velocity escapers, which can carry away a considerable fraction of the cluster's binding energy, leaving the remaining stars more strongly bound (Baumgardt & Kroupa 2007).

Thus the survival probability of an embedded cluster cannot be determined by a single parameter, such as the star formation efficiency, as the complete formation process of stars, clumps of stars, and the entire cluster comes into play. The process whereby stars form in massive star clusters is still poorly explored terrain within astrophysics, and the formation of sub-clumps and clusters is even less well charted.

4.2.2 Observational constraints

What sounds convincing from a theoretical standpoint is often very hard to support with observations. There are a number of interesting observational indications of infant mortality, and of the associated dissolution time scales, but since the embedded phase is short ($\sim 1-2\,$Myr), many parameters are poorly constrained by observations, and the interpretations of models tend to be sensitive to assumptions made about the initial conditions.

Many observed young clusters, particularly the extragalactic population in Tab. 4, appear to be super-virial, which naively would lead to the early termination of the cluster's existence. This is most easily seen in the higher value of their dynamical mass $M_{\rm dyn}$ compared to the photometric mass $M_{\rm phot}$. The former is derived from measurements of the velocity dispersion and the radius of the cluster and the use of Eq. 4. The latter is derived from the total luminosity, calibrated to single stellar population models (see §2). Bastian et al. (2006) determine $M_{\rm phot}$ and $M_{\rm dyn}$ from a compilation of 19 clusters and find that both independent mass estimates are consistent for the somewhat older ($\gtrsim 50-100\,$Myr) clusters, but for young ($\sim 10\,$Myr) star clusters they find $M_{\rm dyn} > M_{\rm phot}$. Goodwin & Bastian (2006) explain this as a signature of the primordial gas expulsion, and of the process of infant mortality.

In Fig. 12 we present an updated version of Fig. 5 of Bastian et al. (2006), showing the ratio of light to dynamical mass of 24 clusters, taken from Table 4, each of which is about 10 megayear old (see §2). The age range is quite narrow because the red supergiant phase, which starts around 10 Myr, makes these clusters extremely bright (especially in the near infrared), whereas younger clusters are still heavily obscured.

Many of the clusters in Fig. 12 and Tab. 4 appear to have dynamical masses too high for their luminosities, and the intuitive explanation is that these clusters are expanding and are possibly even unbound (Goodwin & Bastian 2006). The time needed for a cluster to completely dissolve, or to find a new virial equilibrium after gas expulsion, is about $\sim 20-30\,t_{\rm dyn}$ (see for example Fig. 8 in Baumgardt & Kroupa 2007), where $t_{\rm dyn}$ is the initial dynamical time, when the gas and the stars are still bound. As a result, to 'catch' an unbound or expanding cluster at 10 Myr, the initial $t_{\rm dyn}$ should be $\gtrsim 0.5\,$Myr. This corresponds to an half-mass density of $\rho_{\rm hm} \lesssim 300\,M_\odot\,{\rm pc}^{-3}$ (Eq. 12 and $\rho_{\rm hm} \equiv 3M/8\pi {r_{\rm hm}}^3$).

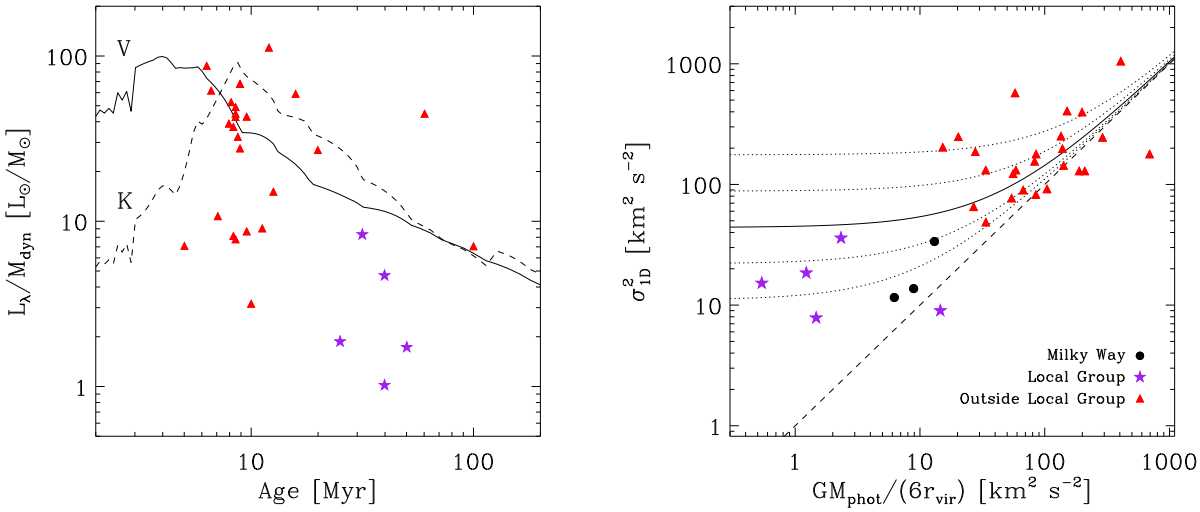

Figure 12: Left: Light to dynamical mass ratio for the clusters in Table 4 that have both quantities available. Photometric evolution from the Bruzual & Charlot (2003) single stellar population models, using a Chabrier IMF, in the V and K bands is indicated by the full and dashed lines, respectively. Right: The measured velocity dispersion squared, presented as a function of a prediction for this quantity based on Eq. 4. The solid line is a prediction of the effect of binaries on $M_{\rm dyn}$, with 1-σ and 2-σ variations due to stochastic fluctuations shown as dashed lines based on the results of Gieles, Sana & Portegies Zwart (2009).

Clusters with shorter initial $t_{\rm dyn}$ (higher density, see Eq. 12) have expanded into the field, or found a new equilibrium a few megayears after gas expulsion, and are not observable as super-virial clusters at 10 Myr.[e]

The initial density of the clusters in Fig. 12 is unknown, but is likely to have been higher in the past that it is today. In addition we may attemp to estimated their initial densities from their current densities. In Fig. 9 we show the radii and masses of the clusters under discussion, together with lines of constant $\rho_{\rm hm}$. The present day densities of the clusters younger than 10 Myr are $\rho_{\rm hm} \approx 10^{3\pm1}\,M_\odot\,{\rm pc}^{-3}$. The densities in the embedded phase were $O(1/f_e^4)$ higher — where the reduction in cluster mass accounts for a factor $1/f_e$ and the consequent adiabatic expansion a factor $1/f_e^3$ (see Eq. 33).

The initial dynamical times were therefore a factor of $1/f_e^2$ shorter than $t_{\rm dyn}$ after phase 1. Based on their physical ages of ~ 10 megayears and the fact that the gas ejection phase does not last beyond the moment of the first supernova (within ~ 3 Myr, see §4.1), these clusters have evolved for at least $10/f_e^2$ to $100/f_e^2$ initial dynamical times, and therefore must be bound (McCrady, Gilbert & Graham 2003; McCrady & Graham 2007), and the observed discrepancy between $M_{\rm phot}$ and $M_{\rm dyn}$ cannot originate from the overall expansion of the cluster.

Fleck et al. (2006) showed that the constant η that relates $\sigma_{\rm 1D}$ and $r_{\rm eff}$ to $M_{\rm dyn}$ (Eq. 30)

[e]The models of Goodwin & Bastian (2006) start with a density in the embedded phase of $\sim 60\,M_\odot\,{\rm pc}^{-3}(t_{\rm dyn} \approx 1\,{\rm Myr})$, which is why their clusters are super-virial for at least 25 Myr.

is up to a factor of three higher when the cluster is mass segregated. This results in a value of $M_{\rm dyn}$ that is too low compared to the true mass when this is not taken into account. So mass segregation is not a plausible explanation for the large downward spread of points in Fig. 12.

We are still left with the question why the observed velocity dispersions in some of these clusters are higher than would be expected from the virial theorem. Several independent and implicit assumptions enter the derivation of $M_{\rm dyn}$ and $M_{\rm phot}$, and each of them could be wrong. The stellar mass function, for example, could be bottom-heavy, i.e. steeper than Salpeter or with an excess of low-mass stars. Such a mass function would result in a velocity dispersion in virial equilibrium higher than that of a cluster with a Salpeter IMF, with little effect on $M_{\rm phot}$. However, to explain the observed discrepancy, the cluster mass function must deviate substantially from the canonical mass functions. We do not favor this conjecture, since the only star cluster for which the mass function was once anticipated to be deficient in low-mass stars, the Arches (Stolte et al. 2005), turns out to have a rather normal mass function at least down to $1\,{\rm M}_\odot$ (Kim et al. 2006).

Another interesting possibility is provided by the binarity of red supergiants, which dominate the observed luminosity. A relatively high fraction of hard binaries (see §3.4.1) leads to an overestimate of the cluster velocity dispersion due to the contribution from their internal orbital motion. This leads to an overestimate of $\sigma_{\rm 1D}$, and therefore of the mass of the cluster (Kouwenhoven & de Grijs 2008). For typical open clusters, with $\sigma_{\rm 1D} \approx 1\,{\rm km\ s^{-1}}$, this can only account for a factor of ~ 2 increase of $M_{\rm dyn}$ (Kouwenhoven & de Grijs 2008). However, young star clusters are dominated by $\sim 13-22\,{\rm M}_\odot$ red supergiants, and a binary fraction of $\sim$25% among these stars could explain an apparent dynamical mass of up to an order of magnitude more than the photometric mass (Gieles, Sana & Portegies Zwart 2009). As a consequence the discrepancy between $M_{\rm dyn}$ and $M_{\rm phot}$ is larger for clusters with high stellar velocity dispersion, or with a small ratios of $M_{\rm phot}/r_{\rm eff}$ (see Eq. 4), which is consistent with the observations. The effect of binaries on $\sigma_{\rm 1D}$ and the ratio of $M_{\rm dyn}/M_{\rm phot}$ is presented in Fig. 12.

Star clusters with $\rho_{\rm hm} \gtrsim 100\,M_\odot\,{\rm pc^{-3}}$ at 10 Myr, such as those listed in Tab. 4 and shown in Fig. 12, have survived the primordial gas expulsion phase and should be considered bound, stable, and likely to survive for a long time (see Eq. 19). They enter the next evolutionary phase, described in §4.3, during which stellar mass loss dominates the evolution of the cluster (phase 2).

4.3 Stellar mass loss

Clusters that survive phase 1 (the embedded phase, §4.2) continue to lose mass through stellar evolution. During phase 2, the most massive ($\gtrsim 50\,{\rm M}_\odot$) stars leave the main-sequence within $\lesssim 4.0\,{\rm Myr}$, and lose about 90% of their mass by the time they collapse to a black hole following a supernova. A $5{\rm M}_\odot$ star loses $\gtrsim 80$% of its mass by the time its core forms a white dwarf at about 100 Myr. For a Kroupa (2001) IMF between $0.1\,{\rm M}_\odot$ and $100\,{\rm M}_\odot$ the total cluster mass decreases by roughly 10%, 20%, and 30% during the first 10, 100, and 500 Myr. The impact of this will be discussed below.

4.3.1 Theoretical considerations

The time scale for mass loss depends on the mode in which it is achieved; supernova explosions, Wolf-Rayet winds and AGB expulsion result in high mass loss rates, whereas the general mass loss for an older stellar population is relatively slow. When the time scales for mass loss by stellar evolution is considerably longer than $t_{\rm dyn}$, the cluster responds adiabatically, expanding through a series of virial equilibria. For small f_e, Eq. 31 reduces to

$$\frac{\delta r_{\rm vir}}{r_{\rm vir}} = \frac{\delta M}{M}, \tag{32}$$

and therefore

$$\frac{r_{\rm vir}}{r_{\rm vir}(t=0)} = \frac{M(t=0)}{M}. \tag{33}$$

Even losing half the mass by slow stellar evolution (which for the canonical IMF would not occur within a Hubble time), the cluster would expand by only a factor of two. In the instantaneous approximation (§4.2 and Eq. 31), such mass loss would lead to the dissolution of the cluster.

In reality, the situation is more complicated, in particular because of the connection between dynamical evolution and stellar mass loss. For real clusters the expansion due to stellar mass loss is considerably more severe than suggested above, and can even result in complete disruption if the cluster is mass segregated before the bulk of the stellar evolution takes place (Vesperini, McMillan & Portegies Zwart 2009). Even an initially unsegregated cluster can still undergo mass segregation during the period when the residual gas is being ejected, and certainly during the early evolution of its stars (Applegate 1986), which can also lead to enhanced expansion at later times. The expansion of a mass segregated cluster, however, will not be homologous, as the massive (segregated) core stellar population tends to lose relatively more mass than the lower-mass halo stars. The result is a more dramatic expansion of the cluster core, with less severe effects farther out.

This effect is illustrated in Fig. 13, which presents the results of an isolated $N = 128k$ body simulation, run on a GRAPE-4 (Makino & Taiji 1998) using the `starlab` software environment (Portegies Zwart et al. 2001). The figure shows the evolution of the core radius with and without stellar evolution. Without stellar evolution the core tends to shrink, and eventually reaches core collapse, whereas with stellar mass loss the core expands (Portegies Zwart, McMillan & Ma

The combined effects of mass loss by stellar evolution and dynamical evolution in the tidal field of the host galaxy have been extensively studied (Fukushige & Heggie 1995, Takahashi & Portegies Zw Baumgardt & Makino 2003). These studies show that when clusters expand to a radius of $\sim 0.5\, r_{\rm J}$ they lose equilibrium and most of their stars overflow $r_{\rm J}$ (see §1.3.2) in a few crossing times.

We conclude that in phase 2 the overall evolution of the cluster is completely dominated by expansion due to stellar mass loss. However, since most of the mass loss comes from massive stars in the core, the core expansion is considerably larger than expected for the global mass function. Phase 2 lasts until the response of the cluster to stellar mass loss deminishes and from that moment the cluster can continue to expand until it completely dissolves or until the cluster core starts to contract again due to internal dynamical effects, at which point phase 3 begins.

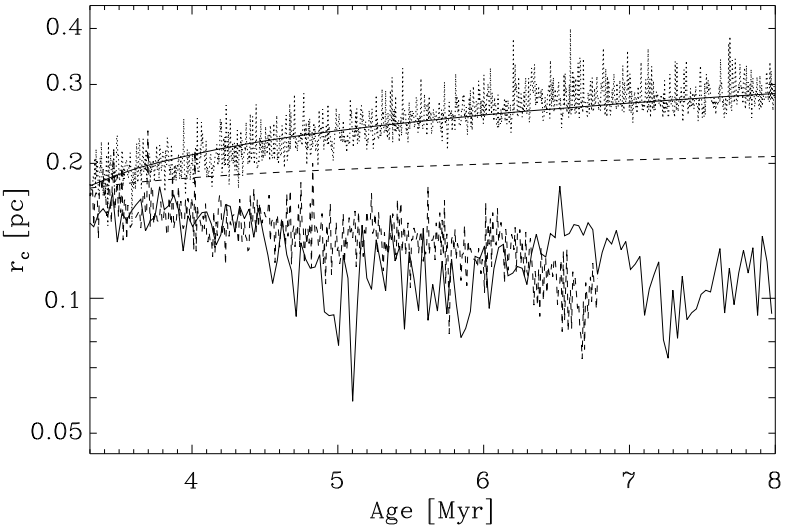

Figure 13: Evolution of the core radius during phase 2 of an N-body simulation ($N = 128k$, $r_{\rm vir} = 3.2\,{\rm pc}$, King $W_0 = 12$, Mass function is Salpeter between $1\,{\rm M}_\odot$ and $100\,{\rm M}_\odot$ Portegies Zwart, McMillan & Makino 2007). After about 3 Myr stellar mass loss dominates the evolution of the cluster core radius. The dotted curve (top curve) is the result of the full simulation, with both stellar evolution and binary dynamics included; the irregular dashed curve is calculated with the same initial realization but without stellar evolution. The wiggely solid curve (bottom) is calculated without stellar mass loss and without binary dynamics by collapsing the binaries in single objects. The smooth dashed line shows the expected expansion of the core, assuming adiabatic mass loss for a Salpeter initial mass. The smooth solid curve is computed assuming mass loss by stellar evolution from a Salpeter mass function with a lower limit of 15 ${\rm M}_\odot$, rather than the $0.1\,{\rm M}_\odot$ used in the simulation.

4.3.2 Observational constraints

Rapid dissolution due to stellar evolution mass loss occurs when $r_{\rm hm}/r_{\rm J} \gtrsim 0.5$. All the clusters in Fig. 9 have, within a factor of two, $r_{\rm hm}/r_{\rm J} \approx 0.03$, suggesting that they are probably all stable against stellar mass loss. Pfalzner (2009) recognizes two evolutionary sequences in young Galactic star clusters, from which she draws a similar conclusion. The first sequence of dense "starburst clusters", containing the Arches cluster, NGC 3603 and Trumpler 14, starts at a density of $\sim 10^5\,M_\odot\,{\rm pc}^{-3}$ at an age of a few megayears. These clusters appear to expand at constant in mass, up to an age of 10–20 Myr, where we find the red supergiant clusters RSGC01 and RSGC02. At that age the cluster density has dropped to $\sim 10^3\,M_\odot\,{\rm pc}^{-3}$. The second sequence of "leaky clusters" (which is identical to our definition of associations, see §2.1) starts at the same age but with much lower densities of $\sim 10\,M_\odot\,{\rm pc}^{-3}$, and expand while $M \propto 1/r_{\rm hm}$ to densities comparable to the field star density. The clusters in Fig. 9 may be compared with the red supergiant clusters in the Milky Way, i.e. the end point of the dense cluster sequence. The associations discussed by Pfalzner (2009, she refers to them as "leaky" clusters) and listed in Table 2 have dynamical

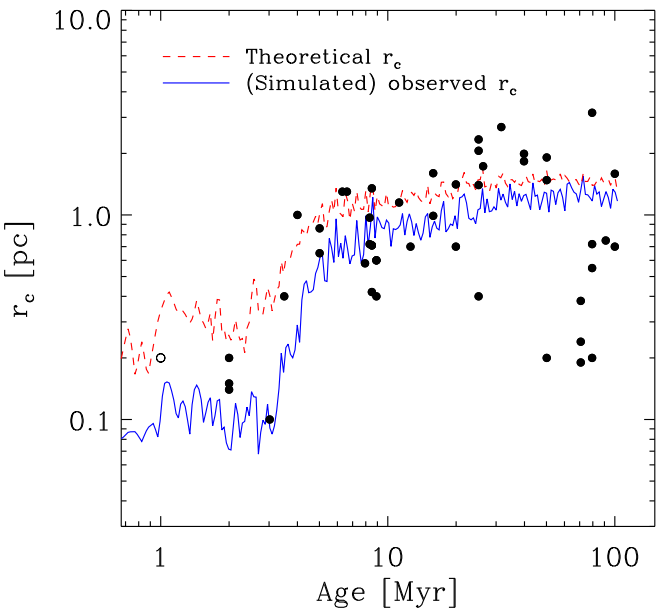

Figure 14: Evolution of observed core radii values of clusters, compared to the results of an N-body simulation including mass loss due to stellar evolution. For the simulation, the projected surface brightness profile was constructed and r_c was determined using and Eq. 5 and Eq. 8 (full line). The dashed line shows the theoretical r_c from Eq. 7 discussed in §1.3.2.

times that exceed the cluster age, and are expected to be unstable against mass loss by stellar evolution.

In §2 we discussed the remarkable increase in the observed core radii of clusters with ages 1–50 Myr (Mackey & Gilmore 2003, Bastian et al. 2008). Earlier studies argued that this effect was the result of early gas expulsion (phase 1), but as discussed in §2 the time scale for finding a new virial equilibrium after gas expulsion is too short to affect the growth of r_c over such a long period. Mass loss from the young stellar population (phase 2) can contribute to some extent to the observed trend, but its effect is probably too weak to explain it completely (Mackey et al. 2007). A more likely solution is dynamical heating from relatively massive objects, such as massive stars and stellar mass black holes, sinking to the cluster center (Merritt et al. 2004).

An additional effect not yet discussed is the difference between the observed r_c, usually resulting from a fit to the surface brightness profile (Eq. 5), and the 3D dynamical core radius described in §1.3.2. If a young star cluster is mass segregated, possibly already from its formation process, then the light is dominated by the few massive stars in the core, which can lead to an underestimate of r_c (Fleck et al. 2005, Gaburov & Gieles 2008). Mackey et al. (2007, 2008) showed that when taking this into account, a remarkable increase of r_c is "observed," while the "real" core radius changes less.

We illustrate this in Fig. 14. The same data points as in Fig. 8 are shown, together with the results of an N-body simulation (lines), where the theoretical value of r_c, as defined in

§1 and the value of r_c resulting from a fit of the EFF87 profile (Eq. 5) to the projected light of the simulated cluster. The cluster consists of $N = 65\,536$ single stars initially distributed according to a Plummer (1911) profile with $r_{vir} = 2\,pc$. Before stellar evolution was turned on, we evolved the cluster for 100 t_{dyn}, which corresponds to $\sim 0.1\,t_{rh}$, to mimic some degree of primordial mass segregation, in which stars with masses $\gtrsim 5\,M_\odot$ are more centrally concentrated than the less massive stars (Eq. 20). Since the massive stars dominate the light, the observed r_c is almost a factor of three smaller than the 3D version at $t = 0$. The observed r_c increase by nearly a factor of ten in a few tens of megayears, while the 3D core radius expands only by a factor of three. After $\sim 30\,Myr$ the two quantities roughly agree. In the simulation r_{hm} increased only by 60% due to the stellar evolution mass loss.

Primordial mass segregation has a profound effect on the evolution of a star cluster, but possibly much more relevant for this review is its consequences for cluster observations. The assumption that a young ($\lesssim 10\,Myr$) cluster is not mass segregated, when in reality it is, can dramatically alter observationally derived quantities, such as the cluster size, velocity dispersion, density profile, and central density.

4.4 External perturbations and evaporation

4.4.1 Theoretical considerations

One important external disruptive factor, first considered by Spitzer (1958, see §4.2), is encounters between clusters and giant molecular clouds. Since GMCs are typically more massive than clusters, the cluster is more affected by an encounter than the cloud (Theuns 1991). The cluster lifetime due to heating by passing clouds is inversely proportional to the volume density of molecular gas, ρ_{gas}, and proportional to the density of the cluster:

$$t_{dis}^{GMC} \approx 1\,Gyr \left(\frac{0.03\,M_\odot\,pc^{-3}}{\rho_{gas}}\right)\left(\frac{\rho_{hm}}{10\,M_\odot\,pc^{-3}}\right). \quad (34)$$

This result is typical for disruption by external tidal perturbations operating on short time scales ($\lesssim t_{dyn}$), also known as tidal shocks and can also be applied to passages through the disc (e.g. Ostriker, Spitzer & Chevalier 1972), bulge (e.g. Gnedin & Ostriker 1997) and spiral arms (Gieles, Athanassoula & Portegies Zwart 2007). Here $0.03\,M_\odot\,pc^{-3}$ is the molecular gas density in the solar neighborhood and the constant is taken from Gieles et al. (2006c), which is an update from the seminal result by Spitzer (1958). The dependence of t_{dis} on ρ_{gas} indicates that the lifetimes of star clusters scales roughly inversely with the observable surface density of molecular gas, Σ_{gas}.

This result enables us to make order of magnitude estimates of the lifetimes of clusters in other galaxies. In spiral galaxies, GMC encounters are especially frequent during the early stages of cluster evolution, since clusters form in the thin gaseous disk where ρ_{gas} is high. Older clusters are typically associated with the thick disk, where ρ_{gas} is low and GMC encounters are less frequent. Since young ($\lesssim$1 Gyr) clusters in spiral galaxies have only a small range in radii (e.g. Larsen 2004), more massive clusters tend to have higher densities, making them less vulnerable to encounters with GMCs, which explains their longer lifetimes compared to their lower-mass counterparts (Gieles et al. 2006c). It is not clear whether the

lack of a mass-radius relation is a universal property imprinted at cluster formation, or the result of evolution.

4.4.2 Observational constraints

If GMC encounters are a dominant disruption process, then it is important to understand the mass-radius correlation of clusters, since $t_{\rm dis}^{\rm GMC} \propto \rho_{\rm hm}$ (§4.4.1). If clusters form with a constant density, i.e. a mass-radius relation of the form $r_{\rm hm} \propto M^{1/3}$, then their destruction time due to GMC encounters is independent of cluster mass. Additional complications arise from the time dependence of a mass-radius relation. Clusters older than those shown in Fig. 9 For young clusters ($\lesssim 10\,$Myr) there seems to be some positive correlation between mass and radius, roughly consistent with a density of $10^{3\pm1}\,M_\odot\,{\rm pc}^{-3}$. Older clusters ($\gtrsim 10\,$Myr) do not seem to exhibit any correlation between mass and radius, consistent with a near-constant radius, i.e. $r_{\rm hm} =$ constant, which could be the consequence of evolutionary effects, such as mass segregation and stellar mass loss. This would lead to a destruction time scale by GMCs ($t_{\rm dis}^{\rm GMC}$) that is dependent of the cluster mass: $t_{\rm dis}^{\rm GMC} \propto M/r_{\rm hm}^3$. In any case, the youngest YMCs listed in Tab. 4 are unlikely to be rapidly destroyed by passing GMCs, since $t_{\rm dis}^{\rm GMC}$ exceeds a Hubble time due to their high densities (see left panel of Fig. 9).

While considering mass loss from star clusters it is convenient to distinguish between two fundamental processes: evaporation and tidal stripping. Evaporation is the steady loss of stars from the cluster driven by the continuous repopulation by relaxation of the high-velocity tail of the Maxwellian velocity distribution (see §3.3.1, Eq. 14 and, e.g. Ambartsumian 1938, Spitzer 1940). This process has been the subject of numerous comprehensive numerical studies (Spitzer 1987, Aarseth 2003, Heggie & Hut 2003, Baumgardt & Makino 2003). Tidal stripping is the prompt removal of stars that find themselves outside the cluster Jacobi radius ($r_{\rm J}$, see 1.3.2) due to internal processes such as stellar mass loss or a change in the external tidal field, for example as the cluster approaches pericenter in its orbit around its parent galaxy. On a $\sim$100 Myr time scale, and for clusters with masses $\gtrsim 10^4\,{\rm M}_\odot$, relaxation is unlikely to be important, and so tidal stripping dominates the cluster mass loss.

Until the 1990s, the main targets of cluster disruption studies were the open clusters in the Milky Way and the YMCs in the Magellanic clouds. Since then, HST observations have established the properties of large populations containing more massive clusters in quiescent spiral galaxies (e.g. Larsen 2002), interacting galaxies (e.g. Whitmore et al. 1999, Bastian et al. 2005), and merger products (e.g. Miller et al. 1997). The primary tool used in studies of cluster disruption is the cluster age distribution. Different groups give different weights to the various factors described in §4.2 in interpreting the results, but empirical cluster disruption studies follow one of two basic models, in which the disruption is either *environment dependent* or *universal*.

In the environment dependent disruption model, the dissolution time follows a simple scaling relation with cluster mass and environment, following the age and mass distributions of luminosity-limited cluster samples in different galaxies (Boutloukos & Lamers 2003). Variations in dissolution time scales are explained by differences in the tidal field strength (Lamers, Gieles & Portegies Zwart 2005) and the GMC density (Gieles et al. 2006c).

The universal disruption model assumes that internal processes dominate the cluster disruption and that roughly 80–90% of all remaining clusters are destroyed during each

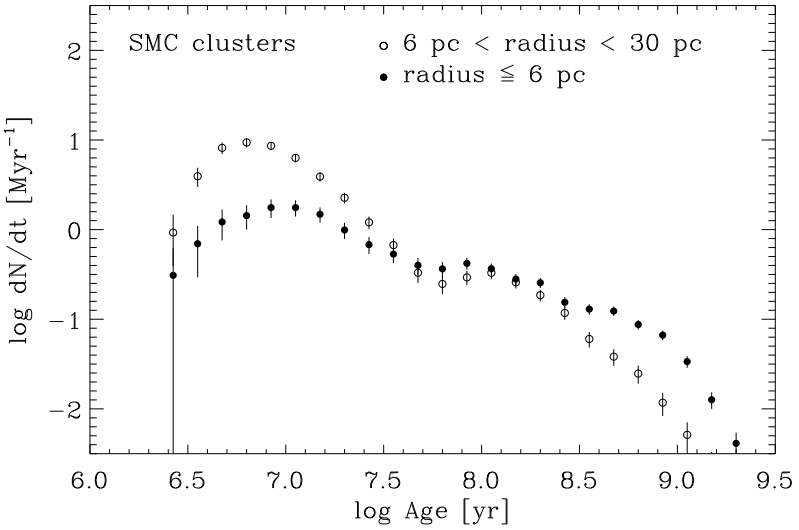

Figure 15: Age distribution of SMC clusters based on the catalog of Chiosi et al. (2006). The sample is split into small and large clusters/associations, with the boundary at a radius of 6 pc. The histograms are made using a 0.5 dex bin width with different starting values (boxcar averaging).

decade in age, resulting in a (mass limited) age distribution that declines inversely with time ($\propto t^{-1}$). The main assumptions are that the majority ($80-90\%$) of clusters dissolve within a few hundred megayears and that the disruption rate does not depend on mass. This model however, is calibrated against the cluster population in the Antennae galaxies, as discussed in §4.2 (Fall, Chandar & Whitmore 2005; Whitmore, Chandar & Fall 2007), and while it is quite consistent with these observations, it is not clear how applicable it is to other galactic environments.

The various cluster dissolution models have led to some controversy, resulting in a number of spirited discussions at conferences and in the literature. Chandar, Fall & Whitmore (2006) demonstrated that the age distribution of SMC clusters declines $\propto t^{-0.85}$, which is consistent with their resuls for the Antennae. Gieles, Lamers & Portegies Zwart (2007) are able to reproduce these results only if they impose an incompleteness in the detection of clusters, which is consistent with the arguments of de Grijs & Goodwin (2008). As a consequence Gieles, Lamers & Portegies Zwart (2007) conclude, using the same data sample used by Chandar, Fall & Whitmore (2006), that the age distribution of massive ($\gtrsim 10^{3.5}\,\mathrm{M}_\odot$) clusters in the LMC younger than a few hundred megayears is not affected by internal processes, contradicting the findings of Chandar, Fall & Whitmore (2006).

The conclusions of Gieles, Lamers & Portegies Zwart (2007) are supported by Boutloukos & Lamers (20 who show that for a constant formation rate of clusters and without disruption, the age distribution of a luminosity-limited cluster sample declines $\propto t^{-\zeta(\beta-1)}$, where $-\beta$ is the index of the cluster initial mass function. The parameter ζ describes how the cluster fades with age, due to stellar evolution: $F_\lambda(t) \propto t^{-\zeta}$, where F_λ is the flux at wavelength λ of a clus-

ter with constant mass. For the U and V-bands $\zeta \approx 1.0$ and 0.7, respectively, which for $\beta = 2$ results in $t^{-\kappa}$, with $0.7 \lesssim \kappa \lesssim 1.0$, due to fading alone. If the distribution of cluster masses is described by a Schechter function (see Eq. 18 in §2.4.2) the age distribution of a luminosity-limited sample that is not affected by disruption is as steep as $0.9 \lesssim \kappa \lesssim 1.4$.

The internal disruption model for the age distribution relies on the assumption that the cluster formation history is constant within the age range considered (a few hundred megayears). Bastian et al. (2009) demonstrate that in the Antennae an increase of the cluster formation rate as predicted by galaxy merger models could alleviate the need to invoke longer duration cluster disruption to explain the decline in the number of clusters with age.

The discussion of the distribution of the number of clusters with age is complicated by the distinction between associations and dense clusters (see §2 and §4.2.2), which may be hard to distinghuish at large distances. This is illustrated in Fig. 15, which shows the age distribution of clusters and associations in the central region of the SMC (Chiosi et al. 2006). The sample is divided into two subsamples of ~ 200 clusters each, based on size. The age distribution of the large ($r_{\rm eff} > 6$pc) clusters falls off much more rapidly than that of the more compact clusters. We note that this is consistent with associations being disrupted by GMC encounters, since they have (on average) much lower densities (see right panel of Fig. 9) and are therefore destroyed much quicker (Eq. 34). The median radii of the two samples are 4.5 pc and 9 pc, respectively, but at a distance of 20 Mpc it would be very difficult to tell these two groups apart. We suggest that by relaxing the cluster size in the observationally selected sample one includes more short-lived associations, which if resolved should probably not be considered genuine star clusters.

4.5 Early evolution and the luminosity function of old globular cluster systems

The LFs of old globular cluster systems is very different from the (power-law) LFs of YMCs discussed in §2.4.1. When approximating the LF of old globular clusters in the Milky Way by a Gaussian, the peak is at $M_V \approx -7.4$ mag (Harris 2001). For a constant mass-to-light ratio of $M/L \approx 2$ the mass function, often referred to as globular cluster mass function (GCMF), which in fact is a present-day mass function. The GCMF is, like the LF, also peaked or bell-shaped (when using logarithmic mass bins). The characteristic mass, or turn-over mass, is $M_{\rm TO} \approx 2 \times 10^5\,{\rm M}_\odot$. It has been argued that old globular clusters formed with this –bell-shaped– mass function (Fall & Rees 1985, Parmentier & Gilmore 2007), which is completely different than the power-law distribution we see for YMCs today. The discrepancy between the bell-shaped curve for old globular clusters and the power-law mass function for YMCs then could originate from the long timescale phase-3 dynamical evolution, this evolution could severre the relatively low-mass ($M \lesssim M_{\rm TO}$) clusters more whereas it leaves the high-mass ($M \gtrsim M_{\rm TO}$) clusters unaffected (Elmegreen & Efremov 1997, Vesperini 1997, Baumgardt 1998, Fall & Zhang 2001, **?**).

The value of $M_{\rm TO}$, however, is remarkably constant between galaxies (Jordán et al. 2007) and even within a single galaxy it hardly varies with the distance to the galaxy center (Vesperini et al. 2003). This is hard to reconsile with the models that start with a power-law mass function and seek to explain the present-day form of the GCMF by phase-3 dynamical

evolution (Vesperini et al. 2003).

For this review only those solutions to this conundrum are relevant that play an important role in the early evolution (i.e. Phase 1 and 2). Baumgardt, Kroupa & Parmentier (2008) provide such a solution; they argue that relatively low-mass clusters are more easily dissolved as a result of phase-1 gas expulsion, leaving the most massive clusters unaffected. They argue that the binding energy of embedded clusters scales with the square of their total masses (gas and stars), whereas the energy input from stellar winds and supernovae depends linearly on the mass of all the stars in the cluster. If the star formation efficiency (f_e) is independent of the mass of the primordial molecular cloud, more massive clusters require more time to clear all the residual gas from the natal cloud. Baumgardt, Kroupa & Parmentier (2008) find that clusters with $M \lesssim 10^5\,\mathrm{M}_\odot$ loose their residual gas on time-scales much shorter than a crossing time, which effectively shocks the cluster and drives it to dissolution (see §4.2) More massive clusters respond adiabatically to the loss of the mass of the cloud (§4.3.1), resulting in a higher survival probability. The weak dependence of $M_{\rm TO}$ on environmental factors emerges quite naturally from this model Baumgardt, Kroupa & Parmentier (2008).

An alternative explanation for the evolution of the mass function of YMCs compared to that of the GCMF is presented by Vesperini & Zepf (2003). They argue that phase-2 stellar mass loss leads to a near universal dissolution rate of low-mass clusters. Old globular clusters of low mass tend to be less concentrated than high-mass clusters (McLaughlin 2000). If this trend is primordial, stellar mass loss would be more effective in destroying low-mass clusters compared to high-mass clusters (Chernoff & Weinberg 1990, Vesperini & Zepf 2003). This mechanism is, as the phase-1 outgassing, independent of environmental factors, like the distance to the galactic center, and would therefore effectively provide a satisfactory explanation of the weak dependence of $M_{\rm TO}$ to the environment.

Each of the three solution to this conundrum have their advantages and disadvantages. It may be evident that this discussion has not yet resulted in a satisfactory solution to the problem, but it promises to continue to be an exciting discussion for the foreseeable future.

5 Lusus Naturæ

Old globular clusters are of interest because of their old age, their assumed relatively homogeneous populations, their relative isolation in their parent galaxies, and because of their abundance of unusual objects, such as blue stragglers, x-ray binaries, radio pulsars, etc., often referred to collectively as *stellar exotica*, or *lusus naturæ*[f]. In the disk of the Milky Way, such objects form through internal evolutionary processes in individual stars or close binary systems. In star clusters, these processes are augmented by stellar interactions, mediated by the high encounter frequency in dense cluster cores.

Stellar encounters generate new channels for the formation of exotic objects, but can also catalyze existing channels. For example, a binary encounter may lead directly to a collision and the formation of a blue straggler, or its effect may be indirect, perhaps resulting in an exchange that eventually (billions of years later) leads to the formation of a low-mass x-ray binary. Repeated encounters can transform binaries and multiple stellar systems, multiplying the channels for the production of exotica (Davies 1995, Hurley & Shara 2002,

[f]Lusus Naturæ is Latin for the freaks of nature, mutants or monsters.

Davies et al. 2006). A clear understanding of the formation and evolution of these objects can provide insight into the past dynamical evolution of the cluster (Davies 2009).

Many of the stellar exotica observed in old globular clusters today are the results of processes that began when the cluster was young. In some cases, they are the products of the interplay between dynamical and evolutionary processes involving stars and binaries during the first $\sim 100\,\mathrm{Myr}$ of the cluster lifetime. The primordial seeds for many lusus naturæ were planted during this period (Portegies Zwart, McMillan & Makino 2007). Later stages (during phase 3, see § 3) of dynamical evolution, such as core collapse, may produce additional generations of exotica. Since the observed YMCs will age to become old globular clusters (see §1), they provide a convenient testbed for the study of the progenitors of stellar exotica.

The progenitors of observed lusus naturæ in old globular clusters are not necessarily easy to identify in the young cluster population, although in some cases the evolutionary link is well established (Glebbeek, Pols & Hurley 2008). There may well be entire populations of peculiar objects in young star clusters that do not lead to observable interesting objects at later stages, and some objects destined for peculiarity may look perfectly ordinary at early times. An example of the latter is the dormant blue straggler population consisting of stars that were rejuvenated by mass transfer or collisions while still on the main sequence, and now lurk among their fellow main-sequence stars until they remain behind after the others traverse the Hertzsprung gap (Portegies Zwart, Hut & Verbunt 1997).

5.1 Binary Stars

Exotic objects in star clusters are closely related to binaries, as they often form via internal binary evolution or during dynamical interactions between binaries and other stars. Examples are the formation of blue stragglers (§5.1.1), colliding wind binaries (§5.1.2), and anomalous x-ray pulsars (§5.2.1), all of which require the presence of binary stars in the system. In some cases, such as the slow evolution of an accreting X-ray pulsar that leads from a low-mass x-ray binary to a binary millisecond pulsar, the evolutionary track is readily established (Bhattacharya & van den Heuvel 1991). In others, however, the punctuated equilibrium through which these objects evolve makes it virtually impossible to catch the key transitions as they occur. Examples are collisions between stars, or the common-envelope phase in the Darwin–Riemann instability of a contact binary.

We will distinguish two fundamental types of binaries in star clusters: (1) "primordial" binaries, which formed contemporaneously with the stars in the cluster as a crucial part of the star-formation process (Goodman & Hut 1989), and (2) "dynamical" binaries, which formed later via stellar interactions, often long after the component stars reached the main sequence. One can wonder to what extend this limited terminology is still usable for binaries that experiences one or more exchange interactions. It is for example, quite possible that two stars that were initially single end-up in a binary after two exchanges. As a practical matter we would still consider such a binary primordial. The second group of dynamical binaries may be further divided into two sub-categories—binaries formed by conservative three- and four-body stellar dynamical interactions, and binaries formed by dissipative two-body tidal capture. The latter process was introduced by Fabian, Pringle & Rees (1975) to explain the relatively high specific frequency of low-mass X-ray binaries in old globular clusters. It has

fallen somewhat out of favor since the late 1980s, but it may be entering a revival of sorts Ogilvie & Lin (2004). Many of the curious objects discussed in this § are related to binarity, either primordial or tidal, although we tentatively will use this distinction in the formation process.

5.1.1 Blue Stragglers

A blue straggler is a star which exceeds the cluster main-sequence turnoff in both temperature and luminosity, but which is not on the horizontal branch. Blue stragglers populate the region blueward of the turnoff, as if they lagged behind on the cluster main sequence while the other stars aged. The first (34) blue stragglers were discovered in the globular cluster M3 by Sandage (1953). At least 8 plausible explanations have been proposed for the formation of blue stragglers (see Leonard 1989). Of these, two are currently in favor:

- direct merger between two stars (Hills & Day 1976),
- mass transfer in a close semi-detached binary star (McCrea 1964).

The latter scenario is supported by the discovery of two blue stragglers, in the young open star clusters NGC 663 and NGC 6649, which have been found to be the donors in Be/X-ray binary systems (Marco, Negueruela & Motch 2007). The discovery of a blue straggler in the old open cluster M67, which appears to be about 2.5 times more massive than the turn-off mass, favors the former view (Leonard 1996).

Both favored mechanisms for blue straggler formation appear plausible in YMCs. However, no blue stragglers have yet been identified in any observed YMC, although this may be explained by the absence of a clear turn-off in the resolved clusters, which makes the identification (and the definition) of a blue straggler impractical. There are, however a number of "odd" stars in YMCs that might possibly evolve to resemble blue stragglers in the future. Objects consistent with this broadened definition include four O3 If/WN6-A stars in the star cluster R136 in the 30 Doradus region of the LMC (Campbell et al. 1992, Brandl et al. 1996).

Several interesting correlations exist between the numbers of blue stragglers in old globular clusters and the numbers of red giants (Ferraro, Fusi Pecci & Bellazzini 1995), and also with the binary fraction (Sollima et al. 2008; Knigge, Leigh & Sills 2009). In addition, Davies, Piotto & de Angeli (2004) find that the number of blue stragglers is be independent of integrated absolute magnitude M_V of the cluster, and use this fact to argue that both production mechanisms are relevant.

5.1.2 Colliding wind binaries

Binaries containing two massive stars, such as Wolf-Rayet stars, with strong stellar winds often exhibit intense radio and/or x-ray emission. Since this process requires copious stellar mass loss in a fast wind, these sources do not occur in old globular clusters, but YMCs appear to be excellent hosts for such systems. Several young and dense star clusters exhibit x-ray and radio emission from colliding wind binaries. In some relatively nearby cases, R136 (Portegies Zwart, Pooley & Lewin 2002), Wd1 (Clark et al. 2005, Crowther et al. 2006), and

the Arches and Quintuplet clusters (Lang et al. 2005), the counterparts of the radio and x-ray sources have been identified.

5.2 Compact objects

A compact object is generally produced in a supernova explosion (see § 5.3.1). During such event the compact object, either a neutron star or a black hole, is likely to receive a high velocity, often referred to as a 'kick'. The direction of the kick is ill constrained, but the velocity distribution of this kick is well determined by observing the velocities of nearby young neutron stars (Lyne & Lorimer 1994; Cordes & Chernoff 1998; Arzoumanian, Chernoff & Cordes 2002) and the galactic scale-height of black hole x-ray transients (White & van Paradijs 1996, Gualandris et al. 2005). It seems that neutron stars receive a considerably higher velocity kick than black holes. As a result the majority ($\sim 95\,\%$) of neutron stars are likely ejected from any YMC (Drukier 1996; Pfahl, Rappaport & Podsiadlowski 2002) whereas most black holes are retained. However, since neutron stars are considerably more massive than the mean mass of a star in a cluster, once formed and retained they tend to stay in the cluster. At a later age compact objects can subsequently dominate the cluster evolution. For black holes this happens at an age of about 100 Myr to a Gyr (Kulkarni, Hut & McMillan 1993; Mackey et al. 2007), whereas for neutron stars the age of domination starts around a Hubble time (Portegies Zwart, McMillan & Makino 2007). The evolution of compact objects in star clusters deserves a separate review, but here we will present a very brief summary of the current observational evidence for compact objects in YMCs.

A number of YMCs have been observed in the radio and x-ray, revealing a wealth of sources, even richer than found in old globular clusters (Clark et al. 2008). Among the x-ray sources is a large population of accreting neutron stars, stellar-mass black holes and possibly intermediate-mass black holes. Because of crowding in the central regions of these clusters, where most of the x-ray sources are found, very few sources have optical counterparts.

With the adopted age limit of 100 Myr, only relatively few white dwarfs have formed—about as many as neutron stars—and cataclysmic variables are not expected. The youth of these clusters seem to make it unlikely that any low-mass x-ray binaries or millisecond pulsars will be found.

5.2.1 Magnetars

Shortly after a supernova (within $\sim 10^5$ years), a newly formed neutron star may become observable as a magnetar, which can have a magnetic field strength exceeding $\sim 10^{15}$ gauss (Kouveliotou et al. 1999). The population of magnetars is subdivided into two classes: soft gamma-ray repeaters (SGRs) and anomalous x-ray pulsars (AXPs)[g]. As the products of supernovae, one might naively expect these objects to reside mainly in YMCs, and indeed about half (3 of 8) of the known SGRs and one-tenth (1 of 10) of the AXPs are known to reside in such systems. These are remarkably high fractions, given that only 0.05% of the stellar mass of the Galaxy resides in star clusters (see §1).

The single cluster AXP is CXOU J164710.2-455216 (Muno et al. 2006) in the Galactic young star cluster Westerlund 1. It exhibits a 20-ms burst with energy $\sim 10^{37}$ erg (15-150

[g]see `http://www.physics.mcgill.ca/~pulsar/magnetar/main.html`.

keV), and spins down at a rate of $P/\dot{P} \simeq -10^{-4}$ (Muno et al. 2007), quite typical of a magnetar.

Several interesting sources are hosted by young star clusters in the LMC. These include the microquasar LS I $+61^\circ\,303$, which may have been ejected from the cluster IC 1805 (Mirabel, Rodrigues & Liu 2004). The relatively low-density young star cluster SL 463, too small for inclusion in this review, seems to be associated with SGR 0526-66 (Klose et al. 2004) at a projected distance of $\sim 30\,\mathrm{pc}$. Two other SGRs associated with relatively low-density young star clusters are SGR 1806-20, at a projected distance of $\sim 0.4\,\mathrm{pc}$ from the core of its parent cluster (Mirabel, Fuchs & Chaty 2000; Corbel & Eikenberry 2004), and SGR 1900+14, at $\sim 0.8\,\mathrm{pc}$ (Mirabel, Fuchs & Chaty 2000; Vrba et al. 2000). This latter SGR has a measured proper motion of 70 mas/yr away from the cluster, suggesting that it indeed was ejected from the parent cluster (DeLuca et al. 2009), which is relatively old ($14 \pm 1\,\mathrm{Myr}$) compared to the usual SGR-producing stars (Davies et al. 2009). The actual association between cluster and SGR is hard to establish in this case since the distances to both objects are ill constrained.

5.2.2 Ultra-luminous X-ray sources

Old globular clusters are known to host an enormous excess of low-mass x-ray binaries compared to the rest of the Galaxy. Much of this excess is attributed to the dynamical environment in dense cluster cores (Fabian, Pringle & Rees 1975; Pooley et al. 2003). Young star clusters are sites of intense dynamical activity, so it is not surprising that YMCs also host many x-ray sources. The majority of x-ray point sources in external galaxies appear to be associated with young star clusters, as is the case for example in the Antennae system (NGC4038/39) Zezas et al. (2002). The nature of most of these x-ray sources is unknown, and we can only guess at their origin.

We limit ourselves here to the most striking x-ray sources, the subclass of ultra-luminous x-ray sources (ULXs), which are characterized by x-ray luminosity $L_x \gtrsim 1.3 \times 10^{39}\,\mathrm{erg/s}$, the maximum isotropic luminosity that can be produced by a $10\,\mathrm{M}_\odot$ black hole accreting pure hydrogen (King et al. 2001). For practical reasons we round the threshold up to $L_x \gtrsim 10^{40}\,\mathrm{erg/s}$, mainly to ensure that such luminosities are unlikely to be produced by stellar-mass black holes accreting at the Eddington rate from a main-sequence companion star. These ULXs are responsible for the brightest stellar x-ray sources in the sky.

Several models attempt to explain the high x-ray luminosity of the ULXs, but at present there is no consensus in the community on the source of the x-rays. The current leading models are:

- anisotropic (collimated or beamed) emission from an accreting stellar-mass black hole (although porosity, turbulence, and bubbles also provide interesting alternatives, King et al. 2001, King 2002),
- accretion from an evolved star onto a stellar-mass black hole, which can, in principle, lead to an accretion rate higher than from a main-sequence star, and therefore a higher x-ray luminosity (Madhusudhan et al. 2006),
- accretion from a companion star onto an "intermediate-mass black hole" (IMBH), with mass $\gtrsim 100\,\mathrm{M}_\odot$ (Portegies Zwart et al. 2004).

ULXs tend to be hosted by starburst and spiral galaxies (Makishima et al. 2000). Some of the brightest are associated with YMCs; a leading example is the ULX in the star cluster MGG 11 in the starburst galaxy M82 (Kaaret et al. 2001). The association with YMCs argues in favor of an accreting black hole of $\sim 1000\,M_\odot$ (Portegies Zwart et al. 2004). The object in MGG 11 is particularly interesting, as it shows a strong quasi-periodic oscillation in the 50-100 mHz frequency range (Strohmayer & Mushotzky 2003), providing a strong argument against beamed emission, and supporting the hypothesis that the x-ray luminosity comes from an accreting black hole of 200–5000 $M_\odot$. Further support is provided by the detected periodic variation of ~ 62 days, which can be explained if the black hole is orbited by a 22–25 $M_\odot$ Roche-lobe filling donor star (Patruno et al. 2006).

ULXs have been associated with YMCs in NGC 5204 (Liu, Bregman & Seitzer 2004), the starburst galaxies M82 (Kaaret et al. 2001) and NGC1313 (Grisé et al. 2008), the edge-on spiral NGC 4565 (Wu et al. 2002), the interacting galaxies M51 (Liu et al. 2002), NGC4038/39 (Antennae Fabbiano, Zezas & Murray 2001) and ESO 350-40 (Cartwheel Gao et al. 2003), and the type 1.5 Seyfert galaxy NGC 1275 (González-Martín, Fabian & Sanders 2006). The higher abundance of ULXs in active, starburst, and interacting galaxies may be related to the empirical fact that YMCs tend to form in these environments; 60% of ULXs are associated with active star-forming regions (Swartz, Tennant & Soria 2009, although the definition of a ULX used here is somewhat faint).

If the counterpart of a ULX hosts an IMBHs, it is likely to be the the acceptor from a windy or Roche-lobe overflowing massive star, as seems to be the case in the 10^{39}–10^{41} erg/s ULX in NGC 5204, where the donor is identified as a B0 Ib supergiant with a 10-day orbital period (Liu, Bregman & Seitzer 2004), and in ULX M51 X-7, which has has an even shorter orbital period of only 2.1 hr (Liu et al. 2002), although no stellar companion has been identified. The black holes that may be responsible for the ULXs NGC 1313 X-1 and X-2 (0.2-10.0 keV, assuming a distance of 3.7 Mpc) may have masses in the range 100–1000 $M_\odot$ (Miller et al. 2003), and in these cases YMCs have been identified as optical counterparts.

5.3 Explosive events

5.3.1 Supernovae

Supernova are relatively rare events, occurring about once every 100 years in a galaxy like the Milky Way (Cappellaro, Evans & Turatto 1999). Although type I supernovae are unlikely to occur in star clusters younger than 100 Myr (Pfahl, Scannapieco & Bildsten 2009), at these ages the seeds may be planted for a rich future of type I events (Shara & Hurley 2002).

Since most massive stars tend to reside in clusters, as discussed in §1 and §2, it is probable that the majority of type Ib/c and type II supernovae occur in star clusters. However, since most supernovae occur in distant galaxies it is hard to find optical counterparts, and very few associations of supernovae with young star clusters have been reported. Based on the peculiar metallicity of SN 1987A, Efremov (1991) argue that the star originated in the young LMC cluster MKM90. SN 2006gy (Foley et al. 2006), which is a candidate for the formation of an IMBH, may have been the result of a collision runaway (§3.4.2) in a YMC (Portegies Zwart & van den Heuvel 2007). However, perhaps the strongest case is the peculiar type IIp supernova SN 2004dj (probably produced by a 12–20 $M_\odot$ star) in the spiral

galaxy NGC 2403; as it faded, the star cluster Sandage-96 reappeared (Wang et al. 2005).

5.3.2 Gamma-ray bursts

Any word written about gamma-ray bursts is likely to trigger its own burst of e-mail, but we cannot resist the temptation to devote a few lines to this fascinating transient phenomenon. Gamma-ray bursts come in two types, of short ($\lesssim 2\,\mathrm{s}$) and long duration, respectively Mészáros (2002). Several theories exist which point to either old globular or young star clusters as possible hosts for gamma-ray bursts. Colliding compact objects are often cited as sources for the short bursts (Narayan, Piran & Shemi 1991). Long bursts are thought to be hosted by massive star forming regions (Paczynski 1998). Of particular interest is the elusive relation between the long bursts and YMCs (Efremov 2000). The models for long-duration gamma-ray bursts should be particularly applicable to YMCs, as they require rapidly rotating high-mass stars (Heger et al. 2003), which could be achieved quite naturally by stellar collisions in a YMC (see §3.4.2).

5.4 Summary of exotica

We have discussed several examples of exotica in YMCs, but other curiosities remain. Many of these exotic objects are well studied in old globular clusters, but similar scrutiny is so far lacking in their younger siblings. Rather than providing a detailed description of each of the oddities found, we simply mention a few developments and recent discoveries of what today we call exotic objects, which one day we may consider "normal." The following list summarizes a number of peculiar clusters, noteworthy because of a unique source or object. The list is far from complete, but at the very least it indicates the diversity of objects found in YMCs.

- **R136** Contains some 13 colliding wind binaries (Portegies Zwart, Pooley & Lewin 2002), and possibly 3 blue stragglers (even though no clear turn-off can be distinguished). In addition, the star cluster shows an OH (1720 MHz) Maser, which is probably related to the surrounding nebula rather than the star cluster itself (Roberts & Yusef-Zadeh 2005).

- The **Arches cluster** contains 10 radio point sources (Lang et al. 2005) and several colliding wind binaries.

- **MGG11** is a YMC in M82 which may contain a ULX (Kaaret et al. 2001), alhtough the Chandra error box is slightly offset.

- The **Quintuplet cluster** contains the Pistol star (Figer et al. 1998), a candidate for the most massive star in the Galaxy, at a projected distance of about 1 pc, as well as 9 radio point sources (Lang et al. 2005).

- **Westerlund 1** hosts the anomalous x-ray pulsar CXOU J164710.2-455216 (Muno et al. 2006), and a wealth of x-ray sources (Clark et al. 2008).

- **Westerlund 2** hosts the massive Wolf-Rayet binary WR 20a, containing two WN6ha stars, at a distance of 1.1 pc from its center (Rauw et al. 2005).

- **NGC 663 and NGC 6649** contain blue stragglers which found to be the donors of Be/X-ray binary systems (Marco, Negueruela & Motch 2007).

- **Sandage-96** is a $\sim 96,000\,\mathrm{M}_\odot$ star cluster in NGC 2403 in which a type IIp supernova was detected (Wang et al. 2005). This star cluster also exhibits multiple stellar populations (Vinkó et al. 2009).

5.4.1 Planetary nebulae and supernova remnants

The nuclear evolution of a sufficiently massive star ($\gtrsim 8\,\mathrm{M}_\odot$) is associated with a supernova explosion (see §5.3.1), while lower mass stars fizzle into the background after a short, bright post-AGB phase. But following these lower mass events a roughly spherical gas shell—a planetary nebula—remains visible for a much longer time than either the supernova or the post-AGB star, illuminated by the central stellar remnant and shocks as the out-flowing gas encounters the interstellar medium.

Every star experiences either a supernova or a post AGB phase and a cluster of 5×10^4 stars will experience some 350 supernovae, leading to an equal number of remnants, while during the first 100 Myr a similar number of planetary nebulae will form. The formation rate of planetary nebulae and supernova remnants is thus ~ 7/Myr. With an observable lifetime for a nebula of about 10^4 yr, we naively expect to see one nebula for every ~ 14 star clusters. Among 80 YMCs in the Milky Way Galaxy Larsen & Richtler (2006) found 3 with a planetary nebula, consistent with our naive estimate. No planetary nebulae or supernova remnants have so far been found in any of the YMCs in the Local Group. But since only 16 of the clusters listed in Tab. 3 are sufficiently old to have formed white dwarfs from single stellar evolution, the lack of planetary nebulae may be a statistical fluctuation.

5.4.2 Brown dwarfs and planets

We will say little here about brown dwarfs and planets in YMCs since the observations are sparse and the general topic deserves its own review. However, a few words are in order.

Young dense star clusters are generally too distant for planets to be detectable using current methods, and no planets have been found to date (Udry & Santos 2007). Old globular clusters seem to be deficient in planets (e.g. 47 Tuc, Gilliland et al. 2000), possibly because of their low metallicities (Weldrake et al. 2005). However, the recent HARPS discovery of a planet around a metal poor star (Mayor et al. 2009) makes this argument less convincing. The planet found orbiting the 11 ms pulsar B1620-26 in the metal poor environment of the globular cluster M4 (Backer 1993; Thorsett, Arzoumanian & Taylor 1993), was formed by a different mechanism than planets around solar-type stars, and we do not (yet) expect such planets in YMCs. Star clusters in high-metallicity environments, such as Westerlund 1 and NGC 3603, could host a large population of planets, but none have yet been found.

We see no reason why YMCs should be deficient in planets. However, the high interaction rate in a dense cluster could make a planetary system short-lived. Disruption of a planetary system may leave the planet separated from its parent star (Spurzem et al. 2009). Several such free-floating objects have been found in the Orion Trapezium cluster (Lucas & Roche 2000). Once dislocated from its parent star, a planet will easily escape the cluster, though.

5.4.3 YMCs in a galactic context

Due to supernovae and winds from massive stars, YMCs are the sources of cluster winds (Silich, Tenorio-Tagle & Rodríguez-González 2004), which may trigger larger-scale winds and chimneys, as in the Perseus arm of the Milky Way Galaxy (Normandeau, Taylor & Dewdney 1996). Although little studied from the point of view of cluster evolution, this is an important topic that provides a possible and rather natural link between the evolution of a YMC and that of its parent galaxy.

6 Concluding Remarks: Young Globular Clusters?

The discovery of large numbers of young massive star clusters, particularly in other galaxies, over the last decade has led to the realization that such clusters are responsible for a significant fraction of all current star formation in the local universe. The study of these systems, and especially their lifetimes, against various stellar evolutionary and dynamical processes, is therefore of critical importance to several branches of stellar and galactic astrophysics.

Star clusters appear to form with a cluster mass function described by a power-law with index -2. This mass function seems to be the same for both open and globular clusters, and does not depend significantly on the local galactic environment or on the specific characteristics of the giant molecular clouds from which the clusters formed. An important parameter for a young bound cluster appears to be its age relative to its current dynamical time scale $t_{\rm dyn}$. For unbound stellar agglomerates or associations, $t_{\rm dyn}$ exceeds the system age, indicating that the cluster is either extremely young or dissolving into the tidal field of its parent galaxy. For the typical bound star clusters discussed in this review, $t_{\rm dyn}$ is smaller than the current age; for an association it is the other way around.

YMCs evolve and eventually dissolve due to the combined effects of a number of physical processes, the most important (for clusters that survive the early expulsion of their natal gas) being mass loss due to stellar evolution. The most massive clusters, such as those found in the Antennae system, have expected lifetimes comparable to the age of the universe, and we could well imagine that the Antennae will someday be a medium-sized elliptical galaxy with an extended population of intermediate-age clusters having overall properties quite comparable to the old globular clusters seen in other ellipticals.

The seeds of the exotica observed in many present-day globular clusters were initiated during the infancy of those systems, in the strongly coupled mix of stellar dynamics and stellar evolution that characterized their early evolution (in particular dring phase 2). YMCs destined to survive to ages comparable to the globular clusters appear to contain much richer populations of stellar exotica (per unit mass) than are found in the field, and may provide important testbeds for this unique period in cluster evolution. Our limiting cluster age of 100 Myr is chosen in part to include the period when this ecological interplay is strongest.

From an observational point of view, little is known of the formation and evolution of stellar exotica in YMCs, mainly because such clusters are relatively rare. The Milky Way contains only half a dozen, and the closest lies ~ 4 kpc away, too distant for detailed study of the individual stars in its central region. However, a number of studies have drawn connections between YMCs and exotic objects, such as unusual supernovae, magenetars,

x-ray binaries, and ultraluminous x-ray sources, possibly placing YMCs in the same league as the old GCs, which are rich in such objects.

Finally, we return to the term "young globular cluster," which we introduced in §1 but have deliberately avoided throughout this review. Is this an appropriate term for a YMC? A fairly common definition of a globular cluster, similar to that found in many textbooks, appears in the Oxford English Dictionary (2009): "*A roughly spherical cluster of stars, typically seen in galactic halos, containing large numbers of old, metal-poor stars.*" This definition contains several qualifiers that would seem to exclude YMCs, but in many ways the definition itself seems to be a relic of a bygone era.

Our own Galaxy contains a significant population of bulge GCs, and there may well be a disk component among GCs in other galaxies, such as the LMC. In any case, it is quite conceivable that YMCs will in many cases come to populate the halos of their parent galaxies. Since there appears to be little dependence of YMC properties on current galactic location, it seems unreasonable to exclude a YMC from the GC definition based solely on this property. The "low metallicity" qualifier in the definition also seems a side effect rather than a requirement. If we required simply that globular clusters be old—or rather long-lived, as in our YMC definition—the metallicity becomes redundant, merely reflecting the epoch at which they formed. Furthermore, the LMC GCs display a broad range of ages, so any cutoff on age or metallicity would be arbitrary. Lastly, any massive cluster more than a few tens of dynamical times old will necessarily have a smooth, roughly spherical appearance, regardless of metallicity or location.

Applying all of these arguments, we can strip away all of the extraneous qualifying terms in the above GC definition until all that remains is the word "massive." In this view, globular clusters are simply "old massive clusters," the logical descendants of YMCs in the early universe.

Acknowledgments

We are particularly grateful to Douglas Heggie, Søren Larsen, Nate Bastian and Fred Rasio for their careful reading of an earlier version of this manuscript and their useful (and often quite critical) comments. In addition we received very helpful comments from Holger Baumgardt, Melvyn Davies, Richard de Grijs, Diederik Kruijssen and Hans Zinnecker. The results of the N-body simulation shown in Fig. 14 was done on one of the GRAPE-6 BLX64 boards of the European Southern Observatory in Garching. This work was made possible with the financial support of DFG cluster of excellence Origin and Structure of the Universe (www.universe-cluster.de), NASA (grant NNX07AG95G), the National Science Foundation (NSF, via grant AST-0708299), Nederlandse Onderzoekschool voor Astronomie (NOVA), het Leids-Kerkhoven Bosscha Fonds (LKBF), the Kavli Institute for Theoretical Physics (KITP, through their hosptality and NSF grant PHY05-51164), and in particular of the Nederlandse Organizatie voor Wetenschappelijk Onderzoek (NWO, via grants #643.200.503 and #639.073.803) and the Nederlandse Computer Faciliteiten (NCF, via project #SH-095-08).

References

Aarseth SJ. 2003. *Gravitational N-Body Simulations*. Gravitational N-Body Simulations, by Sverre J. Aarseth, pp. 430. ISBN 0521432723. Cambridge, UK: Cambridge University Press, November 2003.

Abel T, Bryan GL, Norman ML. 2002. *Science* 295:93–98

Abt HA. 1983. *ARA&A* 21:343–372

Ahmad A, Cohen L. 1973a. *J. of Comp. Phys.* 12:289

Ahmad A, Cohen L. 1973b. *ApJ* 179:885–896

Allison RJ, Goodwin SP, Parker RJ, de Grijs R, Portegies Zwart SF, Kouwenhoven MBN. 2009. *ApJL* 700:L99–L103

Ambartsumian VA. 1938. *Sci. Mem. Leningrade State Univ. #22, ser. Math. Sci. (astronomy)* 4:19

Anders P, de Grijs R, Fritze-v. Alvensleben U, Bissantz N. 2004. *MNRAS* 347:17–28

Andersen M, Zinnecker H, Moneti A, McCaughrean MJ, Brandl B, et al. 2009. *ApJ* 707:1347–1360

Antonov VA. 1962. *Solution of the problem of stability of stellar system Emden's density law and the spherical distribution of velocities*

Applegate JH. 1986. *ApJ* 301:132–144

Arp H, Sandage A. 1985. *AJ* 90:1163–1171

Arzoumanian Z, Chernoff DF, Cordes JM. 2002. *ApJ* 568:289–301

Ascenso J, Alves J, Lago MTVT. 2009. *A&A* 495:147–155

Ascenso J, Alves J, Vicente S, Lago MTVT. 2007. *A&A* 476:199–215

Ashman KM, Zepf SE. 2001. *AJ* 122:1888–1895

Backer DC. 1993. In *Planets Around Pulsars*, ed. J. A. Phillips, S. E. Thorsett, & S. R. Kulkarni, vol. 36 of *Astronomical Society of the Pacific Conference Series*

Bacon D, Sigurdsson S, Davies MB. 1996. *MNRAS* 281:830–846

Bahcall JN, Wolf RA. 1976. *ApJ* 209:214–232

Barmby P, Perina S, Bellazzini M, Cohen JG, Hodge PW, et al. 2009. *AJ* 138:1667–1680

Barnes J, Hut P. 1986. *Nat* 324:446–449

Bastian N. 2008. *MNRAS* 390:759–768

Bastian N, Covey KR, Meyer MR. 2010. *ARA&A , in press (arXiv:1001.2965)*

Bastian N, de Mink SE. 2009. *MNRAS* 398:L11–L15

Bastian N, Gieles M, Goodwin SP, Trancho G, Smith LJ, et al. 2008. *MNRAS* 389:223–230

Bastian N, Gieles M, Lamers HJGLM, Scheepmaker RA, de Grijs R. 2005. *A&A* 431:905–924

Bastian N, Konstantopoulos I, Smith LJ, Trancho G, Westmoquette MS, Gallagher JS. 2007. *MNRAS* 379:1333–1342

Bastian N, Saglia RP, Goudfrooij P, Kissler-Patig M, Maraston C, et al. 2006. *A&A* 448:881–891

Bastian N, Trancho G, Konstantopoulos IS, Miller BW. 2009. *ApJ* 701:607–619

Bate MR, Bonnell IA, Bromm V. 2003. *MNRAS* 339:577–599

Battinelli P, Capuzzo-Dolcetta R. 1991. *MNRAS* 249:76–83

Baumgardt H. 1998. *A&A* 330:480–491

Baumgardt H. 2001. *MNRAS* 325:1323–1331

Baumgardt H, De Marchi G, Kroupa P. 2008. *ApJ* 685:247–253

Baumgardt H, Kroupa P. 2007. *MNRAS* 380:1589–1598

Baumgardt H, Kroupa P, Parmentier G. 2008. *MNRAS* 384:1231–1241

Baumgardt H, Makino J. 2003. *MNRAS* 340:227–246

Baumgardt H, Makino J, Hut P. 2005. *ApJ* 620:238–243

Bell EF, Zucker DB, Belokurov V, Sharma S, Johnston KV, et al. 2008. *ApJ* 680:295–311

Bellazzini M, Fusi Pecci F, Messineo M, Monaco L, Rood RT. 2002. *AJ* 123:1509–1527

Belleman RG, Bédorf J, Portegies Zwart SF. 2008. *New Astronomy* 13:103–112

Benz W, Hills JG. 1987. *ApJ* 323:614–628

Bettwieser E, Sugimoto D. 1984. *MNRAS* 208:493–509

Bhattacharya D, van den Heuvel EPJ. 1991. *PhysRep* 203:1–124

Bik A, Lamers HJGLM, Bastian N, Panagia N, Romaniello M. 2003. *A&A* 397:473–486

Binney J, Tremaine S. 2008. *Galactic Dynamics: Second Edition*. Princeton University Press

Bisseling RH. 2004. *Parallel Scientific Computation: A Structured Approach using BSP and MPI*. Oxford University Press, pp. 324. ISBN 0-19-852939-2, March 2004.

Bonnell IA, Bate MR. 2006. *MNRAS* 370:488–494

Bonnell IA, Bate MR, Vine SG. 2003. *MNRAS* 343:413–418

Bosch G, Terlevich E, Terlevich R. 2009. *AJ* 137:3437–3441

Boutloukos SG, Lamers HJGLM. 2003. *MNRAS* 338:717–732

Brandl B, Sams BJ, Bertoldi F, Eckart A, Genzel R, et al. 1996. *ApJ* 466:254

Brandner W, Clark JS, Stolte A, Waters R, Negueruela I, Goodwin SP. 2008. *A&A* 478:137–149

Bruzual G, Charlot S. 2003. *MNRAS* 344:1000–1028

Caldwell N, Harding P, Morrison H, Rose JA, Schiavon R, Kriessler J. 2009. *AJ* 137:94–110

Campbell B, Hunter DA, Holtzman JA, Lauer TR, Shayer EJ, et al. 1992. *AJ* 104:1721–1742

Campbell MA, Evans CJ, Mackey AD, Gieles M, Alves J, et al. 2010. *MNRAS , in press (arXiv:1002.0288)*

Cantiello M, Brocato E, Blakeslee JP. 2009. *A&A* 503:87–101

Cappellaro E, Evans R, Turatto M. 1999. *A&A* 351:459–466

Carretta E, Bragaglia A, Gratton RG, Lucatello S. 2008. *ArXiv e-prints*

Casertano S, Hut P. 1985. *ApJ* 298:80–94

Chabrier G. 2003. *PASP* 115:763–795

Chandar R, Bianchi L, Ford HC. 2000. *AJ* 120:3088–3097

Chandar R, Bianchi L, Ford HC, Salasnich B. 1999. *PASP* 111:794–800

Chandar R, Fall SM, Whitmore BC. 2006. *ApJL* 650:L111–L114

Chatterjee S, Fregeau JM, Rasio FA. 2008. In *IAU Symposium*, ed. E. Vesperini, M. Giersz, & A. Sills, vol. 246 of *IAU Symposium*

Chernoff DF, Weinberg MD. 1990. *ApJ* 351:121–156

Chiosi E, Vallenari A, Held EV, Rizzi L, Moretti A. 2006. *A&A* 452:179–193

Clark JS, Muno MP, Negueruela I, Dougherty SM, Crowther PA, et al. 2008. *A&A* 477:147–163

Clark JS, Negueruela I, Crowther PA, Goodwin SP. 2005. *A&A* 434:949–969

Clark JS, Negueruela I, Davies B, Larionov VM, Ritchie BW, et al. 2009. *A&A* 498:109–114

Clarke CJ, Bonnell IA, Hillenbrand LA. 2000. *Protostars and Planets IV* :151

Cohn H. 1979. *ApJ* 234:1036–1053

Cohn H. 1980. *ApJ* 242:765–771

Corbel S, Eikenberry SS. 2004. *A&A* 419:191–201

Cordes JM, Chernoff DF. 1998. *ApJ* 505:315–338

Crowther PA, Hadfield LJ, Clark JS, Negueruela I, Vacca WD. 2006. *MNRAS* 372:1407–1424

Davies B. 2009. *ArXiv e-prints*

Davies B, Figer DF, Kudritzki R, Trombley C, Kouveliotou C, Wachter S. 2009. *ArXiv e-prints*

Davies B, Figer DF, Kudritzki RP, MacKenty J, Najarro F, Herrero A. 2007. *ApJ* 671:781–801

Davies B, Figer DF, Law CJ, Kudritzki R, Najarro F, et al. 2008. *ApJ* 676:1016–1028

Davies MB. 1995. *MNRAS* 276:887–905

Davies MB, Amaro-Seoane P, Bassa C, Dale J, de Angeli F, et al. 2006. *New Astronomy* 12:201–214

Davies MB, Piotto G, de Angeli F. 2004. *MNRAS* 349:129–134

de Grijs R, Anders P. 2006. *MNRAS* 366:295–307

de Grijs R, Fritze-v. Alvensleben U, Anders P, Gallagher JS, Bastian N, et al. 2003. *MNRAS* 342:259–273

de Grijs R, Gilmore GF, Johnson RA, Mackey AD. 2002a. *MNRAS* 331:245–258

de Grijs R, Gilmore GF, Mackey AD, Wilkinson MI, Beaulieu SF, et al. 2002b. *MNRAS* 337:597–608

de Grijs R, Goodwin SP. 2008. *MNRAS* 383:1000–1006

de Grijs R, Parmentier G. 2007. *Chinese Journal of Astronomy and Astrophysics* 7:155–186

de Wit WJ, Testi L, Palla F, Zinnecker H. 2005. *A&A* 437:247–255

Decressin T, Meynet G, Charbonnel C, Prantzos N, Ekström S. 2007. *A&A* 464:1029–1044

Dehnen W. 2000. *ApJL* 536:L39–L42

Deiters S, Spurzem R. 2001. *Astronomical and Astrophysical Transactions* 20:47–50

DeLuca A, Caraveo PA, Esposito P, Hurley K. 2009. *ApJ* 692:158–161

D'Ercole A, Vesperini E, D'Antona F, McMillan SLW, Recchi S. 2008. *MNRAS* 391:825–843

Dias WS, Alessi BS, Moitinho A, Lépine JRD. 2002. *A&A* 389:871–873

Djorgovski SG, Meylan G, eds. 1993. *Structure and dynamics of globular clusters*, vol. 50 of *Astronomical Society of the Pacific Conference Series*

Dorband EN, Hemsendorf M, Merritt D. 2003. *Journal of Computational Physics* 185:484–511

Drukier GA. 1996. *MNRAS* 280:498–514

Drukier GA, Fahlman GG, Richer HB. 1992. *ApJ* 386:106–119

Duquennoy A, Mayor M. 1991. *A&A* 248:485–524

Ebisuzaki T, Makino J, Fukushige T, Taiji M, Sugimoto D, et al. 1993. *Publ. Astr. Soc. Japan* 45:269–278

Efremov YN. 1991. *Pis ma Astronomicheskii Zhurnal* 17:404–409

Efremov YN. 2000. *Astronomy Letters* 26:558–564

Eggleton P. 2006. *Evolutionary Processes in Binary and Multiple Stars*

Eggleton PP, Fitchett MJ, Tout CA. 1989. *ApJ* 347:998–1011

Einsel C, Spurzem R. 1999. *MNRAS* 302:81–95

Elmegreen BG. 2007. *ApJ* 668:1064–1082

Elmegreen BG, Efremov YN. 1997. *ApJ* 480:235

Elson RAW, Fall SM. 1985a. *PASP* 97:692–696

Elson RAW, Fall SM. 1985b. *ApJ* 299:211–218

Elson RAW, Fall SM, Freeman KC. 1987. *ApJ* 323:54–78

Elson RAW, Freeman KC, Lauer TR. 1989. *ApJL* 347:L69–L71

Espinoza P, Selman FJ, Melnick J. 2009. *ArXiv e-prints*

Fabbiano G, Zezas A, Murray SS. 2001. *ApJ* 554:1035–1043

Fabian AC, Pringle JE, Rees MJ. 1975. *MNRAS* 172:15P

Fall SM, Chandar R, Whitmore BC. 2005. *ApJL* 631:L133–L136

Fall SM, Rees MJ. 1985. *ApJ* 298:18–26

Fall SM, Zhang Q. 2001. *ApJ* 561:751–765

Fellhauer M, Wilkinson MI, Kroupa P. 2009. *MNRAS* 397:954–962

Ferraro FR, Fusi Pecci F, Bellazzini M. 1995. *A&A* 294:80–88

Figer DF, MacKenty JW, Robberto M, Smith K, Najarro F, et al. 2006. *ApJ* 643:1166–1179

Figer DF, McLean IS, Morris M. 1999. *ApJ* 514:202–220

Figer DF, Najarro F, Gilmore D, Morris M, Kim SS, et al. 2002. *ApJ* 581:258–275

Figer DF, Najarro F, Morris M, McLean IS, Geballe TR, et al. 1998. *ApJ* 506:384–404

Fleck J, Boily C, Lançon A, Heggie D, Deiters S. 2005. In *SF2A-2005: Semaine de l'Astrophysique Francaise*, ed. F. Casoli, T. Contini, J. M. Hameury, & L. Pagani

Fleck JJ, Boily CM, Lançon A, Deiters S. 2006. *MNRAS* 369:1392–1406

Foley RJ, Li W, Moore M, Wong DS, Pooley D, Filippenko AV. 2006. *Central Bureau Electronic Telegrams* 695:1

Forte JC, Vega EI, Faifer F. 2009. *MNRAS* 397:1003–1020

Foster I, Kesselman C, eds. 2004. *The Grid: Blueprint for a New Computing Infrastructure*. Published by Morgan Kaufmann

Fregeau JM, Cheung P, Portegies Zwart SF, Rasio FA. 2004. *MNRAS* 352:1–19

Fregeau JM, Gürkan MA, Joshi KJ, Rasio FA. 2003. *ApJ* 593:772–787

Fregeau JM, Rasio FA. 2007. *ApJ* 658:1047–1061

Freitag M, Benz W. 2001. *A&A* 375:711–738

Freitag M, Benz W. 2005. *MNRAS* 358:1133–1158

Freitag M, Rasio FA, Baumgardt H. 2006. *MNRAS* 368:121–140

Fujii M, Iwasawa M, Funato Y, Makino J. 2007. *Publ. Astr. Soc. Japan* 59:1095–

Fukushige T, Heggie DC. 1995. *MNRAS* 276:206–218

Fukushige T, Heggie DC. 2000. *MNRAS* 318:753–761

Gaburov E, Gieles M. 2008. *MNRAS* 391:190–196

Gaburov E, Harfst S, Portegies Zwart SF. 2009. *New Astronomy* 14:630–637

Gaburov E, Lombardi JC, Portegies Zwart S. 2008. *MNRAS* 383:L5–L9

Gao B, Goodman J, Cohn H, Murphy B. 1991. *ApJ* 370:567–582

Gao Y, Wang QD, Appleton PN, Lucas RA. 2003. *ApJL* 596:L171–L174

Geyer MP, Burkert A. 2001. *MNRAS* 323:988–994

Gieles M. 2009. *MNRAS* 394:2113

Gieles M, Athanassoula E, Portegies Zwart SF. 2007. *MNRAS* 376:809–819

Gieles M, Baumgardt H. 2008. *MNRAS* 389:L28–L32

Gieles M, Lamers HJGLM, Portegies Zwart SF. 2007. *ApJ* 668:268–274

Gieles M, Larsen SS, Bastian N, Stein IT. 2006a. *A&A* 450:129–145

Gieles M, Larsen SS, Scheepmaker RA, Bastian N, Haas MR, Lamers HJGLM. 2006b. *A&A* 446:L9–L12

Gieles M, Portegies Zwart SF, Baumgardt H, Athanassoula E, Lamers HJGLM, et al. 2006c. *MNRAS* 371:793–804

Gieles M, Sana H, Portegies Zwart SF. 2009. *MNRAS, in press (arXiv:0911.1557)*

Giersz M. 1998. *MNRAS* 298:1239–1248

Giersz M. 2001. *MNRAS* 324:218–230

Giersz M. 2006. *MNRAS* 371:484–494

Giersz M, Heggie DC. 1994. *MNRAS* 268:257

Giersz M, Heggie DC. 2009. *MNRAS* 395:1173–1183

Giersz M, Spurzem R. 2003. *MNRAS* 343:781–795

Gies DR. 1987. *ApJS* 64:545–563

Gilliland RL, Brown TM, Guhathakurta P, Sarajedini A, Milone EF, et al. 2000. *ApJL* 545:L47–L51

Girardi L, Chiosi C, Bertelli G, Bressan A. 1995. *A&A* 298:87

Glebbeek E, Gaburov E, de Mink SE, Pols OR, Portegies Zwart SF. 2009. *A&A* 497:255–264

Glebbeek E, Pols OR, Hurley JR. 2008. *A&A* 488:1007–1015

Gnedin OY, Ostriker JP. 1997. *ApJ* 474:223

González-Martín O, Fabian AC, Sanders JS. 2006. *MNRAS* 367:1132–1138

Goodman J, Hut P. 1989. *Nat* 339:40–42

Goodwin SP. 2009. *Ap&SS* :108

Goodwin SP, Bastian N. 2006. *MNRAS* 373:752–758

Gouliermis D, Keller SC, Kontizas M, Kontizas E, Bellas-Velidis I. 2004. *A&A* 416:137–155

Grisé F, Pakull MW, Soria R, Motch C, Smith IA, et al. 2008. *A&A* 486:151–163

Gualandris A, Colpi M, Portegies Zwart S, Possenti A. 2005. *ApJ* 618:845–851

Gürkan MA, Freitag M, Rasio FA. 2004. *ApJ* 604:632–652

Gutermuth RA, Megeath ST, Pipher JL, Williams JP, Allen LE, et al. 2005. *ApJ* 632:397–420

Gvaramadze VV, Bomans DJ. 2008. *A&A* 490:1071–1077

Hamada T, Iitaka T. 2007. *ArXiv Astrophysics e-prints*

Harayama Y, Eisenhauer F, Martins F. 2008. *ApJ* 675:1319–1342

Harfst S, Gualandris A, Merritt D, Spurzem R, Portegies Zwart S, Berczik P. 2007. *New Astronomy* 12:357–377

Harfst S, Portegies Zwart S, Stolte A. 2009. *ArXiv e-prints*

Harris J, Zaritsky D. 2009. *AJ* 138:1243–1260

Harris WE. 1996. *AJ* 112:1487

Harris WE. 2001. In *Saas-Fee Advanced Course 28: Star Clusters*, ed. L. Labhardt & B. Binggeli

Heger A, Fryer CL, Woosley SE, Langer N, Hartmann DH. 2003. *ApJ* 591:288–300

Heggie D, Hut P. 2003. *The Gravitational Million-Body Problem: A Multidisciplinary Approach to Star Cluster Dynamics*. The Gravitational Million-Body Problem: A Multidisciplinary Approach to Star Cluster Dynamics, by Douglas Heggie and Piet Hut. Cambridge University Press, 2003, 372 pp.

Heggie DC. 1975. *MNRAS* 173:729–787

Heggie DC. 1992. *Nat* 359:772–773

Heggie DC. 2001. In *The Restless Universe*, ed. B. A. Steves & A. J. Maciejewski

Heggie DC, Aarseth SJ. 1992. *MNRAS* 257:513–536

Heggie DC, Giersz M. 2008. *MNRAS* 389:1858–1870

Heggie DC, Hut P, Mineshige S, Makino J, Baumgardt H. 2007. *Publ. Astr. Soc. Japan* 59:L11–L14

Heggie DC, Inagaki S, McMillan SLW. 1994. *MNRAS* 271:706

Hénon M. 1965. *Annales d'Astrophysique* 28:62

Henon M. 1973. In *Saas-Fee Advanced Course 3: Dynamical Structure and Evolution of Stellar Systems*, ed. G. Contopoulos, M. Henon, & D. Lynden-Bell

Hillenbrand LA, Hartmann LW. 1998. *ApJ* 492:540

Hills JG. 1975. *AJ* 80:809–825

Hills JG. 1980. *ApJ* 235:986–991

Hills JG, Day CA. 1976. *Astrophys. Lett.* 17:87

Ho LC, Filippenko AV. 1996. *ApJL* 466:L83

Hodge P. 1987. *PASP* 99:724–729

Hodge PW. 1961. *ApJ* 133:413

Hodge PW, Krienke OK, Bellazzini M, Perina S, Barmby P, et al. 2009. *AJ* 138:770–779

Hoekstra A. G, Portegies Zwart S, Bubak M, Sloot P. 2008. *Towards Distributed Petascale Computing*. Petascale Computing: Algorithms and Applications, by David A. Bader (Ed.). Chapman & Hall/CRC computational science series 565pp. (ISBN: 9781584889090, ISBN 10: 1584889098)

Holtzman JA, Faber SM, Shaya EJ, Lauer TR, Groth J, et al. 1992. *AJ* 103:691–702

Huff EM, Stahler SW. 2006. *ApJ* 644:355–363

Hunter DA, Elmegreen BG, Dupuy TJ, Mortonson M. 2003. *AJ* 126:1836–1848

Hunter DA, O'Connell RW, Gallagher JS, Smecker-Hane TA. 2000. *AJ* 120:2383–2401

Hunter DA, Shaya EJ, Holtzman JA, Light RM, O'Neil Jr. EJ, Lynds R. 1995. *ApJ* 448:179

Hurley JR. 2007. *MNRAS* 379:93–99

Hurley JR, Aarseth SJ, Shara MM. 2007. *ApJ* 665:707–718

Hurley JR, Pols OR, Tout CA. 2000. *MNRAS* 315:543–569

Hurley JR, Shara MM. 2002. *ApJ* 570:184–189

Hurley JR, Tout CA, Aarseth SJ, Pols OR. 2001. *MNRAS* 323:630–650

Hurley JR, Tout CA, Pols OR. 2002. *MNRAS* 329:897–928

Hut P, Bahcall JN. 1983. *ApJ* 268:319–341

Hut P, Djorgovski S. 1992. *Nat* 359:806–808

Hut P, Inagaki S. 1985. *ApJ* 298:502–520

Hut P, Makino J, McMillan S. 1988. *Nat* 336:31–35

Hut P, Shara MM, Aarseth SJ, Klessen RS, Lombardi Jr. JC, et al. 2003. *New Astronomy* 8:337–370

Inagaki S, Saslaw WC. 1985. *ApJ* 292:339–347

Innanen KA, Harris WE, Webbink RF. 1983. *AJ* 88:338–360

Jordán A, McLaughlin DE, Côté P, Ferrarese L, Peng EW, et al. 2007. *ApJS* 171:101–145

Joshi KJ, Rasio FA, Portegies Zwart S. 2000. *ApJ* 540:969–982

Kaaret P, Prestwich AH, Zezas A, Murray SS, Kim DW, et al. 2001. *MNRAS* 321:L29–L32

Karakas A, Lattanzio JC. 2007. *Publications of the Astronomical Society of Australia* 24:103–117

Kennicutt Jr. RC. 1998. *ARA&A* 36:189–232

Kennicutt Jr. RC, Chu YH. 1988. *AJ* 95:720–730

Kharchenko NV, Piskunov AE, Röser S, Schilbach E, Scholz RD. 2005. *A&A* 440:403–408

Kim E, Einsel C, Lee HM, Spurzem R, Lee MG. 2002. *MNRAS* 334:310–322

Kim E, Lee HM, Spurzem R. 2004. *MNRAS* 351:220–236

Kim SS, Figer DF, Kudritzki RP, Najarro F. 2006. *ApJL* 653:L113–L116

King AR. 2002. *MNRAS* 335:L13–L16

King AR, Davies MB, Ward MJ, Fabbiano G, Elvis M. 2001. *ApJL* 552:L109–L112

King IR. 1962. *AJ* 67:471

King IR. 1966. *AJ* 71:64–75

Klessen RS. 2001. *ApJ* 556:837–846

Klose S, Henden AA, Geppert U, Greiner J, Guetter HH, et al. 2004. *ApJL* 609:L13–L16

Knigge C, Leigh N, Sills A. 2009. *Nat* 457:288–290

Kouveliotou C, Strohmayer T, Hurley K, van Paradijs J, Finger MH, et al. 1999. *ApJL* 510:L115–L118

Kouwenhoven MBN, de Grijs R. 2008. *A&A* 480:103–114

Kroupa P. 1995. *MNRAS* 277:1491

Kroupa P. 2001. *MNRAS* 322:231–246

Kroupa P. 2008. In *Lecture Notes in Physics, Berlin Springer Verlag*, ed. S. J. Aarseth, C. A. Tout, & R. A. Mardling, vol. 760 of *Lecture Notes in Physics, Berlin Springer Verlag*

Kulkarni SR, Hut P, McMillan S. 1993. *Nat* 364:421–423

Kupi G, Amaro-Seoane P, Spurzem R. 2006. *MNRAS* 371:L45–L49

Lada CJ, Lada EA. 2003. *ARA&A* 41:57–115

Lada CJ, Margulis M, Dearborn D. 1984. *ApJ* 285:141–152

Lamers HJGLM, Gieles M, Bastian N, Baumgardt H, Kharchenko NV, Portegies Zwart S. 2005. *A&A* 441:117–129

Lamers HJGLM, Gieles M, Portegies Zwart SF. 2005. *A&A* 429:173–179

Lang CC, Johnson KE, Goss WM, Rodríguez LF. 2005. *AJ* 130:2185–2196

Larsen SS. 2002. *AJ* 124:1393–1409

Larsen SS. 2004. *A&A* 416:537–553

Larsen SS. 2006. In *Planets to Cosmology: Essential Science in the Final Years of the Hubble Space Telescope*, eds. M Livio, S Casertano

Larsen SS. 2009a. *A&A* 494:539–551

Larsen SS. 2009b. *Phil. Trans. R. Soc. London A , in press (arXiv:0911.0796)*

Larsen SS, Origlia L, Brodie J, Gallagher JS. 2008. *MNRAS* 383:263–276

Larsen SS, Richtler T. 2000. *A&A* 354:836–846

Larsen SS, Richtler T. 2004. *A&A* 427:495–504

Larsen SS, Richtler T. 2006. *A&A* 459:103–111

Larson RB. 1981. *MNRAS* 194:809–826

Leonard PJT. 1989. *AJ* 98:217–226

Leonard PJT. 1996. *ApJ* 470:521

Liu JF, Bregman JN, Irwin J, Seitzer P. 2002. *ApJL* 581:L93–L96

Liu JF, Bregman JN, Seitzer P. 2004. *ApJ* 602:249–256

Lombardi JC, Thrall AP, Deneva JS, Fleming SW, Grabowski PE. 2003. *MNRAS* 345:762–780

Lucas PW, Roche PF. 2000. *MNRAS* 314:858–864

Lutz D. 1991. *A&A* 245:31–40

Lynden-Bell D, Eggleton PP. 1980. *MNRAS* 191:483–498

Lynden-Bell D, Wood R. 1968. *MNRAS* 138:495

Lyne AG, Lorimer DR. 1994. *Nat* 369:127–129

Lynga G. 1982. *A&A* 109:213–222

Ma J, Fan Z, de Grijs R, Wu Z, Zhou X, et al. 2009. *AJ* 137:4884–4896

Mackey AD, Broby Nielsen P. 2007. *MNRAS* 379:151–158

Mackey AD, Gilmore GF. 2003. *MNRAS* 338:85–119

Mackey AD, Wilkinson MI, Davies MB, Gilmore GF. 2007. *MNRAS* 379:L40–L44

Mackey AD, Wilkinson MI, Davies MB, Gilmore GF. 2008. *MNRAS* 386:65–95

Madhusudhan N, Justham S, Nelson L, Paxton B, Pfahl E, et al. 2006. *ApJ* 640:918–922

Maíz-Apellániz J. 2001. *ApJ* 563:151–162

Maíz-Apellániz J. 2002. In *Extragalactic Star Clusters*, eds. DP Geisler, EK Grebel, D Minniti, vol. 207 of *IAU Symposium*

Makino J. 1996. *ApJ* 471:796

Makino J. 2002. *New Astronomy* 7:373–384

Makino J. 2005. *ArXiv Astrophysics e-prints*

Makino J, Aarseth SJ. 1992. *Publ. Astr. Soc. Japan* 44:141–151

Makino J, Hut P, Kaplan M, Saygın H. 2006. *New Astronomy* 12:124–133

Makino J, Taiji M. 1998. *Scientific simulations with special-purpose computers : The GRAPE systems*. Scientific simulations with special-purpose computers : The GRAPE systems /by Junichiro Makino & Makoto Taiji. Chichester ; Toronto : John Wiley & Sons, c1998.

Makishima K, Kubota A, Mizuno T, Ohnishi T, Tashiro M, et al. 2000. *ApJ* 535:632–643

Marco A, Negueruela I, Motch C. 2007. In *Massive Stars in Interactive Binaries*, eds. N St.-Louis, AFJ Moffat, vol. 367 of *Astronomical Society of the Pacific Conference Series*

Mason BD, Hartkopf WI, Gies DR, Henry TJ, Helsel JW. 2009. *AJ* 137:3358–3377

Massey P, Hunter DA. 1998. *ApJ* 493:180

Mayor M, Udry S, Lovis C, Pepe F, Queloz D, et al. 2009. *A&A* 493:639–644

McCrady N, Gilbert AM, Graham JR. 2003. *ApJ* 596:240–252

McCrady N, Graham JR. 2007. *ApJ* 663:844–856

McCrady N, Graham JR, Vacca WD. 2005. *ApJ* 621:278–284

McCrea WH. 1964. *MNRAS* 128:147

McLaughlin DE. 2000. *ApJ* 539:618–640

McLaughlin DE, Anderson J, Meylan G, Gebhardt K, Pryor C, et al. 2006. *ApJS* 166:249–297

McLaughlin DE, van der Marel RP. 2005. *ApJS* 161:304–360

McMillan S, Hut P, Makino J. 1990. *ApJ* 362:522–537

McMillan S, Hut P, Makino J. 1991. *ApJ* 372:111–124

McMillan SLW. 1986. In *The Use of Supercomputers in Stellar Dynamics*, ed. P. Hut & S. L. W. McMillan, vol. 267 of *Lecture Notes in Physics, Berlin Springer Verlag*

McMillan SLW, Aarseth SJ. 1993. *ApJ* 414:200–212

McMillan SLW, Vesperini E, Portegies Zwart SF. 2007. *ApJL* 655:L45–L49

Mengel S, Lehnert MD, Thatte N, Genzel R. 2002. *A&A* 383:137–152

Mengel S, Lehnert MD, Thatte NA, Vacca WD, Whitmore B, Chandar R. 2008. *A&A* 489:1091–1105

Mengel S, Tacconi-Garman LE. 2007. *A&A* 466:151–155

Merritt D, Piatek S, Portegies Zwart S, Hemsendorf M. 2004. *ApJL* 608:L25–L28

Mészáros P. 2002. *ARA&A* 40:137–169

Meurer GR, Heckman TM, Leitherer C, Kinney A, Robert C, Garnett DR. 1995. *AJ* 110:2665

Miller BW, Whitmore BC, Schweizer F, Fall SM. 1997. *AJ* 114:2381

Miller GE, Scalo JM. 1979. *ApJS* 41:513–547

Miller JM, Fabbiano G, Miller MC, Fabian AC. 2003. *ApJL* 585:L37–L40

Miller MC, Hamilton DP. 2002. *MNRAS* 330:232–240

Milone AP, Bedin LR, Piotto G, Anderson J. 2009. *A&A* 497:755–771

Milone AP, Piotto G, Bedin LR, Sarajedini A. 2008. *Memorie della Societa Astronomica Italiana* 79:623

Mirabel IF, Fuchs Y, Chaty S. 2000. In *Gamma-ray Bursts, 5th Huntsville Symposium*, ed. R. M. Kippen, R. S. Mallozzi, & G. J. Fishman, vol. 526 of *American Institute of Physics Conference Series*

Mirabel IF, Rodrigues I, Liu QZ. 2004. *A&A* 422:L29–L32

Moeckel N, Bonnell IA. 2009. *MNRAS* 400:657–664

Moll SL, Mengel S, de Grijs R, Smith LJ, Crowther PA. 2007. *MNRAS* 382:1877–1888

Moore B, Quinn T, Governato F, Stadel J, Lake G. 1999. *MNRAS* 310:1147–1152

Muno MP, Clark JS, Crowther PA, Dougherty SM, de Grijs R, et al. 2006. *ApJL* 636:L41–L44

Muno MP, Gaensler BM, Clark JS, de Grijs R, Pooley D, et al. 2007. *MNRAS* 378:L44–L48

Narayan R, Piran T, Shemi A. 1991. *ApJL* 379:L17–L20

Narbutis D, Vansevičius V, Kodaira K, Bridžius A, Stonkutė R. 2008. *ApJS* 177:174–180

Nitadori K, Makino J. 2008. *New Astronomy* 13:498–507

Nitadori K, Makino J, Hut P. 2006. *New Astronomy* 12:169–181

Normandeau M, Taylor AR, Dewdney PE. 1996. *Nat* 380:687–689

Offner SSR, Hansen CE, Krumholz MR. 2009. *ApJL* 704:L124–L128

Ogilvie GI, Lin DNC. 2004. *ApJ* 610:477–509

Oort JH, Kerr FJ, Westerhout G. 1958. *MNRAS* 118:379

Östlin G, Cumming RJ, Bergvall N. 2007. *A&A* 461:471–483

Ostriker JP, Spitzer LJ, Chevalier RA. 1972. *ApJL* 176:L51

Paczynski B. 1998. *ApJL* 494:L45

Park W, Park HS, Lee MG. 2009. *ApJ* 700:103–113

Parker RJ, Goodwin SP. 2007. *MNRAS* 380:1271–1275

Parmentier G, de Grijs R. 2008. *MNRAS* 383:1103–1120

Parmentier G, Gilmore G. 2007. *MNRAS* 377:352–372

Patruno A, Portegies Zwart S, Dewi J, Hopman C. 2006. *MNRAS* 370:L6–L9

Peacock MB, Maccarone TJ, Knigge C, Kundu A, Waters CZ, et al. 2010. *MNRAS* :28

Perina S, Barmby P, Beasley MA, Bellazzini M, Brodie JP, et al. 2009. *A&A* 494:933–948

Pfahl E, Rappaport S, Podsiadlowski P. 2002. *ApJ* 573:283–305

Pfahl E, Scannapieco E, Bildsten L. 2009. *ArXiv e-prints*

Pfalzner S. 2009. *A&A* 498:L37–L40

Piotto G. 2008. *Memorie della Societa Astronomica Italiana* 79:334

Piotto G, Villanova S, Bedin LR, Gratton R, Cassisi S, et al. 2005. *ApJ* 621:777–784

Piskunov AE, Kharchenko NV, Röser S, Schilbach E, Scholz RD. 2006. *A&A* 445:545–565

Piskunov AE, Schilbach E, Kharchenko NV, Röser S, Scholz RD. 2008. *A&A* 477:165–172

Plummer HC. 1911. *MNRAS* 71:460–470

Pooley D, Lewin WHG, Anderson SF, Baumgardt H, Filippenko AV, et al. 2003. *ApJL* 591:L131–L134

Portegies Zwart SF, Baumgardt H, Hut P, Makino J, McMillan SLW. 2004. *Nat* 428:724–726

Portegies Zwart SF, Belleman RG, Geldof PM. 2007. *New Astronomy* 12:641–650

Portegies Zwart SF, Hut P, Verbunt F. 1997. *A&A* 328:130–142

Portegies Zwart SF, Makino J, McMillan SLW, Hut P. 1999. *A&A* 348:117–126

Portegies Zwart SF, McMillan S, Groen D, Gualandris A, Sipior M, Vermin W. 2008. *New Astronomy* 13:285–295

Portegies Zwart SF, McMillan S, Harfst S, Groen D, Fujii M, et al. 2009. *New Astronomy* 14:369–378

Portegies Zwart SF, McMillan SLW. 2002. *ApJ* 576:899–907

Portegies Zwart SF, McMillan SLW, Hut P, Makino J. 2001. *MNRAS* 321:199–226

Portegies Zwart SF, McMillan SLW, Makino J. 2007. *MNRAS* 374:95–106

Portegies Zwart SF, Pooley D, Lewin WHG. 2002. *ApJ* 574:762–770

Portegies Zwart SF, Takahashi K. 1999. *Celestial Mechanics and Dynamical Astronomy* 73:179–186

Portegies Zwart SF, van den Heuvel EPJ. 2007. *Nat* 450:388–389

Portegies Zwart SF, Verbunt F. 1996. *A&A* 309:179–196

Prantzos N, Charbonnel C. 2006. *A&A* 458:135–149

Price DJ, Bate MR. 2009. *MNRAS* 398:33–46

Proszkow EM, Adams FC, Hartmann LW, Tobin JJ. 2009. *ApJ* 697:1020–1031

Quinlan GD. 1996. *New Astronomy* 1:255–270

Rauw G, Crowther PA, De Becker M, Gosset E, Nazé Y, et al. 2005. *A&A* 432:985–998

Read JI, Wilkinson MI, Evans NW, Gilmore G, Kleyna JT. 2006. *MNRAS* 366:429–437

Roberts DA, Yusef-Zadeh F. 2005. *AJ* 129:805–808

Sabbi E, Sirianni M, Nota A, Tosi M, Gallagher J, et al. 2008. *AJ* 135:173–181

Safronov VS. 1969. *Evoliutsiia doplanetnogo oblaka.*

Salpeter EE. 1955. *ApJ* 121:161

San Roman I, Sarajedini A, Garnett DR, Holtzman JA. 2009. *ApJ* 699:839–849

Sana H, Gosset E, Nazé Y, Rauw G, Linder N. 2008. *MNRAS* 386:447–460

Sandage AR. 1953. *AJ* 58:61–75

Sarajedini A, Mancone CL. 2007. *AJ* 134:447–456

Scally A, Clarke C, McCaughrean MJ. 2005. *MNRAS* 358:742–754

Schechter P. 1976. *ApJ* 203:297–306

Scheepmaker RA, Haas MR, Gieles M, Bastian N, Larsen SS, Lamers HJGLM. 2007. *A&A* 469:925–940

Schilbach E, Röser S. 2008. *A&A* 489:105–114

Schweizer F. 1982. *ApJ* 252:455–460

Shapiro SL. 1985. In *Dynamics of Star Clusters*, ed. J. Goodman & P. Hut, vol. 113 of *IAU Symposium*

Shara MM, Hurley JR. 2002. *ApJ* 571:830–842

Silich S, Tenorio-Tagle G, Rodríguez-González A. 2004. *ApJ* 610:226–232

Sills A, Deiters S, Eggleton P, Freitag M, Giersz M, et al. 2003. *New Astronomy* 8:605–628

Smith LJ, Gallagher JS. 2001. *MNRAS* 326:1027–1040

Smith LJ, Westmoquette MS, Gallagher JS, O'Connell RW, Rosario DJ, de Grijs R. 2006. *MNRAS* 370:513–527

Sollima A, Beccari G, Ferraro FR, Fusi Pecci F, Sarajedini A. 2007. *MNRAS* 380:781–791

Sollima A, Lanzoni B, Beccari G, Ferraro FR, Fusi Pecci F. 2008. *A&A* 481:701–704

Sommariva V, Piotto G, Rejkuba M, Bedin LR, Heggie DC, et al. 2009. *A&A* 493:947–958

Spitzer L. 1987. *Dynamical evolution of globular clusters*. Princeton, NJ, Princeton University Press, 1987, 191 p.

Spitzer Jr. L. 1975. In *Dynamics of the Solar Systems*, ed. A. Hayli, vol. 69 of *IAU Symposium*

Spitzer LJ. 1940. *MNRAS* 100:396

Spitzer LJ. 1958. *ApJ* 127:17

Spitzer LJ. 1969. *ApJL* 158:L139

Spitzer LJ, Chevalier RA. 1973. *ApJ* 183:565–582

Spitzer LJ, Hart MH. 1971. *ApJ* 164:399

Spurzem R. 1999. *Journal of Computational and Applied Mathematics* 109:407–432

Spurzem R, Giersz M, Heggie DC, Lin DNC. 2009. *ApJ* 697:458–482

Stodolkiewicz JS. 1982. *Acta Astronomica* 32:63–91

Stodolkiewicz JS. 1986. *Acta Astronomica* 36:19–41

Stolte A, Brandner W, Grebel EK, Lenzen R, Lagrange AM. 2005. *ApJL* 628:L113–L117

Stolte A, Grebel EK, Brandner W, Figer DF. 2002. *A&A* 394:459–478

Strohmayer TE, Mushotzky RF. 2003. *ApJL* 586:L61–L64

Swartz DA, Tennant AF, Soria R. 2009. *ApJ* 703:159–168

Takahashi K. 1996. *Publ. Astr. Soc. Japan* 48:691–700

Takahashi K. 1997. *Publ. Astr. Soc. Japan* 49:547–560

Takahashi K, Portegies Zwart SF. 1998. *ApJL* 503:L49

Takahashi K, Portegies Zwart SF. 2000. *ApJ* 535:759–775

Theuns T. 1991. *Memorie della Societa Astronomica Italiana* 62:909–914

Thorsett SE, Arzoumanian Z, Taylor JH. 1993. *ApJL* 412:L33–L36

Trenti M, Ardi E, Mineshige S, Hut P. 2007. *MNRAS* 374:857–866

Udry S, Santos NC. 2007. *ARA&A* 45:397–439

Šubr L, Kroupa P, Baumgardt H. 2008. *MNRAS* 385:1673–1680

Vallée JP. 2008. *AJ* 135:1301–1310

van den Bergh S. 1957. *ApJ* 125:445

van den Bergh S. 1971. *A&A* 12:474

van den Bergh S. 1991. *ApJ* 369:1–12

van den Bergh S, McClure RD. 1980. *A&A* 88:360–362

van den Berk J, Portegies Zwart SF, McMillan SLW. 2007. *MNRAS* 379:111–122

Vanbeveren D, Belkus H, van Bever J, Mennekens N. 2009. *Ap&SS* :114

Vansevičius V, Kodaira K, Narbutis D, Stonkutė R, Bridžius A, et al. 2009. *ApJ* 703:1872–1883

Ventura P, D'Antona F, Mazzitelli I, Gratton R. 2001. *ApJL* 550:L65–L69

Vesperini E. 1997. *MNRAS* 287:915–928

Vesperini E, D'Ercole A, D'Antona F, McMillan SLW, Recchi S. 2009. In *Bulletin of the American Astronomical Society*, vol. 41 of *Bulletin of the American Astronomical Society*

Vesperini E, Heggie DC. 1997. *MNRAS* 289:898–920

Vesperini E, McMillan SLW, Portegies Zwart S. 2009. *ApJ* 698:615–622

Vesperini E, Zepf SE. 2003. *ApJL* 587:L97–L100

Vesperini E, Zepf SE, Kundu A, Ashman KM. 2003. *ApJ* 593:760–771

Vinkó J, Sárneczky K, Balog Z, Immler S, Sugerman BEK, et al. 2009. *ApJ* 695:619–635

von Hoerner S. 1957. *ApJ* 125:451

von Hoerner S. 1958. *Zeitschrift fur Astrophysik* 44:221–242

von Hoerner S. 1963. *Zeitschrift fur Astrophysik* 57:47–82

Vrba FJ, Henden AA, Luginbuhl CB, Guetter HH, Hartmann DH, Klose S. 2000. *ApJL* 533:L17–L20

Wang X, Yang Y, Zhang T, Ma J, Zhou X, et al. 2005. *ApJL* 626:L89–L92

Weidner C, Kroupa P. 2004. *MNRAS* 348:187–191

Weidner C, Kroupa P. 2006. *MNRAS* 365:1333–1347

Weidner C, Kroupa P, Larsen SS. 2004. *MNRAS* 350:1503–1510

Weigelt G, Baier G. 1985. *A&A* 150:L18–L20

Weinberg MD. 1994. *AJ* 108:1403–1413

Weldrake DTF, Sackett PD, Bridges TJ, Freeman KC. 2005. *ApJ* 620:1043–1051

White NE, van Paradijs J. 1996. *ApJL* 473:L25

Whitmore BC. 2003. In *A Decade of Hubble Space Telescope Science*, eds. M Livio, K Noll, M Stiavelli

Whitmore BC, Chandar R, Fall SM. 2007. *AJ* 133:1067–1084

Whitmore BC, Schweizer F. 1995. *AJ* 109:960–980

Whitmore BC, Zhang Q, Leitherer C, Fall SM, Schweizer F, Miller BW. 1999. *AJ* 118:1551–1576

Wielen R. 1971. *A&A* 13:309–322

Wielen R. 1988. In *IAU Symp. 126: The Harlow-Shapley Symposium on Globular Cluster Systems in Galaxies*, eds. JE Grindlay, AGD Philip

Wilkinson MI, Hurley JR, Mackey AD, Gilmore GF, Tout CA. 2003. *MNRAS* 343:1025–1037

Wu H, Xue SJ, Xia XY, Deng ZG, Mao S. 2002. *ApJ* 576:738–744

Wyder TK, Hodge PW, Zucker DB. 2000. *PASP* 112:1162–1176

Yungelson LR, van den Heuvel EPJ, Vink JS, Portegies Zwart SF, de Koter A. 2008. *A&A* 477:223–237

Zepf SE, Ashman KM, English J, Freeman KC, Sharples RM. 1999. *AJ* 118:752–764

Zezas A, Fabbiano G, Rots AH, Murray SS. 2002. *ApJ* 577:710–725

Zhang Q, Fall SM. 1999. *ApJL* 527:L81–L84

A Appendix: Dynamical algorithms

Even though the fundamental physics is not hard to understand, simulating star clusters is not a trivial matter. Significant complications arise due to the long-range nature of the gravitational force, which means that every star in the cluster is effectively in constant communication with every other. The result is a potentially enormous number of interactions that must be calculated as we follow the time evolution of the system, leading to high computational cost. Further complications arise from the enormous range in spatial and temporal scales inherent in a star cluster. Computers, by the way they are constructed, have difficulty in resolving such wide ranges, and many of the software problems in simulations of self-gravitating systems arise from this basic limitation. The combination of many physical processes occurring on many scales, with high raw processing requirements, makes numerical gravitational dynamics among the most demanding and challenging areas of computational

science. In this Appendix we discuss some of the issues involved in the numerical modeling of massive star clusters.

The broad spectrum of numerical methodologies currently available is summarized in §4.1. Here we present some of the details of these simulation techniques, starting with *"Continuum" Models*, followed by *Monte Carlo Models* and *Direct N-body Models*. We end this section with brief discussions of computer hardware and multi-core codes, and in particular *Kitchen Sink Models* and *Future Prospects*.

A.1 Continuum methods

The two leading classes of continuum models are gas-sphere (Lynden-Bell & Eggleton 1980, Bettwieser & Sugimoto 1984, Deiters & Spurzem 2001) and Fokker–Planck (Cohn 1979; Shapiro 1985; Chernoff & Weinberg 1990; Drukier, Fahlman & Richer 1992; Takahashi 1996, 1997; Takahashi & Portegie methods. They have mainly been applied to spherically symmetric systems, although axisymmetric extensions to rotating systems have also been implemented (Einsel & Spurzem 1999; Kim et al. 2002; Kim, Lee & Spurzem 2004), and some limited experiments with rudimentary binary treatments have also been performed (Gao et al. 1991).

Both approaches start with the collisional Boltzmann equation as the basic description for a stellar system, then simplify it by averaging the distribution function $f(\mathbf{x}, \mathbf{v})$ in different ways. Gas-sphere methods proceed in a manner closely analogous to the derivation of the equations of fluid motion, taking velocity averages to construct the moments of the distribution: $\rho = \int d^3v\, f(\mathbf{x}, \mathbf{v})$, $\mathbf{u} = \int d^3v\, \mathbf{v} f(\mathbf{x}, \mathbf{v})$, $\sigma^2 = \frac{1}{3} \int d^3v\, v^2 f(\mathbf{x}, \mathbf{v})$, etc. Application of a closure condition leads to a set of equations identical to those of a classical conducting fluid, in which the conductivity depends inversely on the local relaxation time. Fokker–Planck methods transform the Boltzmann equation by orbit-averaging all quantities and recasting the equation as a diffusion equation in $E - J$ space, where E is stellar energy and J is angular momentum. Since both E and J are conserved orbital quantities in a static, spherically symmetric system, two-body relaxation enters into the problem via the diffusion coefficients.

These methods have been of enormous value in developing and refining theoretical insights into the fundamental physical processes driving the dynamical evolution of stellar systems (Bettwieser & Sugimoto 1984). However, as the degree of realism demanded of the simulation increases—adding a mass spectrum, stellar evolution, binaries, etc.—the algorithms rapidly become cumbersome, inefficient, and of questionable validity (Portegies Zwart & Takahashi 1999). As a result, they are generally not applied to the young stellar systems of interest here. The major approaches currently used for simulating young massive clusters are particle-based Monte Carlo or direct N-body codes.

A.2 Monte Carlo methods

Depending on one's point of view, Monte Carlo methods can be regarded as particle algorithms for solving the partial differential equations arising from the continuum models, or approximate schemes for determining the long-term average gravitational interactions of a large collection of particles. The early techniques developed in the 1970s and 1980s (Spitzer & Hart 1971, Henon 1973, Spitzer 1975, Stodolkiewicz 1982, 1986) fall into the former category, but recent studies, in particular (Giersz 1998; Joshi, Rasio & Portegies Zwart 2000;

Freitag & Benz 2001; Giersz 2001; Fregeau et al. 2003; Giersz 2006; Fregeau & Rasio 2007; Heggie & Giersz 2008; Giersz & Heggie 2009), tend to adopt the latter view. The hybrid Monte Carlo scheme of (Giersz 1998, 2001, Giersz & Spurzem 2003) combines a gas-sphere treatment of the "background" stellar population with a Monte Carlo realization of the orbits and interactions of binaries and other objects of interest. These approaches have allowed the first simulations of an entire globular cluster, from a very early (although gas depleted) phase to complete dissolution.

Monte Carlo methods are designed for efficient computation of relaxation effects in collisional stellar systems, a task which they accomplish by reducing stellar orbits to their orbital elements—energy and angular momentum—effectively orbit averaging the motion of each star. Relaxation is modeled by randomly selecting pairs of stars and applying interactions between them in such a way that, on average, the correct rate is obtained. This may be implemented in a number of ways, but interactions are generally realized on time scales comparable to the orbit-averaged relaxation time. As a result, Monte Carlo schemes can be orders of magnitude faster than direct N-body codes. For example, Joshi, Rasio & Portegies Zwart (2000) report a CPU time scaling for their Monte Carlo scheme of $O(N^{1.4})$ for core-collapse problems, compared to N^3 for N-body methods, as discussed below. To achieve these speeds, however, the geometry of the system must be simple enough that the orbital integrals can be computed from a star's instantaneous energy and angular momentum. In practice, this limits the approach to spherically symmetric systems in virial equilibrium, and global dynamical processes occurring on relaxation (or longer) time scales.

A.3 N-body methods

N-body codes incorporate detailed descriptions of stellar dynamics at all levels, using direct integration of the individual (Newtonian) stellar equations of motion for all stars (Aarseth 2003, Heggie & Hut 2003). Their major attraction is that they are assumption-free, in the sense that all stellar interactions are automatically included to all orders, without the need for any simplifying approximations or the inclusion of additional reaction rates to model particular physical processes of interest. Thus, problems inherent to Monte Carlo methods (see §A.2), related to departures from virial equilibrium, spherical symmetry, statistical fluctuations, the form of (and indeed the existence of) phase space distribution functions, and the possibility of interactions not explicitly coded in advance, simply do not arise, and therefore do not require fine-tuning as in the Monte Carlo models.

The price of all these advantages is computational expense. Each of the N particles must interact with every other particle a few hundred times over the course of every orbit, each interaction requires $O(N)$ force calculations, and a typical (relaxation time) run spans $O(N)$ orbits (see Eq. 16). The resulting $O(N^3)$ scaling of the total CPU time means that, even with the best time-step algorithms, integrating even a fairly small system of, say, $N \sim 10^5$ stars requires sustained teraflops speeds for several months (Hut, Makino & McMillan 1988). Radically improved performance can be achieved by writing better software, or by building faster computers (or both). In fact, the remarkable speed-up of N-body codes over the last four decades has mainly been due to advances in hardware, and in a lesser extend due to software.

Substantial performance improvements were realized by adopting better (individual) time

stepping schemes (as opposed to earlier shared time step schemes), in which particles advance using steps appropriate to their individual orbits, rather than a single step for all. Further gains were made by utilizing neighbor schemes (Ahmad & Cohen 1973b), which divide the force on every particle into irregular (rapidly varying) and regular (slowly varying) parts, due (loosely speaking) to nearby and more distant bodies. By recomputing the regular force at every particle step, but extrapolating the more expensive $O(N)$ regular force for most time steps, and recomputing it only on longer time scales, significant improvements in efficiency have been realized. A multi-level generalization of this approach by Dorband, Hemsendorf & Merritt (2003) is incorporated into the collisonal NBODY6++ (Spurzem 1999).

Another important algorithmic improvement was introduced in the mid-1980s with the development of tree codes (Barnes & Hut 1986), which reduce the force calculation complexity from $O(N)$ to $O(\log N)$. Despite their algorithmic efficiency, tree codes have not been widely used in modeling collisional systems (but see McMillan & Aarseth 1993). This seems principally to be because of lingering technical concerns about their long-term accuracy in systems dominated by relaxation processes and their performance in clusters with large dynamic ranges in densities and time scales, even though these objections may no longer be well founded (Moore et al. 1999, Dehnen 2000). Very promising direct–treecode methods have recently been developed to model the dynamical interaction between a cluster and the surrounding galactic population (Fujii et al. 2007, Portegies Zwart et al. 2009).

A.4 Parallelization

Individual time step schemes are generally hard to optimize on parallel machines. For those architectures, block time step schemes (McMillan 1986, Makino et al. 2006) offer substantially better performance. By rounding each star's "natural" step down to the nearest negative integer power of two, such a scheme effectively discretizes the time variable, allowing the possibility that large blocks of stars will be "next" on the time step list, and so can be efficiently integrated in parallel.

The two most important parallel integration techniques are the *ring* and *copy* algorithms. Both have advantages and disadvantages, but the execution times for each, on computers with p processors, scale as N/p, while the communication times scale as p (Harfst et al. 2007). Both algorithms are implemented in a range of N-body codes, including NBODY6++ (Dorband, Hemsendorf & Merritt 2003) and the `kira` integrator in `Starlab` (Portegies Zwart et al. 2008). The two-dimensional lattice parallelization for direct N-body kernels has comparable CPU time scaling, but the communication has a weaker scaling ($\propto 1/\sqrt{p}$), enabling the code to maintain satisfactory performance even on computers with $p \gtrsim 10^3$ processors (Makino 2002, Bisseling 2004). So far, however, this scheme has not been implemented in a production N-body code.

An interesting further step is to use a widely distributed grid of computers (Foster & Kesselman 2004). In this extreme form of parallel computing the computational bottleneck often shifts from the $O(N^2)$ force calculation (see §A.3) to communication (latency and bandwidth). However, even in the worst-case scenario the communication costs scale $\propto N$, so, for a sufficiently large number of stars even intercontinental grid computing can be practical (Hoekstra et al. 2008). In addition, if (as seems likely—see §A.6) future simulation environments will combine a

range of codes in addition to pure stellar dynamics to address the evolution of YMCs in detail, grid computing may provide the solution to the problem of limited supply of local computer resources. This is particularly relevant if the desired algorithms for solving stellar dynamics, stellar evolution, hydrodynamics, etc, require a diversity in computer architectures that may not be locally available.

A.5 Hardware acceleration

A quantum leap in gravitational N-body simulation speed came from the introduction of special purpose computers. All N-body codes, including neighbor schemes and treecodes, suffer from the cost of computing inter-particle forces at every step along the orbit. A technological solution in widespread use is the "GRAPE" (short for "GRAvity PipE") series of machines developed by Sugimoto and co-workers at Tokyo University (Ebisuzaki et al. 1993). Abandoning algorithmic sophistication in favor of simplicity and raw computing power, these machines achieved high performance by mating a fourth-order Hermite integration scheme (Makino & Aarseth 1992) with special-purpose hardware in the form of highly parallel, pipelined "Newtonian force accelerators" implementing the computation of all inter-particle forces entirely in hardware. Operationally, the GRAPE hardware is simple to program, as it merely replaces the function that computes the (regular) force on a particle by a call to the hardware interface libraries; the remainder of the user's N-body code is unchanged.

The effect of GRAPE on simulations of stellar systems has been nothing short of revolutionary. Today, GRAPE-enabled code lies at the heart of almost all detailed N-body simulations of star clusters and dense stellar systems. GRAPE-like optimizations of the innermost force calculation operations using the IA-32 Streaming SIMD Extensions 2 (SSE2), suitable for use on any Intel/AMD processor, are described by Nitadori, Makino & Hut (2006).

Recently, Graphics Processing Units (GPUs) have achieved speeds and price/performance levels previously attainable only by GRAPE systems (see Portegies Zwart, Belleman & Geldof 2007; Hamada & Iitaka 2007; Belleman, Bédorf & Portegies Zwart 2008; Gaburov, Harfst & Portegies Zwart 200 for recent GPU implementations of the GRAPE interface). In addition, the programming model for GPUs (as well as the GRAPE-DR, Makino 2005), means that many other kinds of algorithms can (in principle) be accelerated, although, in practice, it currently seems that CPU-intensive operations such as direct N-body force summation show substantially better acceleration than, say, treecodes running on the same hardware. It appears that commodity components may be poised to outpace special-purpose computers in this specialized area of computational science, just as they have already done in general-purpose computing.

A.6 The kitchen sink

Consistent with our growing understanding of the role of stellar and binary interactions in collisional stellar systems, the leading programs in this field are "kitchen sink" packages that combine treatments of dynamics, stellar and binary evolution, and stellar hydrodynamics within a single simulation. Of these, the most widely used are the N-body codes `NBODY` (Hurley et al. 2001, Aarseth 2003), `kira` which is part of the `starlab` package (e.g. Portegies Zwart et al. 2001), and the Monte Carlo codes developed by Giersz (Giersz 1998,

Heggie & Giersz 2008, Giersz & Heggie 2009), Freitag (Fregeau et al. 2003; Freitag, Rasio & Baumgardt 2
and Fregeau (Fregeau & Rasio 2007).

Despite the differences in their handling of the large-scale dynamics, as just outlined, these codes all employ conceptually similar approaches to stellar and binary evolution and collisions. All use approximate descriptions of stellar evolution, generally derived from look-up tables based on the detailed evolutionary models of Eggleton, Fitchett & Tout (1989) and Hurley, Pols & Tout (2000). They also rely on semi-analytic or heuristic rule-based treatments of binary evolution (Portegies Zwart & Verbunt 1996; Hurley, Tout & Pols 2002), conceptually similar from code to code, but significantly different in detail.

In most cases, collisions are implemented in the simple "sticky-sphere" approximation, where stars are taken to collide (and merge) if they approach within the sum of their effective radii. The effective radii may be calibrated using hydrodynamical simulations, and mass loss may be included in some approximate way. Freitag's Monte Carlo code, geared mainly to studies of galactic nuclei, uses a more sophisticated approach, interpolating encounter outcomes from a pre-computed grid of smoothed particles hydrodynamics (SPH) simulations (Freitag & Benz 2005). An interesting alternative, though currently only operational in AMUSE (see §A.7), is the "Make Me A Star" package (MMAS; Lombardi et al. 2003)[h] and its extension "Make Me a Massive Star" (MMAMS; Gaburov, Lombardi & Portegies Zwart 2008)[i]. MMA(M)S constructs a merged stellar model by sorting the fluid elements of the original stars by entropy or density, then recomputing their equilibrium configuration, using mass loss and shock heating data derived from SPH calculations.

Small-scale dynamics of multiple stellar encounters, such as binary and higher-order encounters, are often handled by look-up from pre-computed cross sections or—more commonly—by direct integration, either in isolation or as part of a larger N-body calculation. Codes employing direct integration may also include post-Newtonian terms in the interactions between compact objects (Kupi, Amaro-Seoane & Spurzem 2006).

A.7 Future prospects

The very comprehensiveness of kitchen-sink codes gives them the great advantage of applicability to complex stellar systems, but also the significant disadvantage of inflexibility. By selecting one of these codes, one is implicitly choosing a particular hard-coded combination of dynamical integrator, stellar and binary evolution schemes, collision prescription, and treatment of multiple dynamics. The structure of these codes is such that implementing a different algorithm within the larger framework is difficult at best, and practically impossible.

However, studies of dense stellar systems force interactions between programs that were never intended to interact with other programs, and by extension require new communication channels between the programmers responsible for them. Closely related to this effort is the "MUSE" (MUltiscale, MUltiphysics Software Environment) project[j] (Portegies Zwart et al. 2009), and its successor AMUSE (Astrophysical MUltipurpose Software Environment), two ambitious open-source efforts in code integration. (A)MUSE aims at the self-consistent integration of dynamics, collisions, stellar evolution, and other relevant physical processes,

[h] See `http://webpub.allegheny.edu/employee/j/jalombar/mmas/`

[i] See `http://castle.strw.leidenuniv.nl/`

[j] `http://muse.li`

thereby realizing one vision of the MODEST[k] community (Hut et al. 2003, Sills et al. 2003, Davies et al. 2006). The long-term goal is a comprehensive environment for modeling dense stellar systems, including multiphysics/legacy codes and flexible interfaces to integrate existing software (written in many languages) within this unifying environment.

Aside from future developments in modular simulation environments, the recent appearance of programmable high-performance hardware has spurred the development of new algorithms for implementing the force-evaluation operations in N-body codes. (Nitadori & Makino 2008) have developed extensions of the standard fourth-order Hermite scheme to higher (sixth and eighth) orders, and Gaburov and Nitadori (2010, in preparation) have incorporated these methods into the well-known Ahmad & Cohen (1973a) neighbor scheme. Other intriguing future prospects come from hybridization of direct methods with hierarchical tree and particle-mesh algorithms, an approach currently under development by Nitadori and Makino (2009, private communication), but not yet operational.

[k]MODEST stands for MOdeling DEnse STellar systems, and can be found at `http://www.manybody.org/modest`.

This figure "a.jpg" is available in "jpg" format from:

http://arxiv.org/ps/1002.1961v1